Complete flux approximation schemes for the compressible Navier-Stokes equations

van Susteren, Hannah

Award date:
2021

Complete flux approximation schemes for the compressible Navier-Stokes equations

Master thesis
Industrial and Applied Mathematics

Hannah van Susteren
0993670

Supervisors:
J.H.M. ten Thije Boonkkamp
B. Koren

July 14, 2021
Eindhoven University of Technology
Department of Mathematics and Computer Science

Abstract

This thesis is on the compressible Navier-Stokes equations. Firstly, the Navier-Stokes equations are derived. Subsequently, the equations are discretized using finite volumes and the complete flux scheme. The resulting system is solved for several choices of boundary conditions and solution variables using the Newton-Raphson method. Subsequently, the results of this numerical implementation are given and a convergence analysis is executed. Additionally, an analytical solution for the momentum equation is given. Lastly, the dimensionless system is given and an alternative discretization approach is proposed.

Contents

1 Introduction **2**

2 Compressible Navier-Stokes equations **4**
2.1 General conservation law 4
2.2 Conservation of mass 4
2.3 Conservation of momentum 5
2.4 Conservation of energy 6
2.5 Equation of state 6
2.6 Caloric equation of state 7
2.7 Compressible Navier-Stokes equations 7

3 Finite volume discretization **8**
3.1 Momentum equation 9
3.2 Energy equation 11
3.3 Discretized system 12

4 Analytical solution for the momentum equation **13**
4.1 Formulation of IVP 13
4.2 Solution methods 14
4.3 Results 15

5 Numerical implementation **22**
5.1 Boundary conditions for system in τ, p 22
5.1.1 Dirichlet and Neumann boundary conditions 22
5.1.2 Dirichlet boundary conditions 24
5.2 Boundary conditions for system in τ, h 27
5.2.1 Dirichlet and Neumann boundary conditions 27
5.2.2 Dirichlet boundary conditions 28

6 Results **30**
6.1 Neumann-Dirichlet boundary conditions 30
6.1.1 Distortions 30
6.1.2 Linear 31
6.1.3 Arbitrary shock 33
6.1.4 Dirichlet shock 35
6.2 Dirichlet boundary conditions 35
6.2.1 Mach = 1.1 36
6.2.2 Mach = 2 38
6.2.3 Mach = 3 41
6.3 Convergence analysis 46

7 Complete flux approach for Prandtl $\neq \frac{3}{4}$ **49**
7.1 Results 50

8 Dimensionless system **54**
8.1 Dimensionless finite volume discretization 54
8.2 Alternative finite volume discretization 55
8.3 Dimensionless Dirichlet boundary conditions 56
8.4 Results dimensionless systems 57
8.4.1 Dimensionless complete flux results 57
8.4.2 Dimensionless alternative approach results 63

9 Conclusion **67**

10 Discussion **68**

A Results complete flux with Neumann-Dirichlet boundary conditions in τ, h **70**

B Results complete flux with Dirichlet boundary conditions in τ, h **71**

1 Introduction

The Navier-Stokes equations are named after engineer and physicist Claude Louis Marie Henri Navier and physicist and mathematician George Gabiel Stokes. The origin of these equations can be dated back to 1687 [1]. In this year, Isaac Newton wrote a papier on viscous fluid motion. Subsequently, the inviscid Euler equations were derived by Daniel Bernoulli in 1738 and Leonhard Euler in 1755. After these equations were derived, fluid flows were researched by several mathematicians, the first being Claude-Louis Navier. However, these mathematicians did not take viscous terms into account. This was done first by George Stokes in 1845 and so the Navier-Stokes equations as we know them today were derived.
Since the equations were derived, many have wondered about the existence and smoothness of these equations. This topic has even become one of the seven Millennium Prize problems stated by the Clay Mathematics Institute in May 2000 [2].

The Navier-stokes equations are used to describe fluid motion. They describe the behaviour of important fluid properties such as density, velocity, pressure, temperature and viscosity. The equations are based on three conservation laws. The conservation laws that are used in the Navier-Stokes equations are the conservation of mass, momentum and energy. These equations can be used for many applications, such as weather prediction, air flow around aircraft and biomedical applications. Because of the wide range of application, more efficient solution methods to these equations are always sought after.

The Navier-Stokes equations exist for compressible flows as well as for incompressible flows. It is important to distinguish these two versions of the Navier-Stokes equations. An incompressible flow is defined by the inability to be compressed when external pressure is applied. This means that the density remains constant within a volume. Furthermore, the Mach number is normally smaller than 0.3 for an incompressible flow [3]. Lastly, incompressible flows are often liquid flows such as water flow.
On the other hand, a compressible flow, as the name suggest, can be compressed. That is, the density can change in a volume. These flows normally have a Mach number larger than 0.3. Examples of compressible flows are gas flows such as aerodynamics. We will only consider the compressible Navier-Stokes equations.

In this thesis, we will construct a numerical method for the compressible Navier-Stokes equations. This approach starts with the finite volume method. That is, the computational domain is divided into finite volumes. Subsequently, we integrate over each volume. This leads to the introduction of the (numerical) fluxes and the discrete conservation law. In order to compute the fluxes, we propose the complete flux scheme. In this scheme, a local boundary value problem is defined. The solution of this boundary value problem defines the numerical flux. This flux is then substituted into the discrete conservation law to form the discretized system. Finally, this system is solved using the Newton-Raphson method.

In addition to the numerical method based on the finite volume method and the complete flux scheme, we also propose an exact solution for the case in which the Prandtl number is equal to $\frac{3}{4}$. The exact solution is computed using the momentum and energy equations. Additionally, boundary conditions at the inflow are imposed. This solution may indicate the behaviour of a correct solution of the Navier-Stokes equation.

In Section 1, we will derive the conservation laws. These laws are generally accompanied

by several equations of state. These equations together form the system of equations known as the Navier-Stokes equations. Subsequently, we will use a finite volume discretization in Section 2. In this discretization, the complete flux scheme will be applied to form the nonlinear discretized system consisting of two equations and an equation of state. Next, before we start the implementation, we first look at an analytical solution of the momentum equation in Section 3. Thereafter, we implement the previously explained discretization in Section 4. In this section, several choices for the boundary conditions are explored as well as options for the solution variables. Furthermore, it is explained how to solve the system using the Newton-Raphson method. Thereafter, the results of this numerical implementation are given in Section 5. The results are evaluated using a convergence analysis. In Section 6, an extension to the original approach, which extends the method to all Prandtl numbers, is described. Finally, the dimensionless system is derived in Section 7. Moreover, an alternative finite volume approach and its results are given.

2 Compressible Navier-Stokes equations

In this chapter, we will derive the one-dimensional compressible Navier-Stokes equations. Starting from a generic conservation law, we will derive three important conservation laws: conservation of mass, momentum and energy. Furthermore, additional equations of state will be introduced. These equations describe the properties of the fluid in question. The three conservation laws along with the equations of state fully describe fluid motion.

We consider an isotropic Newtonian fluid. That is, the properties of the fluid are identical in all directions. Furthermore, a Newtonian fluid adheres to Newton's law of viscosity. This means that the dynamic viscosity is independent of the shear rate. In addition, we consider a fluid as a continuum. In a continuum, the fluid is considered as a whole and not as individual molecules. Therefore, all properties of the fluid can be measured at a point in space as the fluid is considered to be continuous.

2.1 General conservation law

Consider a scalar quantity per unit length U on an arbitrary one-dimensional spatial domain $\Omega = [x_1, x_N]$ in the domain of interest. The domain is stationary, it does not move along with the fluid. A general conservation law for a single fluid reads

$$\frac{\mathrm{d}}{\mathrm{d}t}\int_\Omega U \,\mathrm{d}x + \left[F\right]_{x_1}^{x_N} = \int_\Omega Q_v \,\mathrm{d}x + \left[Q_s\right]_{x_1}^{x_N}, \tag{1}$$

where x is the spatial variable, F is the flux and Q_v, Q_s denote the volume and surface sources, respectively. This conservation law states that the sum of the temporal variation of the chosen quantity per volume and the flux at the boundary is equal to the sum of contributions of the volume sources and the surface sources in the domain Ω.
Using Gauss' theorem, equation (1) can be rewritten to include only volume integrals to obtain

$$\frac{\mathrm{d}}{\mathrm{d}t}\int_\Omega U \,\mathrm{d}x + \int_\Omega \frac{\partial F}{\partial x} \,\mathrm{d}x = \int_\Omega Q_v \,\mathrm{d}x + \int_\Omega \frac{\partial Q_s}{\partial x} \,\mathrm{d}x\,.$$

As this holds for any arbitrary fixed domain, we can now obtain the differential form of the general conservation law:

$$\frac{\partial U}{\partial t} + \frac{\partial F}{\partial x} = Q_v + \frac{\partial Q_s}{\partial x}.$$

Lastly, the flux can be split into the convective flux, F_c, and the diffusive flux, F_d. We then obtain the final version of the general conservation law:

$$\frac{\partial U}{\partial t} + \frac{\partial F_c}{\partial x} + \frac{\partial F_d}{\partial x} = Q_v + \frac{\partial Q_s}{\partial x}.$$

2.2 Conservation of mass

In the conservation of mass equation, we consider the quantity U to be the specific mass of the fluid, that is, the mass per unit volume. This is otherwise known as the density, denoted by ρ. Furthermore, we denote the velocity of the fluid by u. This gives a convective flux F_c of ρu. In the conservation of mass, there is no diffusive flux F_d. Furthermore, mass conservation

is independent of the forces acting on the system and the nature of the fluid. Thus, the source terms Q_v and Q_d are not present. This leaves us with the following conservation law for mass

$$\frac{\partial U}{\partial t} + \frac{\partial F_c}{\partial x} = 0.$$

Finally, substituting U and F_c gives the following conservation of mass

$$\rho_t + (\rho u)_x = 0,$$

where subscript t denotes temporal differentiation and subscript x spatial differentiation.

2.3 Conservation of momentum

We now consider momentum as the chosen quantity U. Momentum is the product of the mass and velocity of a fluid. As we again consider the specific mass, we obtain a momentum of ρu, i.e., $U = \rho u$. The convective flux F_c consists of the chosen quantity multiplied by its velocity. Thus we obtain a convective flux of ρu^2. In the conservation of momentum, there is no diffusive flux F_d. Furthermore, we assume that there are no volume forces, i.e., $Q_v = 0$.

Next is the internal force that works on the boundary, i.e., the term Q_s. The total internal force, also known as the internal stress, is denoted by σ. Thus we obtain $Q_s = \sigma$. The internal stress consists of the isotropic pressure and the viscous shear stress. Firstly, the isotropic pressure is the force per unit area of the fluid acting in the direction of the outward pointing normal. Thus the isotropic pressure working on the fluid flow is denoted by $-p$ where p denotes pressure. Secondly, we have the viscous shear stress, denoted by $\bar{\tau}$. This force is a result of the deformation caused by the resistance to flow. It can be shown that the shear stress depends only on the rate of deformation [4]. The rate of deformation depends on the derivatives of the velocity components in all spatial directions. For an isotropic Newtonian fluid, this means that the shear stress in the direction x is

$$\bar{\tau} = \lambda u_x + 2\mu u_x, \tag{2}$$

where μ is the dynamic viscosity and λ is the second viscosity coefficient. Now we can use Stokes' hypothesis, which relates the dynamic viscosity and the second viscosity coefficient as follows

$$3\lambda + 2\mu = 0,$$

implying that

$$\lambda = -\tfrac{2}{3}\mu. \tag{3}$$

Substituting (3) into (2), we obtain

$$\bar{\tau} = \tfrac{4}{3}\mu u_x.$$

A more detailed derivation of the shear stress can be found in [11]. Combining the shear stress and the isotropic pressure, we obtain the total internal stress

$$\sigma = -p + \tfrac{4}{3}\mu u_x. \tag{4}$$

Finally, substituting the convective flux ρu^2 and the total internal stress σ, we obtain the following law of conservation of momentum

$$(\rho u)_t + (\rho u^2)_x = (-p + \tfrac{4}{3}\mu u_x)_x. \tag{5}$$

2.4 Conservation of energy

According to the first law of thermodynamics, energy cannot be created or destroyed, it can only be transformed. The law states that the change in energy is equal to the heat flux at the boundaries plus the work done by the system. We consider U to be the product of the total specific internal energy e (energy per unit mass) and the specific mass, i.e., $U = \rho e$. Note that the meaning of specific can change. For specific mass, it means per unit volume. For specific energy, it means per unit mass. The convective flux is again the chosen quantity times the velocity. Thus, we obtain that $F_c = \rho u e$.
The diffusive flux F_d consists of the heat flux q. According to Fourier's law of heat conduction, the heat flux q is proportional to the negative temperature derivative, i.e.,

$$q = -\kappa T_x,$$

where κ denotes the thermal conductivity. This coefficient is a property of a material that describes the ability to conduct heat.
Furthermore, the surface source results from work done due to the internal stress acting on the surface. This is the product of the internal stress σ and the velocity u, i.e., $Q_s = \sigma u$. Using (4), we obtain

$$Q_s = -pu + \tfrac{4}{3}\mu u u_x.$$

Finally, again no volume forces exist, i.e. $Q_v = 0$.
Substituting all terms into the general conservation law gives

$$(\rho e)_t + (\rho u e - \kappa T_x)_x = (-pu + \tfrac{4}{3}\mu u u_x)_x. \tag{6}$$

Lastly, we introduce the specific enthalpy h. This is the sum of the specific energy and the work due to pressure and volume:

$$h = e + \frac{p}{\rho}.$$

Substituting the specific enthalpy into (6) gives the final form of the conservation of energy equation:

$$(\rho e)_t + (\rho u h)_x = (\tfrac{4}{3}\mu u u_x + \kappa T_x)_x.$$

2.5 Equation of state

An equation of state denotes the relation between state variables of a fluid. These state variables are pressure, volume and temperature. As the equation describes properties of a fluid, it can differ per fluid.
From now on, we will consider an ideal gas as the fluid. Therefore, we will use the ideal gas law, known as

$$p = \rho R T,$$

where R is the specific gas constant. Furthermore, the specific gas constant can be related to the specific heat constants, i.e., $R = c_p - c_v$, where c_p is the specific heat for constant pressure and c_v the specific heat for constant volume. Furthermore, the ratio between the two specific heat constants is called the heat capacity ratio, defined as $\gamma = \frac{c_p}{c_v}$. The specific heat capacity at constant pressure denotes the amount of energy that is needed to increase the temperature of the fluid by one unit per unit of mass at constant pressure. Similarly, the specific heat at constant volume denotes the amount of energy needed to increase the temperature by one unit for one unit mass at constant volume.

2.6 Caloric equation of state

In this equation of state, the specific enthalpy h is defined. The specific enthalpy is the total energy in a system per unit of mass, due to temperature and pressure. The total energy consists of the thermal and kinetic energy. Firstly, the specific kinetic energy equals $\frac{1}{2}u^2$. Secondly, we can use the specific heat at constant pressure to determine the thermal energy. As c_p denotes the amount of energy needed to increase the temperature by one unit, the product of c_p and the temperature T equals the amount of energy due to temperature, also known as the thermal energy. Now combining the thermal and kinetic energy, we obtain the following equation for the specific enthalpy

$$h = c_p T + \tfrac{1}{2}u^2.$$

2.7 Compressible Navier-Stokes equations

Putting all equations together, we obtain the one-dimensional compressible Navier-Stokes equations:

$$\rho_t + (\rho u)_x = 0, \tag{7a}$$
$$(\rho u)_t + (\rho u^2 + p)_x = (\tfrac{4}{3}\mu u_x)_x, \tag{7b}$$
$$(\rho e)_t + (\rho u h)_x = (\tfrac{4}{3}\mu u u_x + \kappa T_x)_x, \tag{7c}$$
$$p = \rho R T, \tag{7d}$$
$$h = c_p T + \tfrac{1}{2}u^2. \tag{7e}$$

These equations will be discretized to form the discretized system and subsequently will be solved.

3 Finite volume discretization

We will now discretize the compressible Navier-Stokes equations.
Firstly, we assume that the fluid system is in steady state. Thus we consider the following compressible Navier-Stokes equations

$$(\rho u)_x = 0, \tag{8a}$$
$$(\rho u^2 + p)_x = (\tfrac{4}{3}\mu u_x)_x, \tag{8b}$$
$$(\rho u h)_x = (\tfrac{4}{3}\mu u u_x)_x + (\kappa T_x)_x, \tag{8c}$$
$$p = \rho R T, \tag{8d}$$
$$h = c_p T + \tfrac{1}{2}u^2. \tag{8e}$$

We will rewrite this system of equations to obtain a new system that includes two differential equations together with two equations of state. Subsequently, we will apply the finite volume method. Furthermore, we will define the numerical flux using the complete flux method [5]. To this purpose we introduce two scaled boundary-value problems (BVP). Finally, the numerical flux is substituted into the finite volume scheme to obtain the final nonlinear discretized system.

First we define the mass flux as the product of density and velocity, i.e., $m = \rho u$. From (8a), we then obtain

$$m_x = 0,$$

thus we know that m is constant. Furthermore, we introduce the specific volume τ defined as $\tau = \frac{1}{\rho}$. Using these new variables, we can now write $\rho u^2 = m^2\tau$ and $u = m\tau$. Thus we can also write $u_x = m\tau_x$, as m is constant. Substituting these new expressions into (8b), we obtain

$$(m^2\tau - \tfrac{4}{3}\mu m\tau_x + p)_x = 0.$$

Furthermore, we can rewrite (8c) to obtain

$$(mh)_x = (\tfrac{4}{3}\mu(\tfrac{1}{2}u^2)_x)_x + (\kappa T_x)_x.$$

Substituting $\frac{1}{2}u^2 = h - c_p T$ from (8e) into these equations gives

$$(mh)_x = (\tfrac{4}{3}\mu(h - c_p T)_x)_x + (\kappa T)_x,$$

or equivalently,

$$(mh - \tfrac{4}{3}\mu h_x)_x = (\kappa(1 - \tfrac{4}{3}\mathrm{Pr})T_x)_x, \tag{9}$$

where the Prandtl number, defined as

$$\mathrm{Pr} = \frac{\mu c_p}{\kappa},$$

is introduced. The Prandtl number denotes the ratio between momentum diffusivity and thermal diffusivity. Fluids with a low Prandtl number, i.e., $\mathrm{Pr} \ll 1$ have dominant thermal diffusion whereas fluids with $\mathrm{Pr} \gg 1$ have dominant momentum diffusion.
Next we rewrite (8d) as

$$p\tau = RT, \tag{10}$$

and substitute this into (9) to obtain

$$(mh - \tfrac{4}{3}\mu h_x)_x = (\alpha(p\tau)_x)_x,$$

where $\alpha = \frac{\kappa}{R}(1 - \frac{4}{3}\mathrm{Pr})$.
Finally we rewrite (8e) as

$$h = \frac{\gamma}{\gamma - 1} p\tau + \tfrac{1}{2}(m\tau)^2, \tag{11}$$

where we used that $\gamma = \frac{c_p}{c_v}$ and $R = c_p - c_v$.
In summary, we have rewritten the conservation laws to obtain

$$(m^2\tau - \tfrac{4}{3}\mu m\tau_x + p)_x = 0, \tag{12a}$$

$$(mh - \tfrac{4}{3}\mu h_x)_x = (\alpha(p\tau)_x)_x, \tag{12b}$$

for the three unknowns p, τ and h, where we have used equations of state (10) and (11). We will refer to equations (12a) and (12b) as the specific volume and enthalpy equations, respectively.

3.1 Momentum equation

First we discretize the specific volume equation (12a). We define the momentum flux f_τ as

$$f_\tau = m^2\tau - \tfrac{4}{3}\mu m\tau_x + p.$$

Using this definition, we then obtain

$$(f_\tau)_x = 0.$$

We cover the domain with N equidistant points with boundary points x_1 and x_N. This gives $N - 1$ volumes of size $\Delta x = \frac{x_N - x_1}{N-1}$. Now we apply the finite volume method on control volumes $V_j = [x_{j-\frac{1}{2}}, x_{j+\frac{1}{2}}]$ for $j = 2, ...N - 1$. The grid and control volumes are depicted below.

Figure 1: Spatial grid

Integrating the momentum flux over the control volume leads to

$$f_\tau(x_{j+\frac{1}{2}}) - f_\tau(x_{j-\frac{1}{2}}) = 0.$$

We introduce the numerical flux as $F_{\tau,j+\frac{1}{2}}$. Hence the discrete conservation law becomes

$$F_{\tau,j+\frac{1}{2}} - F_{\tau,j-\frac{1}{2}} = 0.$$

Now we define a local boundary value problem as follows

$$\begin{cases} (f_\tau)_x = 0, & x_j < x < x_{j+1}, \\ \tau(x_j) = \tau_j, & \tau(x_{j+1}) = \tau_{j+1}. \end{cases}$$

This boundary value problem defines the numerical flux. That is, the solution of this BVP equals the numerical flux. This results from the observation that f_τ is constant and therefore $F_{\tau,j+\frac{1}{2}}$ is also equal to this constant, i.e., $f_\tau = F_{\tau,j+\frac{1}{2}}$. In the BVP, Dirichlet conditions are chosen to successfully adapt the complete flux approach and to form the discretized system later on.
To simplify computations, we rescale this BVP using $\sigma(x) = \frac{x-x_j}{\Delta x}$ where $\Delta x = x_{j+1} - x_j$. It then holds that $0 \leq \sigma(x) \leq 1$. The scaled BVP reads

$$\begin{cases} (m^2\tau - \varepsilon m\tau' + p)' = 0, & 0 < \sigma < 1, \\ \tau(0) = \tau_j, \quad \tau(1) = \tau_{j+1}, \end{cases}$$

where prime ($'$) refers to differentiation w.r.t. σ and $\varepsilon = \frac{4\mu}{3\Delta x}$.
Rewriting the numerical flux using the integrating factor (assuming $m \neq 0$) gives

$$F_{\tau,j+\frac{1}{2}} = -\varepsilon m \left(e^{-m\sigma/\varepsilon}\tau\right)' e^{m\sigma/\varepsilon} + p,$$

where we assume ε to be constant in order to simplify matters. Subsequently, we multiply with $-\frac{1}{\varepsilon m}e^{\frac{-m\sigma}{\varepsilon}}$ to isolate the derivative as follows

$$(e^{-m\sigma/\varepsilon}\tau)' - \frac{1}{\varepsilon m}e^{-m\sigma/\varepsilon}p(\sigma) = -\frac{1}{\varepsilon m}e^{-m\sigma/\varepsilon}F_{\tau,j+\frac{1}{2}}.$$

Now that the derivative is isolated, we integrate and apply the boundary conditions to obtain

$$e^{-m/\varepsilon}\tau_{j+1} - \tau_j - \frac{1}{\varepsilon m}\int_0^1 e^{-m\sigma/\varepsilon}p(\sigma)\ \mathrm{d}\sigma = -\frac{1}{\varepsilon m}\int_0^1 e^{-m\sigma/\varepsilon}\ \mathrm{d}\sigma\ F_{\tau,j+\frac{1}{2}}.$$

The right-handside integral equals

$$\int_0^1 e^{-m\sigma/\varepsilon}\ \mathrm{d}\sigma = \frac{\varepsilon}{m}\big(1 - e^{-m/\varepsilon}\big).$$

Thus, we obtain

$$F_{\tau,j+\frac{1}{2}} = \frac{-m^2}{1-e^{-m/\varepsilon}}\big(e^{-m/\varepsilon}\tau_{j+1} - \tau_j\big) + \frac{m}{\varepsilon}\frac{1}{1-e^{-m/\varepsilon}}\int_0^1 e^{-m\sigma/\varepsilon}p(\sigma)\ \mathrm{d}\sigma.$$

Now we split the flux into two parts, namely $F^1_{\tau,j+\frac{1}{2}}$ $F^2_{\tau,j+\frac{1}{2}}$, where the second part includes the pressure term. The first part of the flux equals

$$F^1_{\tau,j+\frac{1}{2}} = m\varepsilon\left(B\Big(\frac{-m}{\varepsilon}\Big)\tau_j - B\Big(\frac{m}{\varepsilon}\Big)\tau_{j+1}\right),$$

where $B(z) = \frac{z}{e^z-1}$. Introducing the Péclet number $\mathrm{Pe} = \frac{m}{\varepsilon}$, the flux becomes

$$F^1_{\tau,j+\frac{1}{2}} = m\varepsilon\Big(B(-\mathrm{Pe})\tau_j - B(\mathrm{Pe})\tau_{j+1}\Big). \tag{13}$$

The second part of the flux takes the effect of the pressure into account. We assume that the pressure can be written as a linear function, i.e. $p(\sigma) = p_j + (p_{j+1} - p_j)\sigma$, where again $0 \leq \sigma \leq 1$. Using this linear pressure, we can use integration by parts on the integral as follows

$$\begin{aligned}\int_0^1 e^{-m\sigma/\varepsilon}p(\sigma)\ \mathrm{d}\sigma &= p_j\int_0^1 e^{-m\sigma/\varepsilon}\ \mathrm{d}\sigma + (p_{j+1}-p_j)\int_0^1 e^{-m\sigma/\varepsilon}\sigma\ \mathrm{d}\sigma \\ &= p_j\frac{\varepsilon}{m}(1-e^{-m/\varepsilon}) + (p_{j+1}-p_j)\frac{\varepsilon}{m}\left(\frac{\varepsilon}{m}\left(1-e^{-m/\varepsilon}\right) - e^{-m/\varepsilon}\right).\end{aligned}$$

Thus the second part equals

$$F^2_{\tau,j+\frac{1}{2}} = \left[\frac{e^{-m/\varepsilon} - 1 + \frac{m}{\varepsilon}}{-\frac{m}{\varepsilon}(e^{-m/\varepsilon} - 1)}\right] p_j + \left[\frac{e^{m/\varepsilon} - 1 - \frac{m}{\varepsilon}}{\frac{m}{\varepsilon}(e^{m/\varepsilon} - 1)}\right] p_{j+1}$$
$$= W(-\mathrm{Pe})p_j + W(\mathrm{Pe})p_{j+1}, \tag{14}$$

where $W(z) = \frac{e^z - 1 - z}{z(e^z - 1)}$. For this function it holds that $0 \leq W(z) \leq 1$ and $W(z) + W(-z) = 1$. Now combining (13) and (14), we obtain the total numerical flux

$$F_{\tau,j+\frac{1}{2}} = F^1_{\tau,j+\frac{1}{2}} + F^2_{\tau,j+\frac{1}{2}}$$
$$= m\varepsilon\Big(B(-\mathrm{Pe})\tau_j - B(\mathrm{Pe})\tau_{j+1}\Big) + W(-\mathrm{Pe})p_j + W(\mathrm{Pe})p_{j+1}.$$

Although we assume that $m \neq 0$, the same results can be obtained for $m = 0$ using the Taylor series of the exponential function. However, when $m = 0$, there is no fluid flow since either the density or velocity is zero.

3.2 Energy equation

Now we will discretize the enthalpy equation (12b). First moving all the terms to one side, we obtain

$$\Big(mh - \tfrac{4}{3}\mu h_x - \alpha(p\tau)_x\Big)_x = 0.$$

We define the enthalpy flux f_h as $f_h = mh - \frac{4}{3}\mu h_x - \alpha(p\tau)_x$. Thus we obtain that

$$(f_h)_x = 0.$$

Similarly as before, we apply the finite volume method on control volume $V_j = [x_{j-\frac{1}{2}}, x_{j+\frac{1}{2}}]$ to obtain

$$f_h(x_{j+\frac{1}{2}}) - f_h(x_{j-\frac{1}{2}}) = 0.$$

Thus we again obtain the discrete conservation law

$$F_{h,j+\frac{1}{2}} - F_{h,j-\frac{1}{2}} = 0,$$

where we have introduced the numerical flux $F_{h,j+\frac{1}{2}}$. We can now formulate the following BVP which, similarly as before, defines the numerical flux

$$\begin{cases} (f_h)_x = 0, & x_j < x < x_{j+1}, \\ h(x_j) = h_j, & h(x_{j+1}) = h_{j+1}. \end{cases}$$

We observe that f_h is constant and therefore

$$f_h = F_{h,j+\frac{1}{2}}.$$

Thus the solution of the BVP defines the numerical flux. Furthermore, we again consider Dirichlet conditions for the reasons previously mentioned.
Again, to simplify computations, we scale the BVP to obtain

$$\begin{cases} (mh - \varepsilon h' - \frac{\alpha}{\Delta x}(p\tau)')' = 0, & 0 < \sigma < 1, \\ h(0) = h_j, & h(1) = h_{j+1}. \end{cases}$$

Furthermore, we can rewrite $F_{h,j+\frac{1}{2}}$ as follows

$$F_{h,j+\frac{1}{2}} = -\varepsilon(e^{-m\sigma/\varepsilon}h)'e^{\frac{m\sigma}{\varepsilon}} - \frac{\alpha}{\Delta x}(p\tau)'. \tag{15}$$

We now assume that $\mathrm{Pr} = \frac{3}{4}$, leading to $\alpha = 0$. Then, the numerical flux reduces to

$$F_{h,j+\frac{1}{2}} = -\varepsilon\Big(e^{-m\sigma/\varepsilon}h\Big)'e^{\frac{m\sigma}{\varepsilon}}.$$

Multiplying with $\frac{1}{\varepsilon}e^{\frac{-m\sigma}{\varepsilon}}$ gives

$$-\frac{1}{\varepsilon}e^{-m\sigma/\varepsilon}F_{h,j+\frac{1}{2}} = \Big(e^{-m\sigma/\varepsilon}h\Big)'.$$

Subsequently, assuming $m \neq 0$, integrating and applying the boundary conditions gives

$$F_{h,j+\frac{1}{2}} = \varepsilon\left(B(-\mathrm{Pe})h_j - B(\mathrm{Pe})h_{j+1}\right).$$

This result can also be obtained using Taylor series for $m = 0$.
Lastly, we note that this approach can also be seen as the homogeneous flux scheme as there is no source term. However, one could also take the pressure term as a source term in order to resemble the complete flux more. Both approaches lead to the same result.

3.3 Discretized system

In summary, we have computed the numerical momentum flux and the numerical enthalpy flux, which read

$$F_{\tau,j+\frac{1}{2}} = m\varepsilon\Big(B(-\mathrm{Pe})\tau_j - B(\mathrm{Pe})\tau_{j+1}\Big) + W(-\mathrm{Pe})p_j + W(\mathrm{Pe})p_{j+1}, \tag{16a}$$

$$F_{h,j+\frac{1}{2}} = \varepsilon\Big(B(-\mathrm{Pe})h_j - B(\mathrm{Pe})h_{j+1}\Big). \tag{16b}$$

Furthermore, we assumed that p can be written as a linear function $p(\sigma) = p_j + (p_{j+1} - p_j)\sigma$ and that $\mathrm{Pr} = \frac{3}{4}$. For both numerical fluxes, we use the finite volume method to obtain

$$F_{\tau,j+\frac{1}{2}} - F_{\tau,j-\frac{1}{2}} = 0, \tag{17a}$$

$$F_{h,j+\frac{1}{2}} - F_{h,j-\frac{1}{2}} = 0. \tag{17b}$$

Substituting (16a) into (17a) gives

$$m\varepsilon\left[-B^-\tau_{j-1} + (B^- + B^+)\tau_j - B^+\tau_{j+1}\right] - W^-p_{j-1} + (W^- - W^+)p_j + W^+p_{j+1} = 0,$$

where $B^- = B(-\mathrm{Pe}),\ B^+ = B(\mathrm{Pe})$ and similarly for W.
For the enthalpy flux, we substitute (16b) into (17b) to obtain

$$\varepsilon\left[-B^-h_{j-1} + (B^- + B^+)h_j - B^+h_{j+1}\right] = 0.$$

Thus we have the following nonlinear discretized system

$$m\varepsilon\left[-B^-\tau_{j-1} + (B^- + B^+)\tau_j - B^+\tau_{j+1}\right] - W^-p_{j-1} + (W^- - W^+)p_j + W^+p_{j+1} = 0, \tag{18a}$$

$$\varepsilon\left[-B^-h_{j-1} + (B^- + B^+)h_j - B^+h_{j+1}\right] = 0, \tag{18b}$$

$$h = \frac{\gamma}{\gamma - 1}p\tau + \tfrac{1}{2}(m\tau)^2. \tag{18c}$$

This nonlinear system can now be solved.

4 Analytical solution for the momentum equation

Before continuing with the discretized system, we first propose an analytical solution. Here, we again assume that $\text{Pr} = \frac{3}{4}$.

4.1 Formulation of IVP

Before we consider the momentum equation, we briefly consider the energy equation (8c). Integrating the energy equation gives

$$\rho u h - \tfrac{4}{3}\mu u u_x - \kappa T_x = C_1, \tag{19}$$

where C_1 is an integration constant. Substituting $m = \rho u$ and $h = \frac{1}{2}u^2 + c_p T$ into (19) gives

$$-\tfrac{4}{3}\mu h_x + mh = \kappa(1 - \tfrac{4}{3}\text{Pr})T_x + C_1,$$

where Pr is the Prandtl number. We assume that $\text{Pr} = \frac{3}{4}$, giving

$$-\tfrac{4}{3}\mu h_x + mh = C_1.$$

Imposing inflow boundary condition at $x = -\infty$: $h = h_{\text{in}}$ and $h_x = 0$ leads to $C_1 = mh_{\text{in}}$. Thus, the differential equation becomes

$$-\frac{4}{3}\mu h_x + mh = mh_{\text{in}}.$$

Therefore, the solution for h is

$$h(x) = h_{\text{in}} + C_2 e^{3mx/4\mu}.$$

As enthalpy is a fluid property, it should be bounded for $x \to \infty$, leading to $C_2 = 0$. Thus, we have that $h = h_{\text{in}}$.

Now consider the momentum equation (8b). Integrating this equation gives

$$\rho u^2 + p = \tfrac{4}{3}\mu u_x + C_3, \tag{20}$$

where C_3 is a constant. We can now substitute $m = \rho u$ and $p = \rho RT = RTm/u$. Furthermore, we can rewrite

$$RT = \frac{R}{c_p} c_p T = \frac{c_p - c_v}{c_p}(h - \tfrac{1}{2}u^2) = \frac{\gamma - 1}{\gamma}(h - \tfrac{1}{2}u^2).$$

Substituting m and p into the integrated momentum equation (20) and multiplying with u/m gives

$$\frac{4\mu}{3m} u_x u = \frac{\gamma + 1}{2\gamma} u^2 + \frac{\gamma - 1}{\gamma} h_{\text{in}} - \frac{u}{m} C_3, \tag{21}$$

where we used that $h(x) = h_{\text{in}}$. Note that we again assume that $m \neq 0$, otherwise there would be no fluid flow.
The boundary conditions that we impose for the velocity at the inflow $x = -\infty$ are $u = u_{\text{in}}$, $u_x = 0$. Substituting this in (21) gives

$$C_3 = \left(\frac{\gamma + 1}{2\gamma} u_{\text{in}}^2 + \frac{\gamma - 1}{\gamma} h_{\text{in}} \right) \frac{m}{u_{\text{in}}}.$$

Subsequently substituting C_3 into (21) gives

$$\frac{4\mu}{3m}uu_x = -\frac{u}{u_{\text{in}}}\left(\frac{\gamma+1}{2\gamma}u_{\text{in}}^2 + \frac{\gamma-1}{\gamma}h_{\text{in}}\right) + \frac{\gamma+1}{2\gamma}u^2 + \frac{\gamma-1}{\gamma}h_{\text{in}}.$$

Now we introduce the scaled velocity $v = u/u_{\text{in}}$. Rewriting the equation above finally gives

$$vv_x = \theta(v-1)(v-\beta), \tag{22}$$

where $\theta = \frac{3m(\gamma+1)}{8\mu\gamma}$, $\beta = \frac{\gamma-1}{\gamma+1} + \frac{2}{(\gamma+1)M_{\text{in}}^2}$ and $M_{\text{in}} = \frac{u_{\text{in}}}{c_{\text{in}}}$ is the Mach number at the inflow. Furthermore, $c = \sqrt{\frac{\gamma p}{\rho}}$ is the speed of sound. The Mach number classifies the type of flow. If $M < 1$, we have a subsonic flow; if $M = 1$, we have a sonic flow and if $M > 1$, we have a supersonic flow.

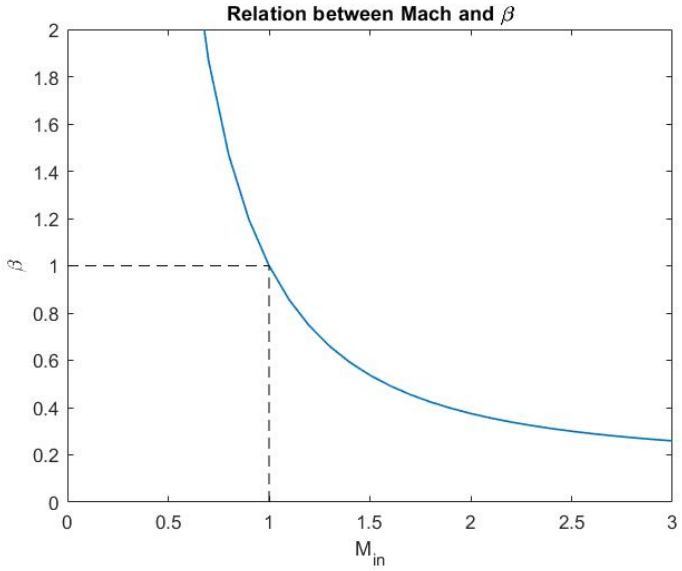

Figure 2: Relation β and Mach for $\gamma = \frac{7}{5}$

In Figure 2, we can see the relation between the Mach number and β. If β is larger than one, the Mach number is smaller than one and vice versa. Thus, $\beta < 1$ gives a supersonic flow while $\beta > 1$ gives a sonic flow. Finally, $\beta = 1$ describes a sonic flow.
In order to solve (22), we impose an initial condition to obtain the following initial value problem

$$vv_x = \theta(v-\beta)(v-1),\ x > x_0, \tag{23a}$$
$$v(x_0) = v_0, \tag{23b}$$

where $v_0 \in [0.5, 1.5]$. We will later see how important the choice of x_0 and v_0 is.

4.2 Solution methods

The exact solution of (23) can be found by changing the variable that is differentiated. That is, we rewrite the differential equation for v to obtain a differential equation for x. First we rewrite

$\mathrm{d}v/\mathrm{d}x$ to obtain a term $\mathrm{d}x/\mathrm{d}v$ as follows

$$\frac{\mathrm{d}v}{\mathrm{d}x} = \frac{\theta}{v}(v-\beta)(v-1),$$
$$\frac{\mathrm{d}x}{\mathrm{d}v} = \frac{v}{\theta(v-\beta)(v-1)}.$$

Using partial fraction decomposition, we obtain

$$\frac{\mathrm{d}x}{\mathrm{d}v} = \frac{1}{\theta(1-\beta)}\left(\frac{-\beta}{v-\beta} + \frac{1}{v-1}\right).$$

Now we integrate over the interval $[v_0, v]$ to obtain the following equation for x as a function of v

$$x(v) = \frac{1}{\theta(1-\beta)}\Big(-\beta\log|v-\beta| + \log|v-1| + \beta\log|v_0-\beta| - \log|v_0-1|\Big) + x_0. \tag{24}$$

From (24), we see that x can not be computed for a sonic flow, i.e., for $\beta = 1$. Thus for a sonic flow, we have to compute the expression for x separately. We start with

$$\frac{\mathrm{d}v}{\mathrm{d}x} = \frac{\theta}{v}(v-1)^2.$$

Then using a similar method as for the subsonic and supersonic flows, we obtain

$$\begin{aligned}\frac{\mathrm{d}x}{\mathrm{d}v} &= \frac{v}{\theta(v-1)^2},\\ &= \frac{1}{\theta}\left(\frac{1}{v-1} + \frac{1}{(v-1)^2}\right).\end{aligned}$$

Now integrating, we get

$$x = \frac{1}{\theta}\left(\log|v-1| - \log|v_0-1| - \frac{1}{v-1} + \frac{1}{v_0-1}\right). \tag{25}$$

From (24) we can already see that there is no solution for $v = \beta$ and $v = 1$. These are the equilibrium solutions also seen in the direction fields in Figure 3. Using (24) and (25), we can choose an interval for v and compute x as a function of v. Subsequently, we can plot these results in an (x, v) plot.
Alternatively, (23) can be solved numerically using an ode-solver in `Matlab`. We have used the `ode45` solver.

4.3 Results

From (23a) we see that there are two equilibrium solutions $v = 1$ and $v = \beta$. To analyze the stability of these solutions, we plot the direction field for supersonic, sonic and subsonic flows in Figure 3.

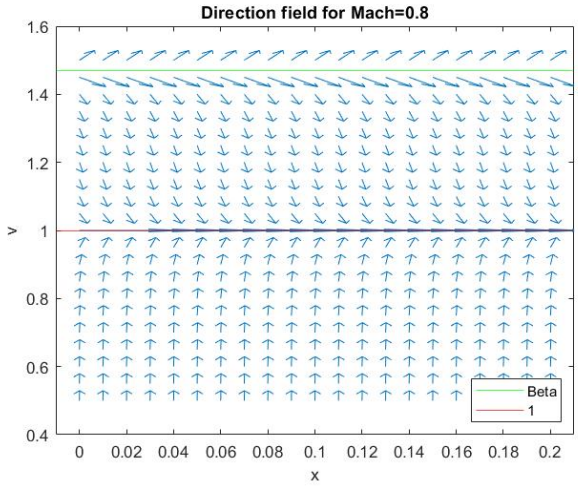

(a) $M_{\text{in}} = 0.8$, subsonic flow

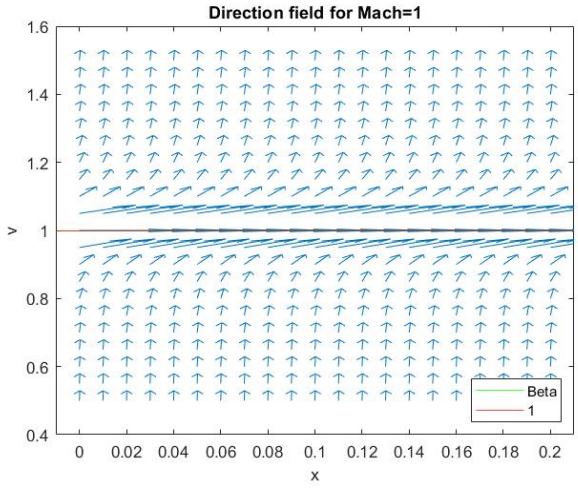

(b) $M_{\text{in}} = 1$, sonic flow

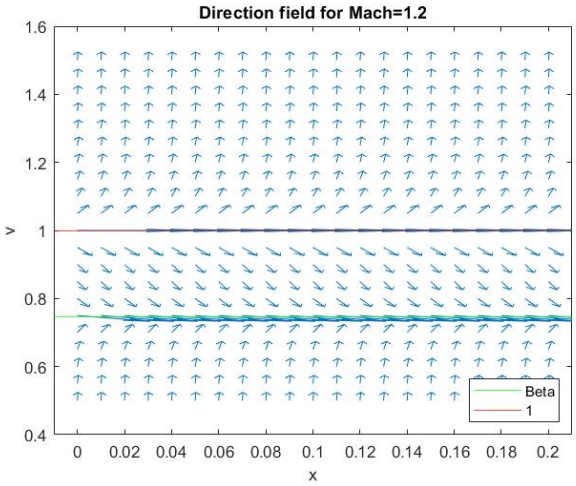

(c) $M_{\text{in}} = 1.2$, supersonic flow

Figure 3: Direction fields, $m = 1, \mu = 1.e-3, \gamma = 1.4, \theta = 642.86$

From Figure 3, we see that for a subsonic flow, $v = \beta$ is an unstable solution, while $v = 1$ is a stable solution. For the supersonic flow $v = \beta$ is a stable solution while $v = 1$ is an unstable solution. For the sonic flow $v = \beta = 1$ is a semi-stable solution.
The stability of equilibrium solutions can also be computed using (23a). Firstly, we write (23a) as $v_x = f(v)$. Secondly, we compute $f_v(v) = \theta(1 - \beta/v^2)$ for $v = 1, \beta$ for all Mach numbers. If this derivative is negative, the equilibrium solution is stable. If it is positive, the equilibrium solution is unstable. Lastly, if it is equal to zero, it is a semi-stable equilibrium solution. For $M_{\text{in}} = 0.8$, $f_v(1) < 0, f_v(\beta) > 0$. For $M_{\text{in}} = 1$, $f_v(1) = f_v(\beta) = 0$. Finally, for $M_{\text{in}} = 1.2$, $f_v(1) > 0, f_v(\beta) < 0$. These results coincide with the direction fields in Figure 3.

From (23) we can already see that the solution will presumably be invariant of x_0. However, the range of x will influence how much of the shock solution can be seen. We demonstrate this in

the following figure.

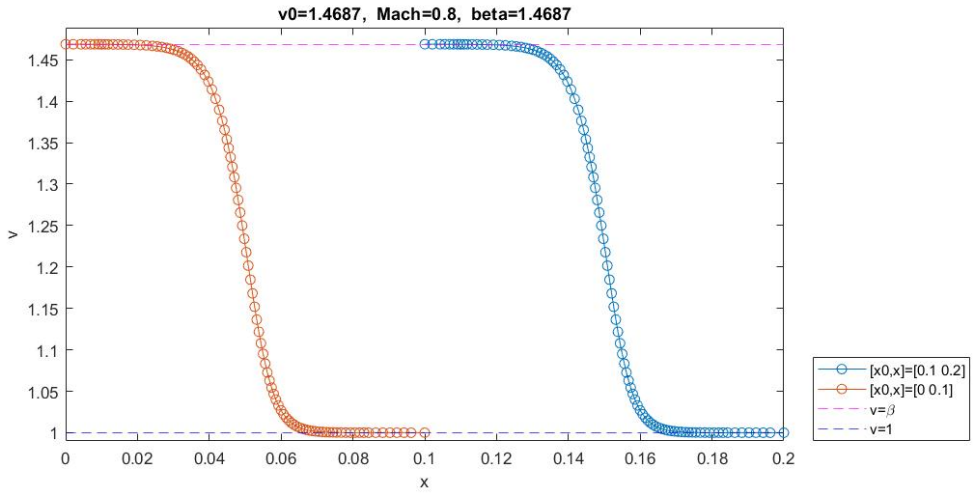

Figure 4: Numerical solution for different spatial intervals

In Figure 4 we see that for different spatial intervals of equal width, the solution remains the same. The width of the left plateau depends on the choice of v_0. If v_0 is chosen closer to β, the plateau will become even wider. The width of the right plateau depends on the width of the spatial interval. Although we have only shown this phenomena for a subsonic flow, it also holds for a (super)sonic flow.

Next we compute the analytical and numerical results for a subsonic flow.

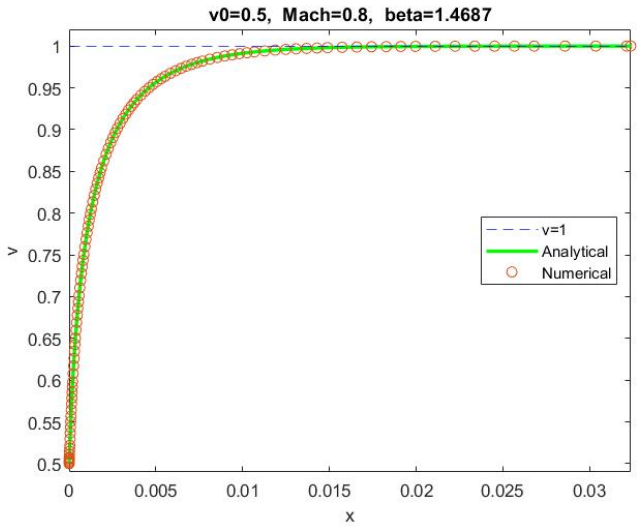

(a) Initial condition $v(0) = 0.5$

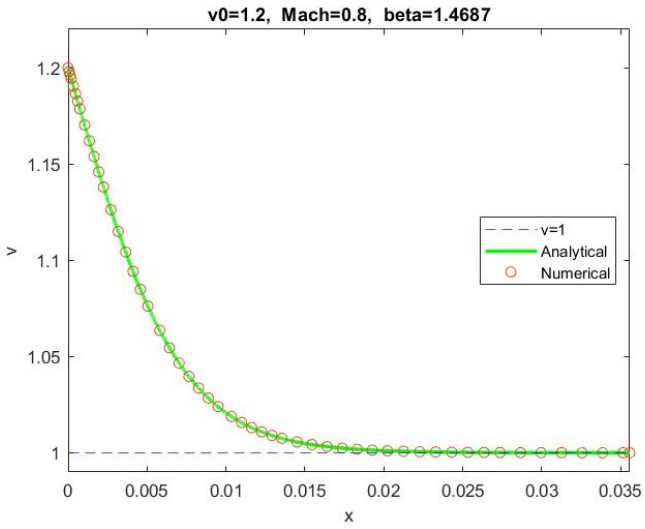

(b) Initial condition $v(0) = 1.2$

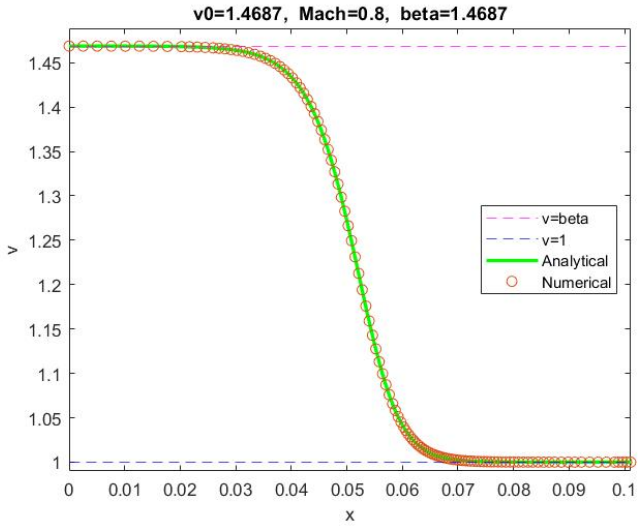

(c) Initial condition $v(0) = \beta - 0.00001$

Figure 5: Solution for subsonic flow

As seen in Figure 3, it is expected that all solutions with an initial solution smaller than β tend towards the equilibrium solution $v = 1$. This is exactly what can be seen in Figure 5. As can be seen in Figure 5c, even if the initial solution is very close to β, the solution still tends towards $v = 1$. As $v = u/u_{\text{in}}$, this means that the velocity always tends towards the inflow velocity. Furthermore, we note that for each initial solution v_0, the x-axis differs. This is a result of the analytical solution. For the analytical solution, the range of v is chosen in order to compute x. Therefore, x can vary for each initial solution. Lastly, we note that only for v_0 close to β, we can see a whole shock. Such a shock is a result which is expected for the Navier-Stokes equations. Next, we compute the solution for a sonic flow.

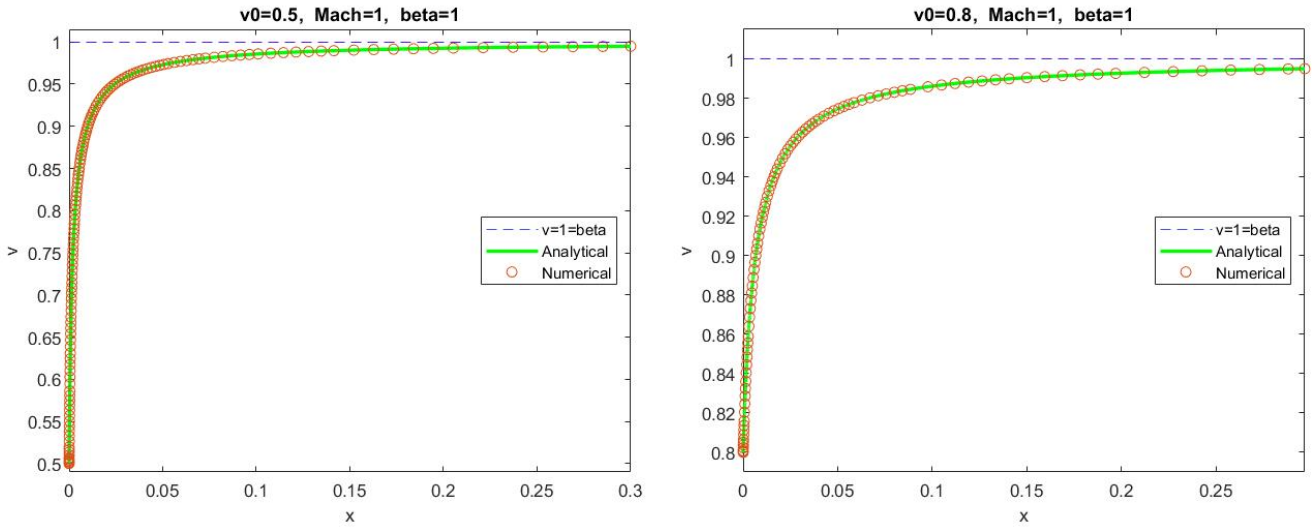

(a) Initial condition $v(0) = 0.5$

(b) Initial condition $v(0) = 0.8$

Figure 6: Solution for sonic flow

As can be seen in Figure 6, the solution again tends towards equilibrium solution $v = \beta = 1$. This behaviour only happens for initial solutions smaller than 1, as can be seen from the direction field plot. When using an initial solution bigger than 1, the solution diverges to infinity. For the sonic flow, we were not able to compute a whole shock as previously done. Lastly, we compute the solution for a supersonic flow.

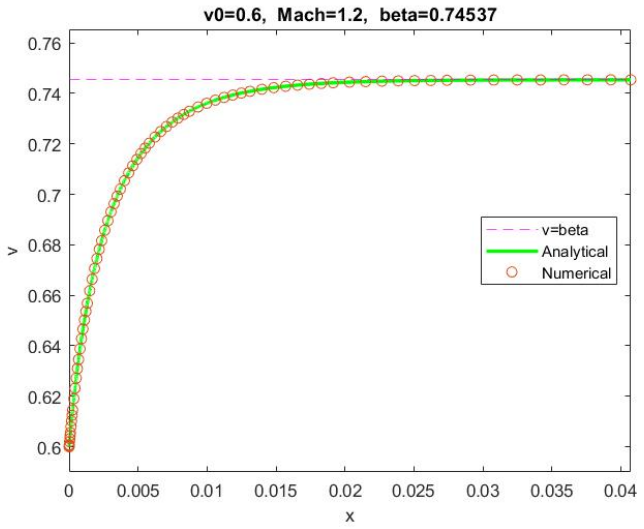

(a) Initial condition $v(0) = 0.6$

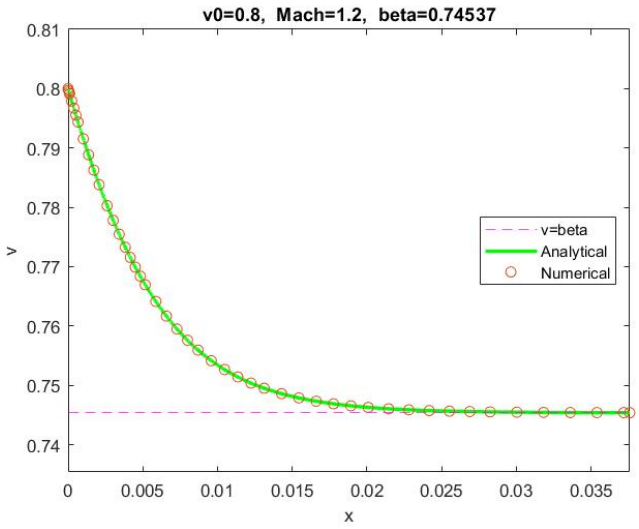

(b) Initial condition $v(0) = 0.8$

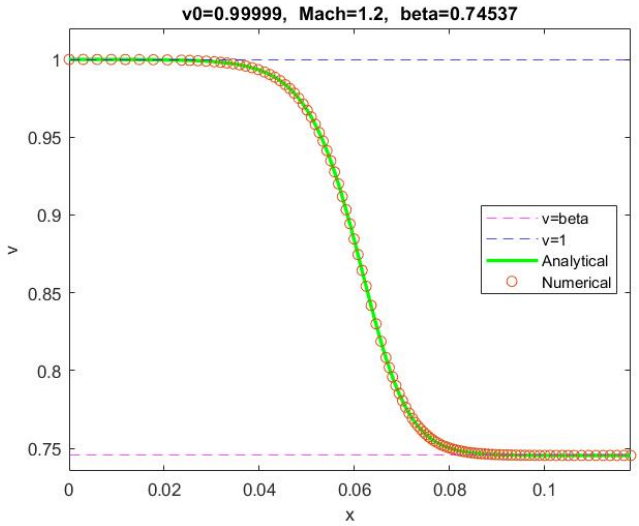

(c) Initial condition $v(0) = 1 - 0.00001$

Figure 7: Solution for supersonic flow

For all initial solutions smaller than 1, the solution tends towards the stable equilibrium solution $v = \beta$. As β is roughly $\frac{3}{4}$, the velocity tends towards $\frac{3}{4}$ of the inflow velocity, thus the velocity decreases. In Figure 7c, we can again see a full shock. This is a result which is expected and will presumably resemble a solution of the complete flux approach.

In conclusion, the analytical and numerical solution are both highly dependent on the initial solution v_0 and the range of v and x, respectively. However, when a suitable interval is chosen, the complete shock can be seen in the solution.

With the use of the analytical and numerical solutions, we can also compute other solution components such as the density and pressure. As we can only compute $v = u/u_{\text{in}}$, we have to make two assumptions in order to compute other variables. Firstly, we assume that u_{in}, the velocity at the inflow, is equal to 1.1. The value of u_{in} is based on the Dirichlet boundary conditions of a supersonic flow with Mach equal to 1.1, as we will see later on in this report. Secondly, we use h is constant for $\text{Pr} = \frac{3}{4}$. We can then obtain the following result

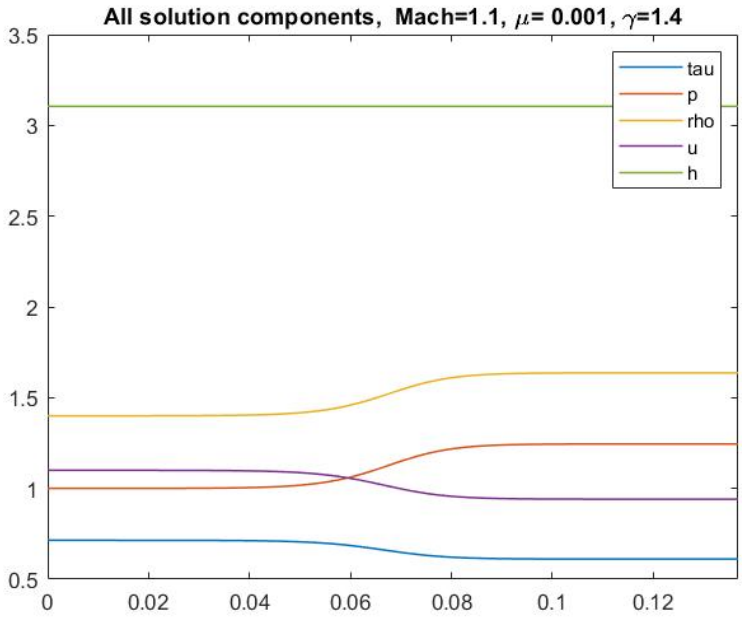

Figure 8: Solution based on the exact solution for $\text{Pr} = \frac{3}{4}$

In Figure 8, we can see a very promising solution. In this solution, we can see a flow moving across a shock wave. Across this shock wave, the variables change. For example, the velocity decreases and as a result, the density increases as it is a compressible flow. The physical interpretation will be discussed more extensive later on.

Now that the analytical solution is computed and we have seen the first results, we can continue the discretization.

5 Numerical implementation

We will now solve the discretized system (18). In order to solve the system, a few choices have to be made. Firstly, we have to choose what kind of boundary conditions to apply. Secondly, a choice in variables has to be made. System (18) consists of three equations and three variables which will be reduced to two equations for two variables. This will presumably simplify computations. These options will be explored and the results will be discussed.

5.1 Boundary conditions for system in τ, p

Suppose we have the spatial domain $[x_1, x_N]$. We need boundary conditions at x_1 and at x_N. We assume that the fluid flow is in positive x-direction. Thus the boundary at x_1 is the inflow boundary while x_N is the outflow boundary. Suppose we use the variables τ and p, which are obtained by substituting (18c) into (18b).

5.1.1 Dirichlet and Neumann boundary conditions

A possibility is to impose Dirichlet conditions at the inflow boundary and Neumann conditions at the outflow boundary. These boundary conditions can be written as

$$\begin{aligned} \tau(x_1) &= \tau_1 = \tau_L, \qquad & \tau'(x_N) &= \tau'_N = 0, \\ p(x_1) &= p_1 = p_L, \qquad & p'(x_N) &= p'_N = 0. \end{aligned}$$

In order to solve the nonlinear system (18) with the chosen boundary conditions, we need a suitable solution method. In this report, we propose the the Newton-Raphson method defined as

$$\underline{y}_{k+1} = \underline{y}_k - (\mathbf{F}'(\underline{y}_k))^{-1} \underline{F}(\underline{y}_k),$$

where k denotes the iteration and system (18) can be written as $\underline{F}(\underline{y}) = 0$ for solution vector $\underline{y}$ that consists of the variables τ and p. We will now formulate the Newton-Raphson method for system (18).

We want to solve $\underline{F}(\underline{y}) = \underline{0}$ where $\underline{F}$ consists of two parts, i.e., $\underline{F} = (\underline{F}_1 \, , \, \underline{F}_2)^\mathsf{T}$ that coincide with equations (18a) and (18b). The solution vector $\underline{y}$ is defined as

$$\underline{y} = (\tau_2, p_2, \ldots \tau_N, p_N)^\mathsf{T}.$$

Note that the solution vector could also be chosen differently. This choice influences the Jacobian.

Implementation of the Dirichlet condition is straightforward. For the Neumann condition, we use central differences at $x = x_N$ to obtain the relations $\tau_{N-1} = \tau_{N+1}$ and $p_{N-1} = p_{N+1}$. For

the momentum equation (18a), we can write $\underline{F}_1$ as follows

$$\underline{F}_1 = m\varepsilon \begin{pmatrix} B^- + B^+ & -B^+ & & & \\ -B^- & B^- + B^+ & -B^+ & & \\ & \ddots & \ddots & \ddots & \\ & & -B^- & B^- + B^+ & -B^+ \\ & & & -B^- - B^+ & B^- + B^+ \end{pmatrix} \begin{pmatrix} \tau_2 \\ \vdots \\ \vdots \\ \tau_N \end{pmatrix} +$$
$$\begin{pmatrix} W^- - W^+ & W^+ & & & \\ -W^- & W^- - W^+ & W^+ & & \\ & \ddots & \ddots & \ddots & \\ & & -W^- & W^- - W^+ & W^+ \\ & & & -W^- + W^+ & W^- - W^+ \end{pmatrix} \begin{pmatrix} p_2 \\ \vdots \\ \vdots \\ p_N \end{pmatrix} + \begin{pmatrix} -m\varepsilon B^- \tau_L - W^- p_L \\ 0 \\ \vdots \\ 0 \\ 0 \end{pmatrix} = \underline{0},$$

where again $B^- = B(-\mathrm{Pe})$, $B^+ = B(\mathrm{Pe})$ and similarly for W.
The energy equation (18b) can be written as $\underline{F}_2$ as follows

$$\underline{F}_2 = \varepsilon \begin{pmatrix} B^- + B^+ & -B^+ & & & \\ -B^- & B^- + B^+ & -B^+ & & \\ & \ddots & \ddots & \ddots & \\ & & -B^- & B^- + B^+ & -B^+ \\ & & & -B^- - B^+ & B^- + B^+ \end{pmatrix} \begin{pmatrix} \tilde{\gamma} p_2 \tau_2 + \frac{1}{2} m^2 \tau_2^2 \\ \vdots \\ \vdots \\ \tilde{\gamma} p_N \tau_N + \frac{1}{2} m^2 \tau_N^2 \end{pmatrix} +$$
$$\begin{pmatrix} -\varepsilon B^- (\tilde{\gamma} \tau_L p_L + \frac{1}{2} m^2 \tau_L^2) \\ 0 \\ \vdots \\ 0 \\ 0 \end{pmatrix} = \underline{0},$$

where $\tilde{\gamma} = \frac{\gamma}{\gamma - 1}$.
Thus we have a system $F(\underline{y}) = \underline{0}$ that consists of $2N - 2$ equations for $2N - 2$ unknowns. The system in matrix notation is briefly written as

$$\underline{F}_1 = m\varepsilon \mathbf{B} \underline{\tau} + \mathbf{W} \underline{p} + \underline{f}_1,$$
$$\underline{F}_2 = \varepsilon \mathbf{B} \underline{h} + \underline{f}_2,$$

where $\mathbf{B}, \mathbf{W}$ are square matrices of size $N - 1$ and $\underline{f}_1, \underline{f}_2$ are vectors including the boundary conditions.

In order to implement the Newton-Raphson method, we compute the Jacobian of $\underline{F}_1$ and $\underline{F}_2$ to form $\mathbf{F}' = (\mathbf{F}'_1 \;\; \mathbf{F}'_2)^\mathsf{T}$. Differentiating $\underline{F}_1$ and $\underline{F}_2$ w.r.t. all elements of $\underline{y}$ gives

$$\mathbf{F}'_1 = \begin{pmatrix} m\varepsilon(B^- + B^+) & W^- - W^+ & m\varepsilon(-B^+) & W^+ & & & & \\ m\varepsilon(-B^-) & -W^- & m\varepsilon(B^- + B^+) & W^- - W^+ & m\varepsilon(-B^+) & W^+ & & \\ & \ddots & \ddots & \ddots & \ddots & \ddots & \ddots & \\ & & m\varepsilon(-B^-) & -W^- & m\varepsilon(B^- + B^+) & W^- - W^+ & m\varepsilon(B^+) & W^+ \\ & & & & m\varepsilon(-B^- - B^+) & -W^- + W^+ & m\varepsilon(B^- + B^+) & W^- - W^+ \end{pmatrix},$$

$$\mathbf{F}_2' = \varepsilon \begin{pmatrix} (B^- + B^+) & (B^- + B^+) & (-B^+) & (-B^+) & & & & \\ (-B^-) & (-B^-) & (B^- + B^+) & (B^- + B^+) & (-B^+) & (-B^+) & & \\ & \ddots & \ddots & \ddots & \ddots & \ddots & \ddots & \\ & & (-B^-) & (-B^-) & (B^- + B^+) & (B^- + B^+) & (-B^+) & (-B^+) \\ & & & & (-B^- - B^+) & (-B^- - B^+) & (B^- + B^+) & (B^- + B^+) \end{pmatrix}$$

$$\begin{pmatrix} \tilde{\gamma}p_2 + m^2\tau_2 & & & & & & & \\ & \tilde{\gamma}\tau_2 & & & & & & \\ & & \tilde{\gamma}p_3 + m^2\tau_3 & & & & & \\ & & & \tilde{\gamma}\tau_3 & & & & \\ & & & & \ddots & & & \\ & & & & & \ddots & & \\ & & & & & & \tilde{\gamma}p_N + m^2\tau_N & \\ & & & & & & & \tilde{\gamma}\tau_N \end{pmatrix}.$$

5.1.2 Dirichlet boundary conditions

Alternatively, one can choose to use Dirichlet boundary conditions at both boundaries:

$$\begin{aligned} \tau(x_1) &= \tau_1 = \tau_L, & \tau(x_N) &= \tau_N = \tau_R, \\ p(x_1) &= p_1 = p_L, & p(x_N) &= p_N = p_R. \end{aligned}$$

Using the solution vector

$$\underline{y} = (\tau_2, p_2, \ldots \tau_{N-1}, p_{N-1})^{\mathsf{T}},$$

the system to be solved can again be written as $\underline{F} = (\underline{F}_1 \quad \underline{F}_2)^\mathsf{T}$ where

$$\underline{F}_1 = m\varepsilon \begin{pmatrix} B^- + B^+ & -B^+ & & & \\ -B^- & B^- + B^+ & -B^+ & & \\ & \ddots & \ddots & \ddots & \\ & & -B^- & B^- + B^+ & -B^+ \\ & & & -B^- & B^- + B^+ \end{pmatrix} \begin{pmatrix} \tau_2 \\ \vdots \\ \vdots \\ \tau_{N-1} \end{pmatrix} +$$

$$\begin{pmatrix} W^- - W^+ & W^+ & & & \\ -W^- & W^- - W^+ & W^+ & & \\ & \ddots & \ddots & \ddots & \\ & & -W^- & W^- - W^+ & W^+ \\ & & & -W^- & W^- - W^+ \end{pmatrix} \begin{pmatrix} p_2 \\ \vdots \\ \vdots \\ p_{N-1} \end{pmatrix} + \begin{pmatrix} -m\varepsilon B^- \tau_L - W^- p_L \\ 0 \\ \vdots \\ 0 \\ -m\varepsilon B^+ \tau_R + W^+ p_R \end{pmatrix} = \underline{0}.$$

$$\underline{F}_2 = \varepsilon \begin{pmatrix} B^- + B^+ & -B^+ & & & \\ -B^- & B^- + B^+ & -B^+ & & \\ & \ddots & \ddots & \ddots & \\ & & -B^- & B^- + B^+ & -B^+ \\ & & & -B^- & B^- + B^+ \end{pmatrix} \begin{pmatrix} \tilde{\gamma} p_2 \tau_2 + \frac{1}{2} m^2 \tau_2^2 \\ \vdots \\ \vdots \\ \tilde{\gamma} p_{N-1} \tau_{N-1} + \frac{1}{2} m^2 \tau_{N-1}^2 \end{pmatrix} +$$

$$\begin{pmatrix} -\varepsilon B^- (\tilde{\gamma} \tau_L p_L + \frac{1}{2} m^2 \tau_L^2) \\ 0 \\ \vdots \\ 0 \\ -\varepsilon B^+ (\tilde{\gamma} \tau_R p_R + \frac{1}{2} m^2 \tau_R^2) \end{pmatrix} = \underline{0},$$

where $\tilde{\gamma} = \frac{\gamma}{\gamma - 1}$.
Note that we now have $2N - 4$ equations for $2N - 4$ variables. The Jacobian now becomes

$$\mathbf{F}'_\mathbf{1} = \begin{pmatrix} m\varepsilon(B^- + B^+) & W^- - W^+ & m\varepsilon(-B^+) & W^+ & & & & \\ m\varepsilon(-B^-) & -W^- & m\varepsilon(B^- + B^+) & W^- - W^+ & m\varepsilon(-B^+) & W^+ & & \\ & \ddots & \ddots & \ddots & \ddots & \ddots & \ddots & \\ & & m\varepsilon(-B^-) & -W^- & m\varepsilon(B^- + B^+) & W^- - W^+ & m\varepsilon(B^+) & W^+ \\ & & & & m\varepsilon(-B^-) & -W^- & m\varepsilon(B^- + B^+) & W^- - W^+ \end{pmatrix},$$

$$\mathbf{F}'_\mathbf{2} = \varepsilon \begin{pmatrix} (B^- + B^+) & (B^- + B^+) & (-B^+) & (-B^+) & & & & \\ (-B^-) & (-B^-) & (B^- + B^+) & (B^- + B^+) & (-B^+) & (-B^+) & & \\ & \ddots & \ddots & \ddots & \ddots & \ddots & \ddots & \\ & & (-B^-) & (-B^-) & (B^- + B^+) & (B^- + B^+) & (-B^+) & (-B^+) \\ & & & & (-B^-) & (-B^-) & (B^- + B^+) & (B^- + B^+) \end{pmatrix}$$

$$\begin{pmatrix} \tilde{\gamma} p_2 + m^2 \tau_2 & & & & & & & \\ & \tilde{\gamma} \tau_2 & & & & & & \\ & & \tilde{\gamma} p_3 + m^2 \tau_3 & & & & & \\ & & & \tilde{\gamma} \tau_3 & & & & \\ & & & & \ddots & & & \\ & & & & & \ddots & & \\ & & & & & & \tilde{\gamma} p_{N-1} + m^2 \tau_{N-1} & \\ & & & & & & & \tilde{\gamma} \tau_{N-1} \end{pmatrix}.$$

5.1.2.1 Conditions for Dirichlet boundaries

When using Dirichlet boundary conditions at both boundaries, a solution is not always guaranteed. To determine criteria that guarantee solvability, we look at the momentum and energy differential equations and integrate them over the interval $[x_1, x_N]$. Furthermore, we assume a uniform flow at both boundaries, i.e., $\tau_x = p_x = h_x = 0$ at the boundaries. We then obtain:

$$m^2\tau_L + p_L = m^2\tau_R + p_R \tag{26a}$$

$$mh_L = mh_R, \tag{26b}$$

where $h = \frac{1}{2}m^2\tau^2 + \frac{\gamma}{\gamma-1}p\tau$.
Equations (26a) and (26b) can be seen as a version of the Rankine-Hugoniot conditions. These conditions explain the relation between two states on either side of a shock wave in one-dimensional fluid flows [6].
From (26a) we obtain

$$p_R = p_L + m^2(\tau_L - \tau_R). \tag{27}$$

Subsequently substituting h and p_R into (26b) and rewriting gives

$$\tfrac{1}{2}m^3(\tau_L - \tau_R)(\tau_L + \tau_R) = \frac{\gamma}{\gamma - 1}m\left(-p_L(\tau_L - \tau_R) + m^2\tau_R(\tau_L - \tau_R)\right).$$

As we do not seek the trivial solution $\tau_L = \tau_R$, $p_L = p_R$, etc., we eliminate these trivial solutions and rewrite to obtain:

$$\tau_R = \frac{2\gamma}{m^2(\gamma+1)}p_L + \frac{\gamma-1}{\gamma+1}\tau_L. \tag{28}$$

Thus, we now have equations for τ_R and p_R dependent on τ_L and p_L. We can choose the values at the inflow and subsequently compute the values at the outflow.

However, there is one more condition which has to be satisfied. Namely, the second law of thermodynamics, also known as the entropy condition, has to be satisfied. This law states that it must hold that the entropy does not decrease [7]. Entropy is a measure of the amount of energy unavailable to do work. In a closed system where energy is conserved, the amount of available energy cannot increase. Therefore, entropy cannot decrease. We denote entropy by s. It can be shown that across a shock, it should hold that $s_{j+1} \geq s_j$ for $j = 1, \ldots N-1$. This can be shown using the balance equation for entropy, a detailed derivation can be found in [7]. The entropy for an ideal gas can be approximated as $s = p\tau^\gamma$ [8]. It should then hold that

$$p_R\tau_R^\gamma \geq p_L\tau_L^\gamma. \tag{29}$$

Furthermore, the entropy condition should hold on all volumes, i.e., it should hold that

$$p_{j+1}\tau_{j+1}^\gamma \geq p_j\tau_j^\gamma \text{ for } j = 1, N-1.$$

In order to establish when the entropy condition holds, we first define the shock relations. These can be found by dividing (28) by τ_L and (27) by p_L, respectively. Furthermore, we use that

$M^2 = \frac{u^2}{c^2} = \frac{m^2\tau}{\gamma p}$ to obtain:

$$\begin{aligned}
\frac{\tau_R}{\tau_L} &= \frac{2\gamma p_L}{m^2(\gamma+1)\tau_L} + \frac{\gamma-1}{\gamma+1}, \\
\frac{p_R}{p_L} &= 1 + \frac{m^2(\tau_L - \tau_R)}{p_L}, \\
M_R^2 &= \frac{m^2\tau_R}{\gamma p_R}.
\end{aligned}$$

After rewriting these equations, we obtain the shock relations:

$$\frac{\tau_R}{\tau_L} = \frac{2 + (\gamma-1)M_L^2}{(\gamma+1)M_L^2}, \tag{30a}$$

$$\frac{p_R}{p_L} = \frac{2\gamma M_L^2 - (\gamma-1)}{\gamma+1}, \tag{30b}$$

$$M_R^2 = \frac{2 + (\gamma-1)M_L^2}{2\gamma M_L^2 - (\gamma-1)}. \tag{30c}$$

The shock relations are well known and can be found in literature, e.g., in [9]. Substituting (30a) and (30b) into (29), one can derive that the entropy condition only holds for $M_L \geq 1$, that is, a sonic or supersonic fluid flow. It then also holds that $\tau_R \leq \tau_L$, $p_R \geq p_L$ and $M_R \leq M_L$. Thus, rarefaction shocks, which are multiple waves over which the density decreases, are not possible [10]. For a perfect gas, one can expect a supersonic inflow with a compression shock. This means that there will be a dividing wave between the stationary and moving fluid, also known as a shock wave. A shock wave occurs when force is applied to the fluid. Due to this force, the fluid starts to move and becomes compressed [10].
In conclusion, when using Dirichlet boundary conditions at both boundaries, we can prescribe the inflow conditions and compute the outflow conditions using (28) and (27). These boundary conditions satisfy the entropy condition and are only possible for supersonic inflows.

5.2 Boundary conditions for system in τ, h

Until now, we have only considered τ and p as variables. However, we could also choose τ, h or p, h, although p, h does not seem like a suitable choice as $\underline{F}_1$ is linear in τ. Therefore, we now consider τ, h as variables. Using (18c), we can write p in terms of h to obtain

$$p_j = \frac{h_j - \frac{1}{2}m^2\tau_j^2}{\tilde{\gamma}\tau_j}.$$

5.2.1 Dirichlet and Neumann boundary conditions

Using Neumann-Dirichlet boundary conditions similar to those described in section 5.1.1, we now get

$$\begin{aligned}
\tau(x_1) = \tau_1 = \tau_L, \qquad & \tau'(x_N) = \tau'_N = 0, \\
h(x_1) = h_1 = h_L, \qquad & h'(x_N) = h'_N = 0,
\end{aligned}$$

with solution vector

$$\underline{y} = (\tau_2, h_2, \ldots \tau_N, h_N)^\mathsf{T}.$$

Furthermore, system (18) can now again be written as $\underline{F} = (\underline{F}_1\,,\,\underline{F}_2)^\mathsf{T}$ where

$$\underline{F}_1 = m\varepsilon \begin{pmatrix} B^- + B^+ & -B^+ & & & \\ -B^- & B^- + B^+ & -B^+ & & \\ & \ddots & \ddots & \ddots & \\ & & -B^- & B^- + B^+ & -B^+ \\ & & & -B^- - B^+ & B^- + B^+ \end{pmatrix} \begin{pmatrix} \tau_2 \\ \vdots \\ \vdots \\ \tau_N \end{pmatrix} +$$

$$\begin{pmatrix} W^- - W^+ & W^+ & & & \\ -W^- & W^- - W^+ & W^+ & & \\ & \ddots & \ddots & \ddots & \\ & & -W^- & W^- - W^+ & W^+ \\ & & & -W^- + W^+ & W^- - W^+ \end{pmatrix} \begin{pmatrix} \frac{h_2 - \frac{1}{2}m^2\tau_2^2}{\tilde{\gamma}\tau_2} \\ \vdots \\ \vdots \\ \frac{h_N - \frac{1}{2}m^2\tau_N^2}{2\tilde{\gamma}\tau_N} \end{pmatrix} + \begin{pmatrix} -m\varepsilon B^-\tau_L - W^-(\frac{2h_L - m^2\tau_L^2}{2\tilde{\gamma}\tau_L}) \\ 0 \\ \vdots \\ 0 \end{pmatrix} = \underline{0}.$$

$$\underline{F}_2 = \varepsilon \begin{pmatrix} B^- + B^+ & -B^+ & & & \\ -B^- & B^- + B^+ & -B^+ & & \\ & \ddots & \ddots & \ddots & \\ & & -B^- & B^- + B^+ & -B^+ \\ & & & -B^- - B^+ & B^- + B^+ \end{pmatrix} \begin{pmatrix} h_1 \\ \vdots \\ \vdots \\ h_N \end{pmatrix} + \begin{pmatrix} -\varepsilon B^- h_L \\ 0 \\ \vdots \\ 0 \end{pmatrix} = \underline{0}.$$

Note that for the system in τ, h, $\underline{F}_2$ becomes linear. The Jacobian of F_1 is

$$\mathbf{F}_1' = \begin{pmatrix} m\varepsilon(B^- + B^+) & (W^- - W^+)p_{2,h} & m\varepsilon(-B^+) & W^+p_{3,h} & & & & \\ m\varepsilon(-B^-) & -W^-p_{2,h} & m\varepsilon(B^- + B^+) & (W^- - W^+)p_{3,h} & m\varepsilon(-B^+) & W^+p_{4,h} & & \\ & \ddots & \ddots & \ddots & \ddots & \ddots & \ddots & \\ & & m\varepsilon(-B^-) & -W^-p_{N-2,h} & m\varepsilon(B^- + B^+) & (W^- - W^+)p_{N-1,h} & m\varepsilon(B^+) & W^+p_{N,h} \\ & & & & m\varepsilon(-B^- - B^+) & (-W^- + W^+)p_{N-1,h} & m\varepsilon(B^- + B^+) & (W^- - W^+)p_{N,h} \end{pmatrix} \cdot$$

$$\begin{pmatrix} (W^- - W^+)p_{2,\tau} & 0 & W^+p_{3,\tau} & 0 & & & & \\ -W^-p_{2,\tau} & 0 & (W^- - W^+)p_{3,\tau} & 0 & W^+p_{4,\tau} & 0 & & \\ & \ddots & \ddots & \ddots & \ddots & \ddots & \ddots & \\ & & 0 & -W^-p_{N-2,\tau} & 0 & (W^- - W^+)p_{N-1,\tau} & 0 & W^+p_{N,\tau} \\ & & & & 0 & (-W^- + W^+)p_{N-1,\tau} & 0 & (W^- - W^+)p_{N,\tau} \end{pmatrix},$$

where $p_{j,\tau} = \frac{1}{\tilde{\gamma}}(-\frac{1}{2}m^2 - \frac{h_j}{\tau_j^2})$ and $p_{j,h} = \frac{1}{\tilde{\gamma}\tau_j}$ are the partial derivatives of p w.r.t τ and h. The Jacobian of F_2 becomes significantly easier:

$$\mathbf{F}_2' = \begin{pmatrix} 0 & \varepsilon(B^- + B^+) & 0 & \varepsilon(-B^+) & & & & \\ 0 & \varepsilon(-B^-) & 0 & \varepsilon(B^- + B^+) & 0 & \varepsilon(-B^+) & & \\ & \ddots & \ddots & \ddots & \ddots & \ddots & \ddots & \\ & & 0 & \varepsilon(-B^-) & 0 & \varepsilon(B^- + B^+) & 0 & \varepsilon(-B^+) \\ & & & & 0 & \varepsilon(-B^- - B^+) & 0 & \varepsilon(B^- + B^+) \end{pmatrix}.$$

5.2.2 Dirichlet boundary conditions

Consider using Dirichlet boundary conditions at both boundaries:

$$\begin{aligned} \tau(x_1) &= \tau_1 = \tau_L, \qquad & \tau(x_N) &= \tau_N = \tau_R, \\ h(x_1) &= h_1 = h_L, \qquad & h(x_N) &= h_N = h_R. \end{aligned}$$

Similar as in Section 5.1.2, these boundary conditions must satisfy certain criteria in order to guarantee a solution and the entropy condition. Using the same method used as in Section 5.1.2, but now eliminating p, we obtain the following relations

$$\tau_R = \frac{2(\gamma-1)h_L}{(1+\gamma)m^2\tau_L},$$
$$h_R = h_L.$$

For solution vector

$$\underline{y} = (\tau_2, h_2, \dots \tau_{N-1}, h_{N-1})^{\mathsf{T}},$$

system (18) can now again be written as $\underline{F} = (\underline{F}_1\,,\,\underline{F}_2)^{\mathsf{T}}$ where

$$\underline{F}_1 = m\varepsilon \begin{pmatrix} B^- + B^+ & -B^+ & & & \\ -B^- & B^- + B^+ & -B^+ & & \\ & \ddots & \ddots & \ddots & \\ & & -B^- & B^- + B^+ & -B^+ \\ & & & -B^- & B^- + B^+ \end{pmatrix} \begin{pmatrix} \tau_2 \\ \vdots \\ \vdots \\ \tau_{N-1} \end{pmatrix} +$$
$$\begin{pmatrix} W^- - W^+ & W^+ & & & \\ -W^- & W^- - W^+ & W^+ & & \\ & \ddots & \ddots & \ddots & \\ & & -W^- & W^- - W^+ & W^+ \\ & & & -W^- & W^- - W^+ \end{pmatrix} \begin{pmatrix} \frac{2h_2 - m^2\tau_2^2}{2\tilde{\gamma}\tau_2} \\ \vdots \\ \vdots \\ \frac{2h_{N-1} - m^2\tau_{N-1}^2}{2\tilde{\gamma}\tau_{N-1}} \end{pmatrix} + \begin{pmatrix} -m\varepsilon B^-\tau_L - W^-(\frac{2h_L - m^2\tau_L^2}{2\tilde{\gamma}\tau_1}) \\ 0 \\ \vdots \\ 0 \\ -m\varepsilon B^+\tau_R + W^+(\frac{2h_R - 2m^2\tau_R^2}{2\tilde{\gamma}\tau_R}) \end{pmatrix} = \underline{0}.$$

$$\underline{F}_2 = \varepsilon \begin{pmatrix} B^- + B^+ & -B^+ & & & \\ -B^- & B^- + B^+ & -B^+ & & \\ & \ddots & \ddots & \ddots & \\ & & -B^- & B^- + B^+ & -B^+ \\ & & & -B^- & B^- + B^+ \end{pmatrix} \begin{pmatrix} h_2 \\ \vdots \\ \vdots \\ h_{N-1} \end{pmatrix} + \begin{pmatrix} -\varepsilon B^- h_L \\ 0 \\ \vdots \\ 0 \\ -\varepsilon B^+ h_R \end{pmatrix} = \underline{0},$$

The Jacobian becomes

$$\mathbf{F}_1' = \begin{pmatrix} m\varepsilon(B^- + B^+) & (W^- - W^+)p_{2,h} & m\varepsilon(-B^+) & W^+p_{3,h} & & & & \\ m\varepsilon(-B^-) & -W^-p_{2,h} & m\varepsilon(B^- + B^+) & (W^- - W^+)p_{3,h} & m\varepsilon(-B^+) & W^+p_{4,h} & & \\ & \ddots & \ddots & \ddots & \ddots & \ddots & \ddots & \\ & & m\varepsilon(-B^-) & -W^-p_{N-3,h} & m\varepsilon(B^- + B^+) & (W^- - W^+)p_{N-2,h} & m\varepsilon(B^+) & W^+p_{N-1,h} \\ & & & & m\varepsilon(-B^-) & -W^-p_{N-2,h} & m\varepsilon(B^- + B^+) & (W^- - W^+)p_{N-1,h} \end{pmatrix}$$
$$+ \begin{pmatrix} (W^- - W^+)p_{2,\tau} & 0 & W^+p_{3,\tau} & 0 & & & & \\ -W^-p_{2,\tau} & 0 & (W^- - W^+)p_{3,\tau} & 0 & W^+p_{4,\tau} & 0 & & \\ & \ddots & \ddots & \ddots & \ddots & \ddots & \ddots & \\ & & 0 & -W^-p_{N-3,\tau} & 0 & (W^- - W^+)p_{N-2,\tau} & 0 & W^+p_{N-1,\tau} \\ & & & & 0 & -W^-p_{N-2,\tau} & 0 & (W^- - W^+)p_{N-1,\tau} \end{pmatrix},$$

$$\mathbf{F}_2' = \begin{pmatrix} 0 & \varepsilon(B^- + B^+) & 0 & \varepsilon(-B^+) & & & & \\ 0 & \varepsilon(-B^-) & 0 & \varepsilon(B^- + B^+) & 0 & \varepsilon(-B^+) & & \\ & \ddots & \ddots & \ddots & \ddots & \ddots & \ddots & \\ & & 0 & \varepsilon(-B^-) & 0 & \varepsilon(B^- + B^+) & 0 & \varepsilon(-B^+) \\ & & & & 0 & \varepsilon - B^- & 0 & \varepsilon(B^- + B^+) \end{pmatrix}.$$

The result of all different implementation options will be shown in the next section.

6 Results

In this section we will look at the results of the complete flux approach. This will be done for the Neumann-Dirichlet boundary conditions as well as for the Dirichlet boundary conditions. We primarily use variables τ, p to compute the results and do not show results in τ, h as they often coincide. If the results do differ, we also show results in τ, h. The results of the system in τ, h that are not shown here, can be found in Appendix A and B. All results are computed for $\mathrm{Pr} = \frac{3}{4}$.

All solution are shown in the following variables with units:

1. ρ in $\mathrm{kg/m^3}$,
2. τ in $\mathrm{m^3/kg}$,
3. p in $\mathrm{N/m^2}$,
4. u in $\mathrm{m/s}$,
5. h in $\mathrm{J/kg}$.

6.1 Neumann-Dirichlet boundary conditions

First we consider the Neumann-Dirichlet boundary conditions. For this combination, a non-trivial solution is not always guaranteed. This is highly dependent on the initial solution. Therefore, we try several initial solutions. For all initial solutions, we use Mach = 1.1 and $\mu = 1\mathrm{e}{-5}\,\mathrm{kg/ms}$. Computations using a low Mach number are easier and therefore have a higher possibility of obtaining a nontrivial solution.

6.1.1 Distortions

Firstly, we use a trivial solution with a sinus distortion as a test case. This test case checks whether the solution converges to the trivial solution for an initial solution that is close enough to the trivial solution.

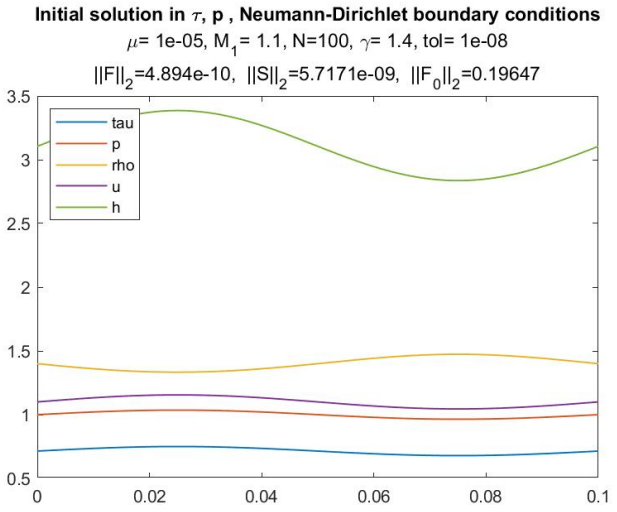

(a) Initial solution

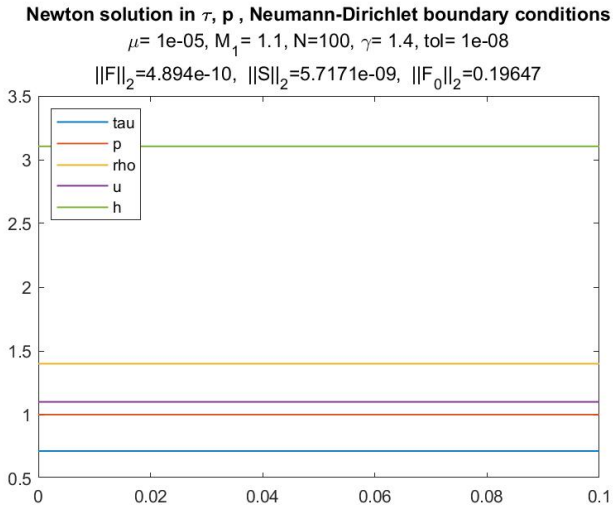

(b) Final solution

Figure 9: Initial solution with distortion, system in τ, p

As can be seen in Figure 9, the solution does indeed converge to a trivial solution. This verifies that the method is able to converge.

6.1.2 Linear

In order to find a nontrivial solution, the first initial solution that we propose is a linear initial solution between values at the left and right boundary. The boundary values that were chosen here are

$$\tau_L = \tfrac{1}{\gamma}, \qquad \tau_R = \tau_L - 0.2, \tag{31a}$$

$$p_L = 1, \qquad p_R = p_L + 0.1. \tag{31b}$$

Using these boundary values, a linear line is constructed between the left and right boundary. Subsequently, the values for h and u are computed. Note that the values at the right boundary are chosen arbitrarily and could also have been chosen differently.

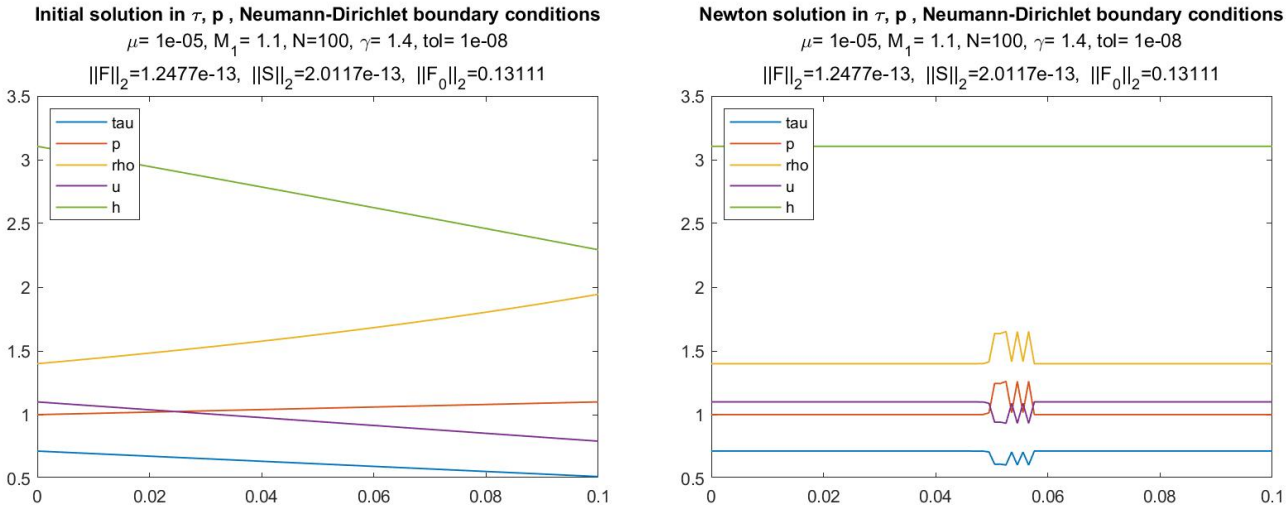

(a) Initial solution

(b) Final solution

Figure 10: Initial linear solution, system in τ, p

In Figure 10 we can see that using a linear initial solution results in a trivial solution where additionally oscillations occur. As oscillations are not expected in a nontrivial solution, we suspect that the linear initial solution is not a good choice for the system in τ, p when using these boundary values.

When we use the system in variables τ, h, we do obtain a nontrivial solution. This presumably is a result of the construction of the initial solution. In the system for τ, h, the graphs for τ and h are first computed and then the graph for p is computed. The graph for h is chosen to be constant as we have previously seen that h should be constant for $\mathrm{Pr} = \frac{3}{4}$.
For the system in τ, p, the graphs for τ and p are first chosen and then h is computed. Therefore, h is not necessarily constant as h is not an 'input' variable.

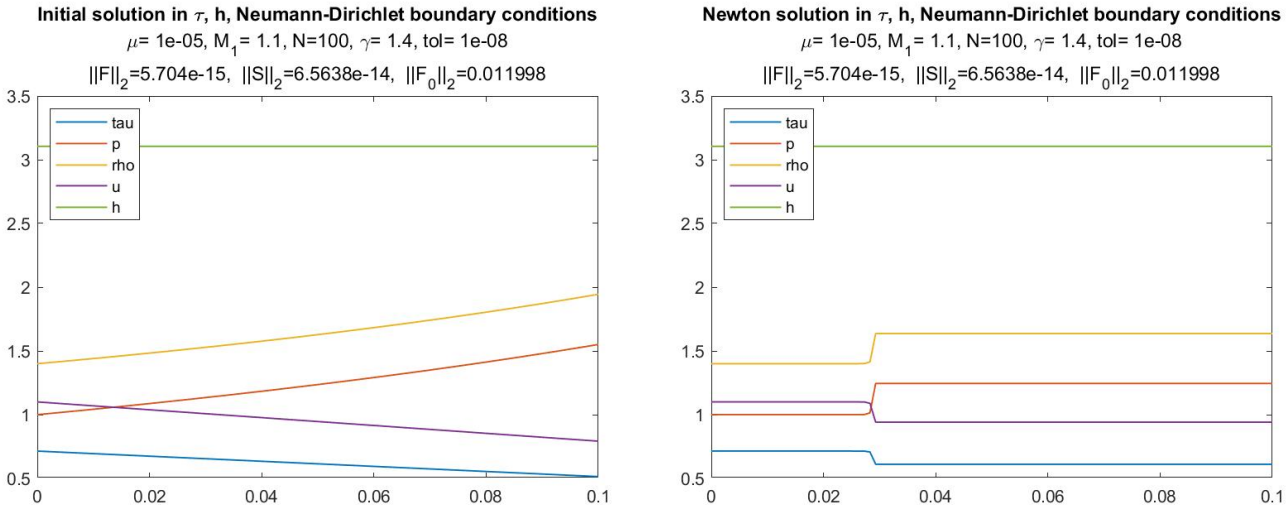

(a) Initial solution

(b) Final solution

Figure 11: Initial linear solution, system in τ, h

In Figure 11, we see a nontrivial solution. This solution resembles a shock which is an expected solution. The main difference in the initial solutions between the two systems is the choice of h. Therefore, we suspect that there is a better chance of computing a nontrivial solution when h is constant in the initial solution.

6.1.3 Arbitrary shock

Next we propose a shock as the initial solution. The right boundary values τ_R and p_R are again (31a) and (31b), respectively. The shock is placed in the middle of the spatial domain, i.e., at $x = 0.05$. The shock is a jump from the left boundary values to the right boundary values and has a width equal to Δx.

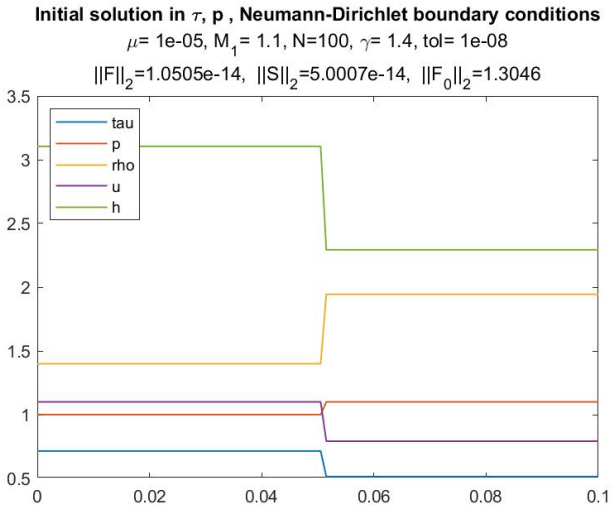

(a) Initial solution

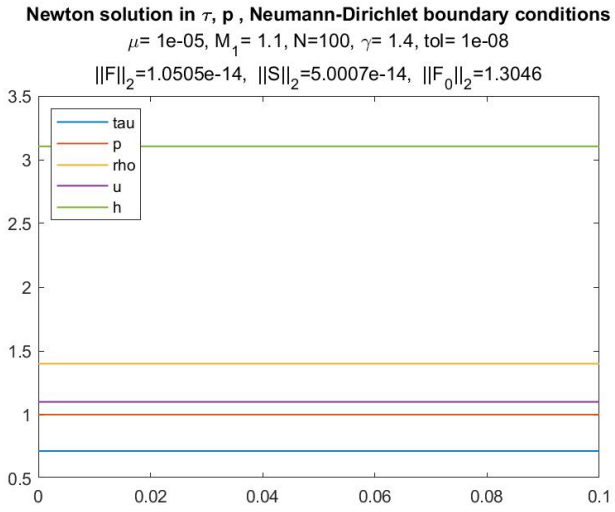

(b) Final solution

Figure 12: Initial solution with shock, system in τ, p

As can be seen in Figure 12, we again find the trivial solution.

However, when we use this initial solution for the system in variables τ, h, we find a different result.

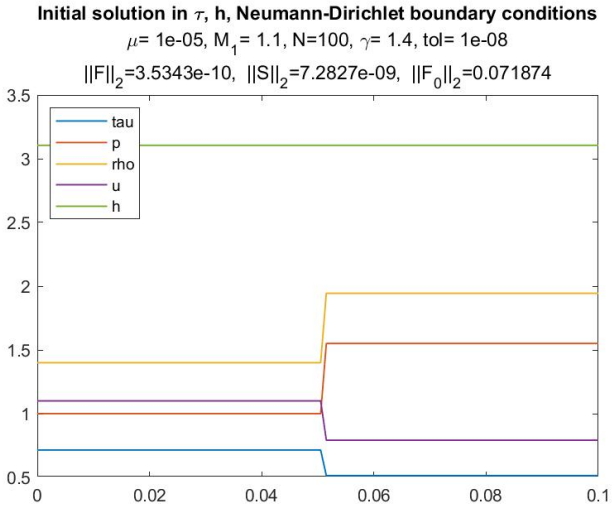

(a) Initial solution

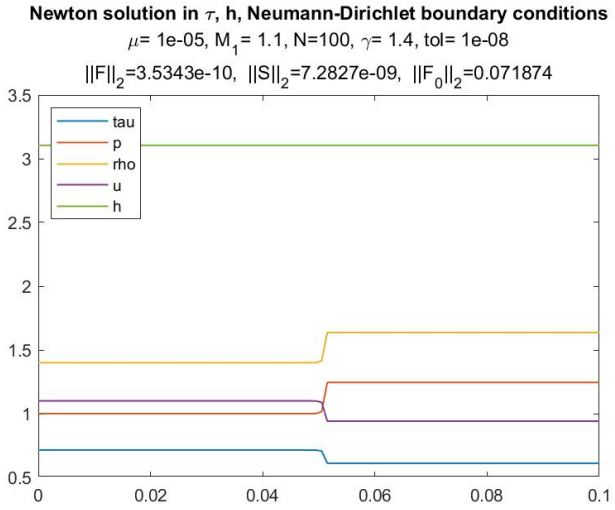

(b) Final solution

Figure 13: Initial solution with shock, system in τ, h

In Figure 13, we find a nontrivial solution. The main difference between the initial solutions in τ, p and τ, h is again that h is constant in the latter option. Furthermore, we see that h remains

constant in the final solution. Lastly, we see that the nontrivial solution depicts a shock. The shock is similar to the shock found when using the linear initial solution for τ, h. The only difference is the location of the shock.

6.1.4 Dirichlet shock

As a last initial solution, we use the Dirichlet boundary values computed in Section 5.1.2. These values are used to construct a shock in the middle of the spatial domain. The Dirichlet boundary values guarantee a nontrivial solution when using Dirichlet boundary conditions at both sides. We suspect that these values also guarantee a nontrivial solution when using Neumann-Dirichlet boundary conditions but using the Dirichlet values in the initial solution. In addition, we have chosen h to be constant in this initial solution for both systems as we previously have seen that an initial solution where h is constant shows better results.

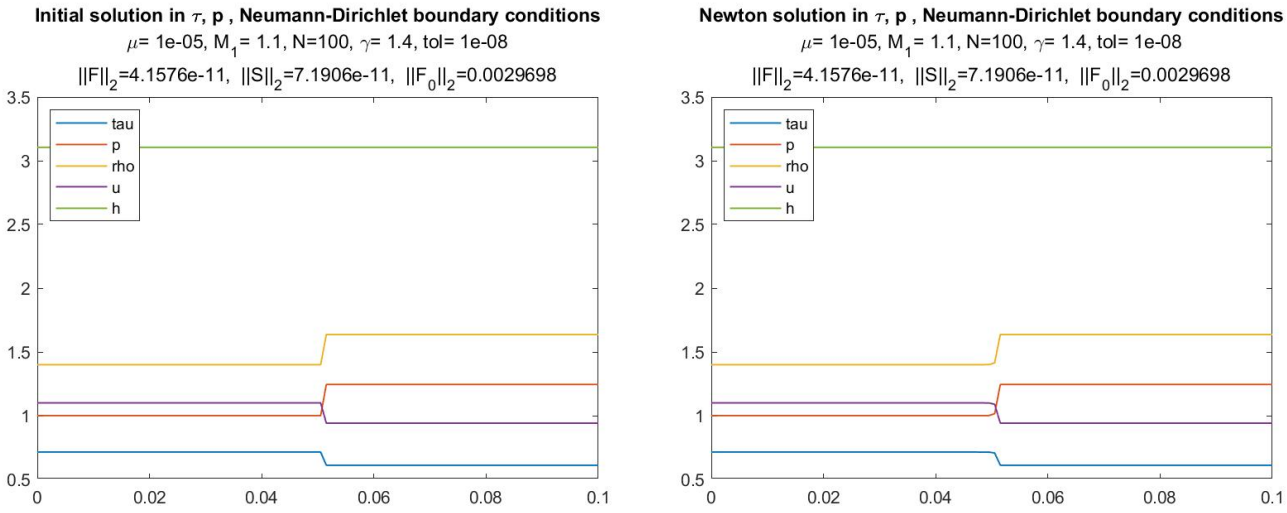

(a) Initial solution

(b) Final solution

Figure 14: Initial solution with Dirichlet shock, system in τ, p

In Figure 14 we again find a nontrivial solution that has a shock structure. We note that the solution is very similar to the initial solution. Therefore, we suspect that the use of Dirichlet boundary values at both sides of the spatial domain gives better results. We find the same solution when using variables τ, h.
In conclusion, finding a nontrivial solution when using Neumann-Dirichlet boundary conditions is not guaranteed. The use of a constant h in the initial solution presumably helps with finding a nontrivial solution. Furthermore, using the Dirichlet boundary values in the initial solution gives better results.

6.2 Dirichlet boundary conditions

Now that we have concluded that Dirichlet boundary conditions presumably guarantee a nontrivial solution, we use Dirichlet boundary conditions at both boundaries.

For the following results, we have used

$$\begin{aligned}
&\gamma = \tfrac{7}{5},\\
&\mathrm{M_{in}} \in (1, 3],\\
&\mu \in [1\mathrm{e}{-2}, 1\mathrm{e}{-5}],\\
&\mathrm{Pr} = \tfrac{3}{4},\\
&\tau_1 = \tfrac{1}{\gamma} \quad \mathrm{m}^3/\mathrm{kg},\\
&p_1 = 1 \quad \mathrm{N}/\mathrm{m}^2,\\
&h_1 = \frac{1}{\gamma - 1} + \frac{m^2}{2\gamma^2} \quad \mathrm{J/kg}.
\end{aligned}$$

Note that for these values, the speed of sound at the inflow, c_1, is always equal to 1 m/s . We again show the results for the system in τ, p. The results for the system in τ, h can be found in Appendix B. As a nontrivial solution is guaranteed for these computations, we also analyze the evolution of the Mach number and the entropy. A physical explanation of the results is given at the end, as all results show similar physical behaviour.

6.2.1 Mach = 1.1

We first compute the results for Mach = 1.1. We do this for $\mu = 1\mathrm{e}{-3}$ and $\mu = 1\mathrm{e}{-5}$.

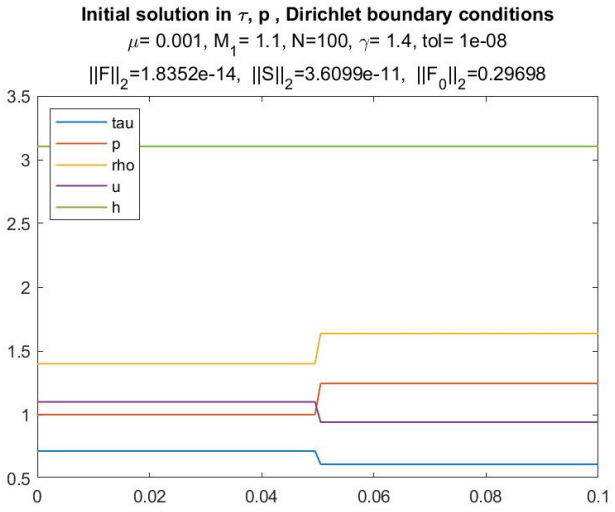

(a) Initial solution

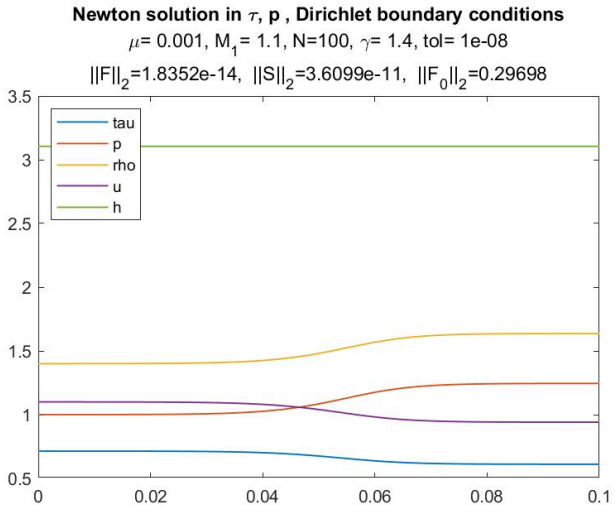

(b) Final solution

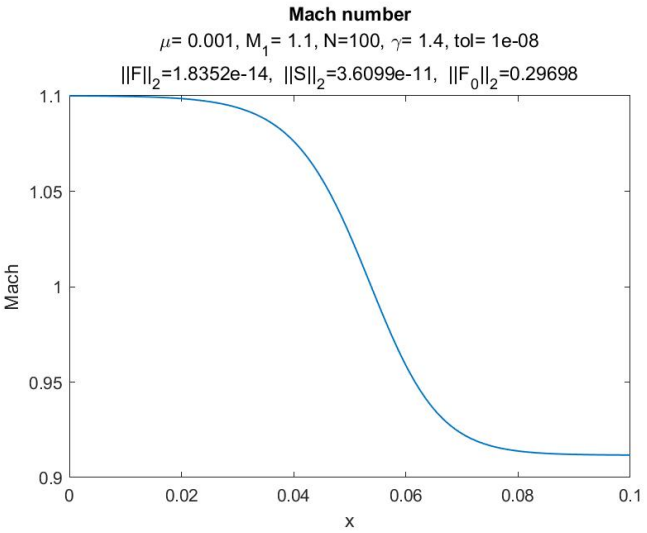

(c) Mach

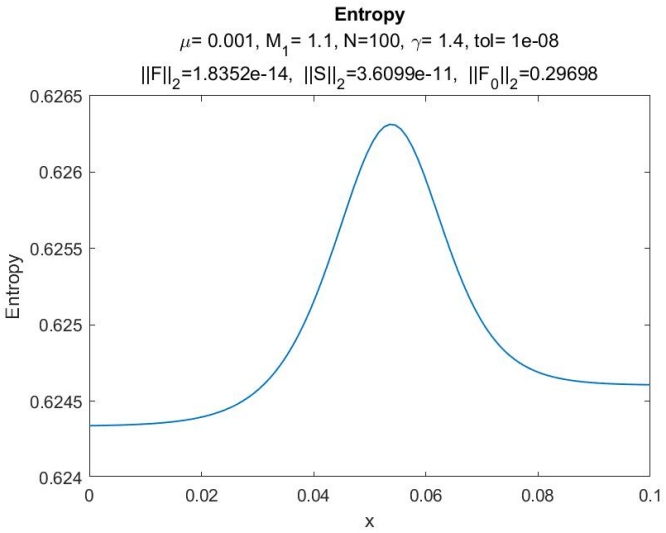

(d) Entropy

Figure 15: Initial solution with shock, system in τ, p

In Figure 15, we see that the initial shock becomes smoother but does not disappear. Furthermore, we see that the Mach number decreases nicely, as predicted by the shock relations. We note that although the entropy at the right boundary is higher than the entropy at the left boundary, there is an interval where the entropy decreases. The decrease of the entropy is a phenomenon which is usually not allowed. Although the decrease does occur, we note that the decrease is only of 0.002 J/K. Lastly, we note that we obtained the same result in Figure 8 for the analytical solution.

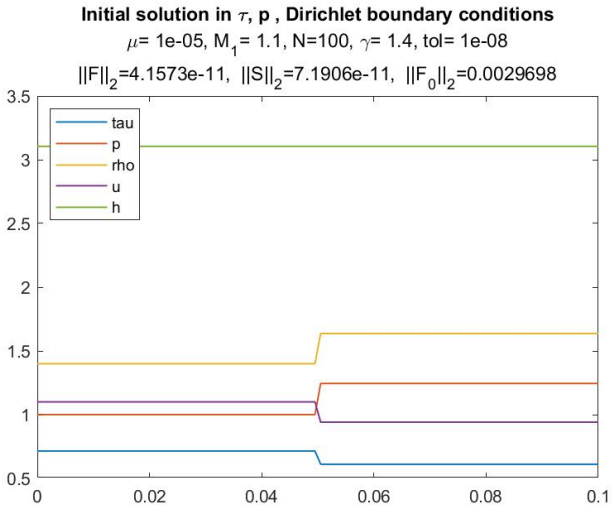

(a) Initial solution

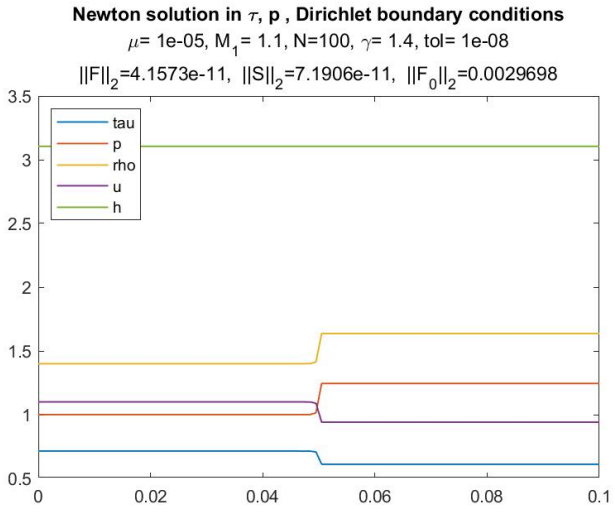

(b) Final solution

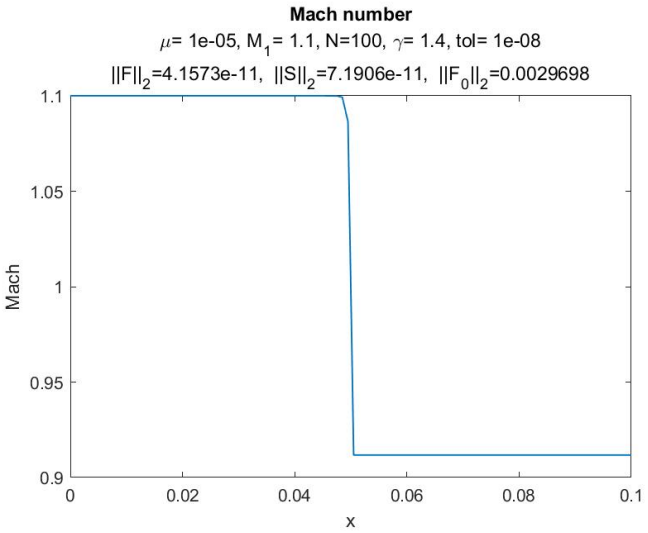

(c) Mach

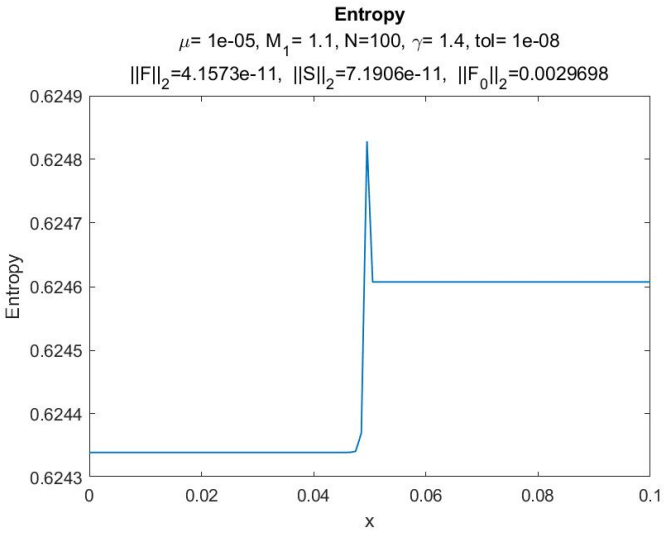

(d) Entropy

Figure 16: Initial solution with shock, system in τ, p

For a lower dynamic viscosity, as shown in Figure 16, we see that the shock width decreases. Furthermore, the graphs for the Mach number and the entropy become sharper. Unfortunately, we again see a small peak in the entropy.

6.2.2 Mach $= 2$

Now we increase the Mach number to Mach $= 2$ and compute results for $\mu = 1\text{e}{-2}$ and $\mu = 1\text{e}{-5}$.

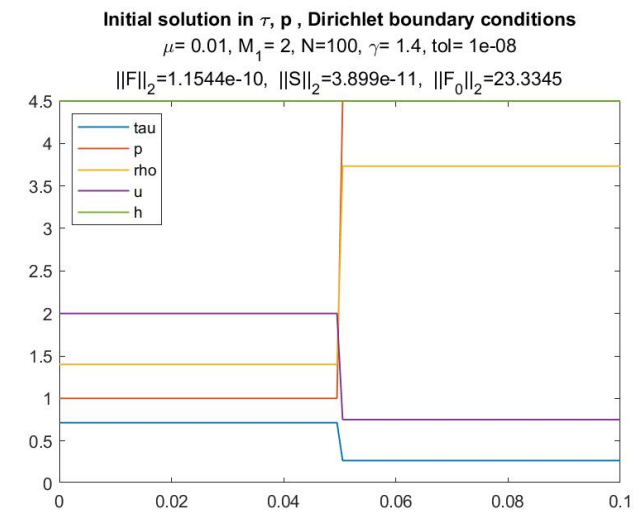

(a) Initial solution

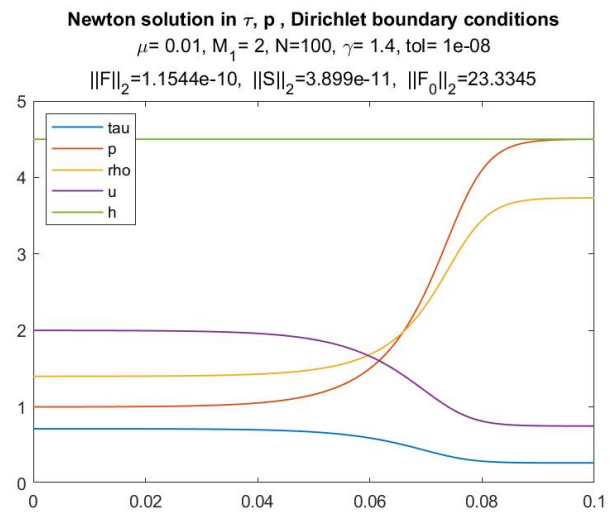

(b) Final solution

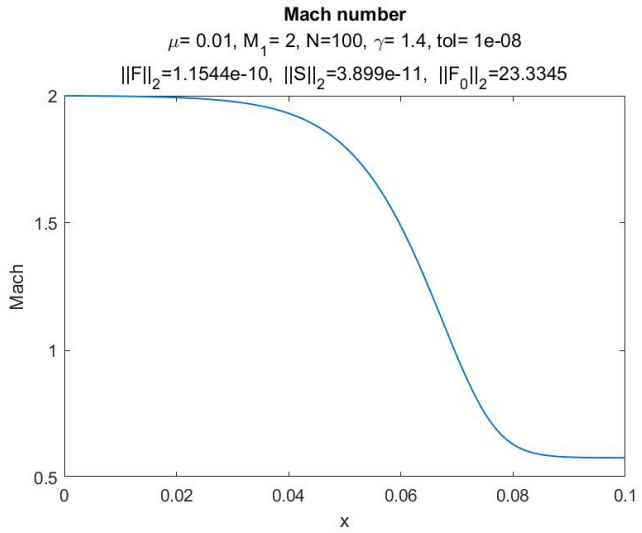

(c) Mach

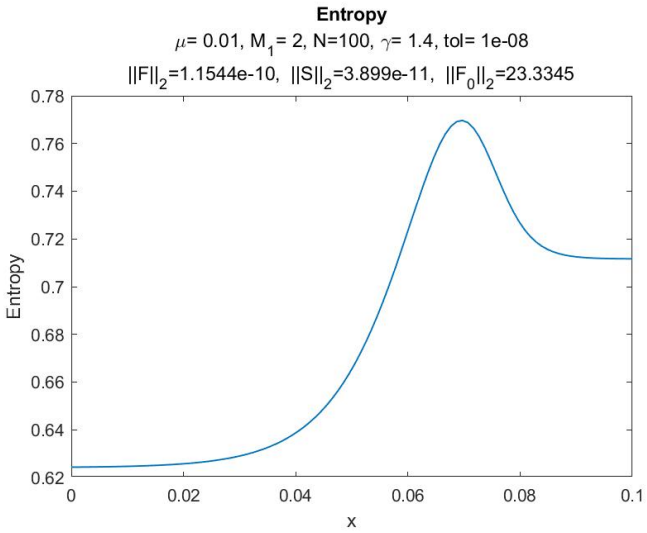

(d) Entropy

Figure 17: Initial solution with shock, system in τ, p

Firstly, in Figure 17, we see that for $\mu = 1e{-}2$, the shock width becomes even larger than before. Furthermore, we see that the shock has moved to the right side of the spatial domain. This is a result of the higher Mach number. Lastly, we note that the range of the variables increases for a larger Mach number. That is, the pressure and density increase and the velocity and specific volume decrease w.r.t. Mach = 1.1.

Note that for Mach = 2, we have used $\mu = 1e{-}2$ instead of $\mu = 1e{-}3$. This is a result of a problem of the method. For certain combinations of the Mach number and the dynamic viscosity, the method does not work. This phenomenon will be discussed in more detail in the discussion.

Based on Figure 17, the spatial domain seems to be too restricted. For larger Mach numbers, the shock travels to the right of the spatial domain. It can be argued whether the variable derivatives at the right boundary are truly zero. Therefore we expand the spatial domain to $[0, 0.2]$.

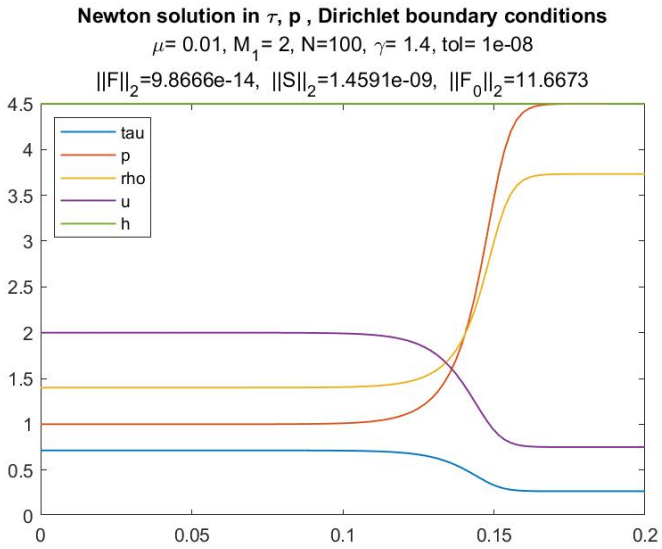

Figure 18: Spatial domain enlarged

From Figure 18, we first note that the shock has moved. We have chosen the spatial domain twice as long. However, the shock has moved along with this enlarged domain. The position of the shock has remained the same. That is, the shock is still located at roughly $\frac{3}{4}$ of the spatial domain. From this we can see that the solution is invariant of x.
Furthermore, we see that the result is very similar but the shock becomes sharper. The plateau at the right boundary has become longer. As a result, the derivatives seem to be truly zero. Thus, if the shock tends too much towards the right boundary, an enlarged spatial domain can slightly improve the solution.
Lastly we note that the number of grid points N has remained equal to 100. Therefore Δx has increased which has a influence on the Péclet number. The choice of x_{max} only influences Δx when N remains unchanged. Thus the difference in the size of the plateau is presumably a result of a different Péclet number.

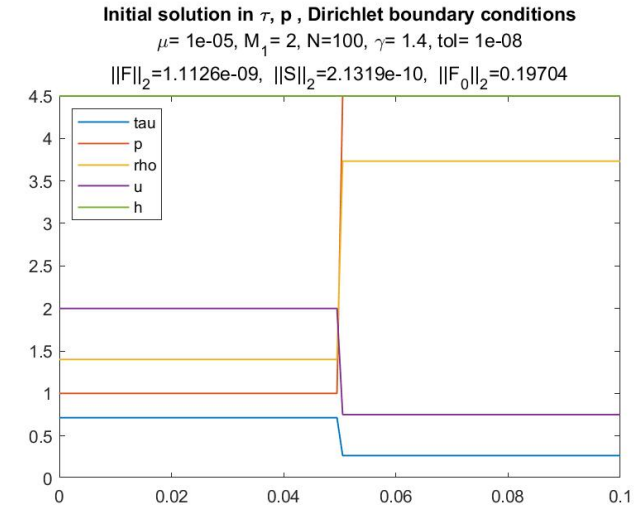

(a) Initial solution

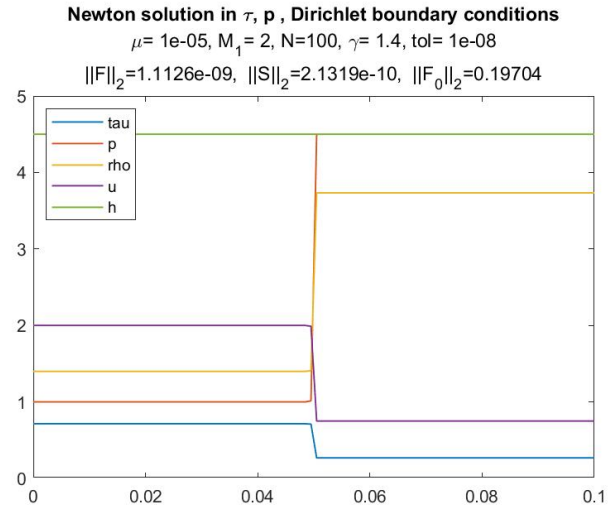

(b) Final solution

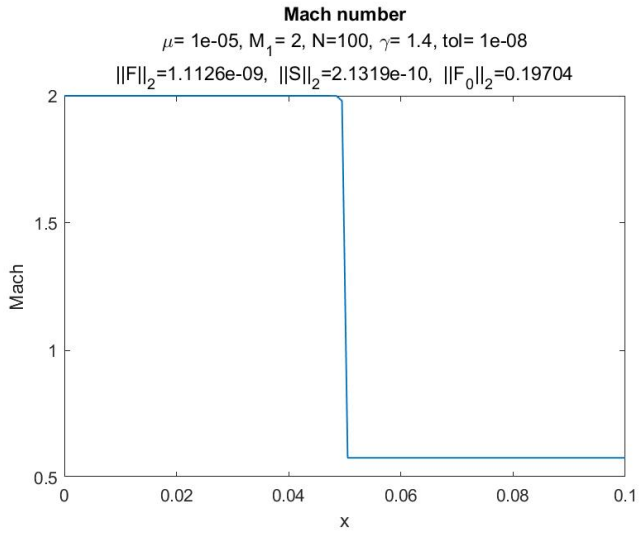

(c) Mach

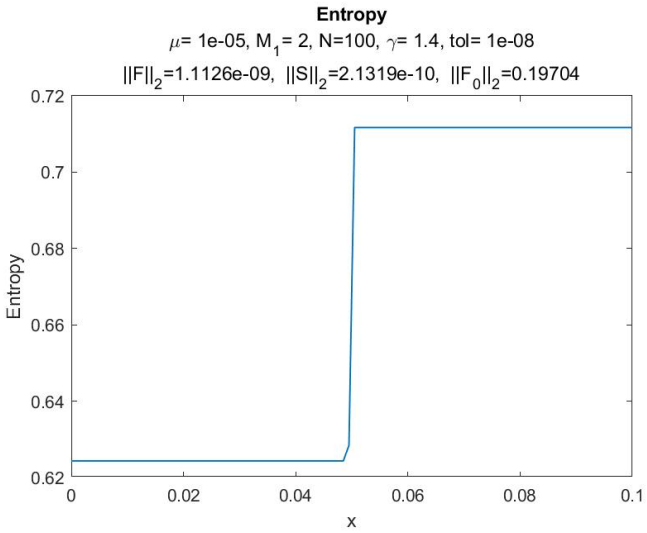

(d) Entropy

Figure 19: Initial solution with shock, system in τ, p

In Figure 19, we see that for a high Mach number and a low dynamic viscosity, the shock width becomes minimal and the graphs become very sharp. Visually, there is a minimal difference between the initial solution and the final solution. In the graph for the entropy, we finally see only an increase. This is the behaviour that is expected of entropy. However, we can not verify why the entropy has a small decrease for lower Mach numbers and lower dynamic viscosities.

6.2.3 Mach $= 3$

Finally, we analyze results for Mach $= 3$ and $\mu = 1\text{e}{-3}$ and $\mu = 1\text{e}{-5}$.

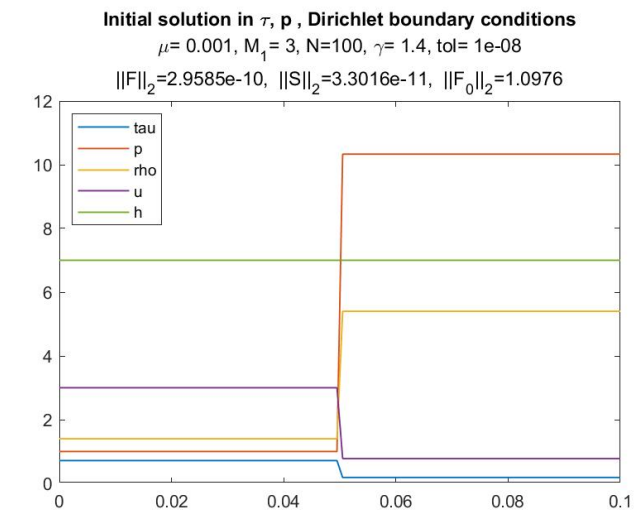

(a) Initial solution

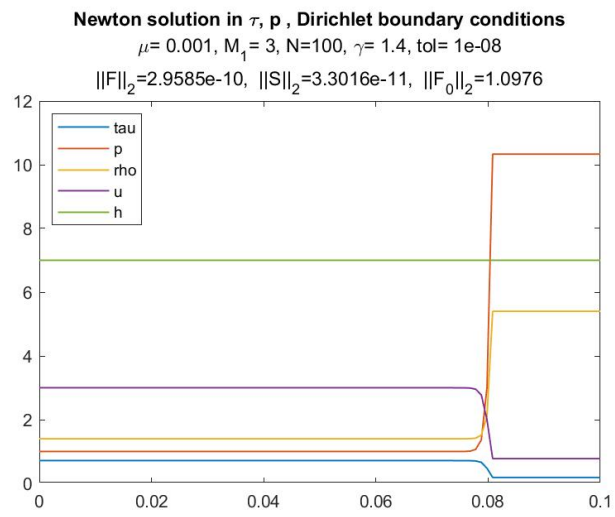

(b) Final solution

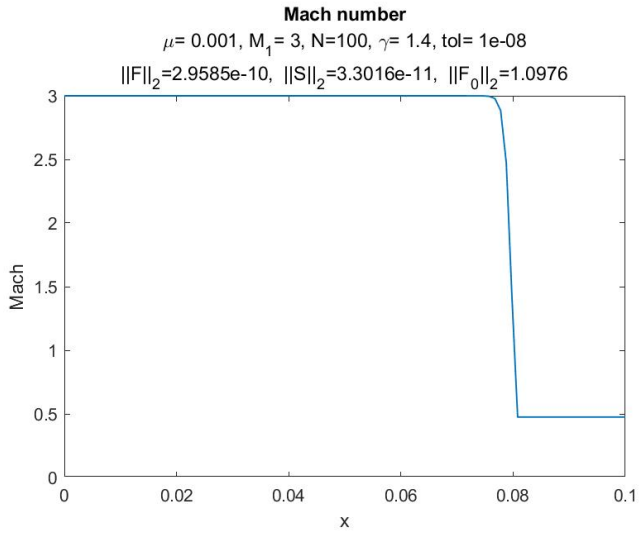

(c) Mach

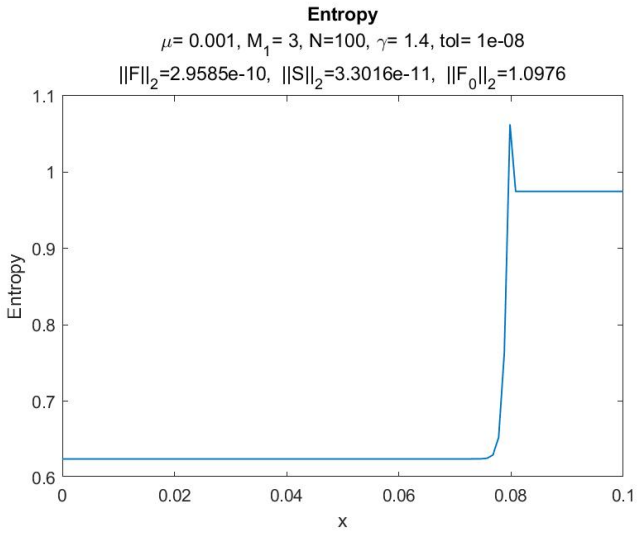

(d) Entropy

Figure 20: Initial solution with shock, system in τ, p

In Figure 20, it can be seen that the shock has again moved to the right in the spatial domain. However, we can clearly see that the derivatives at the right boundary are zero. Furthermore, the range of the variables becomes even larger. In the entropy, we again see a small peak.

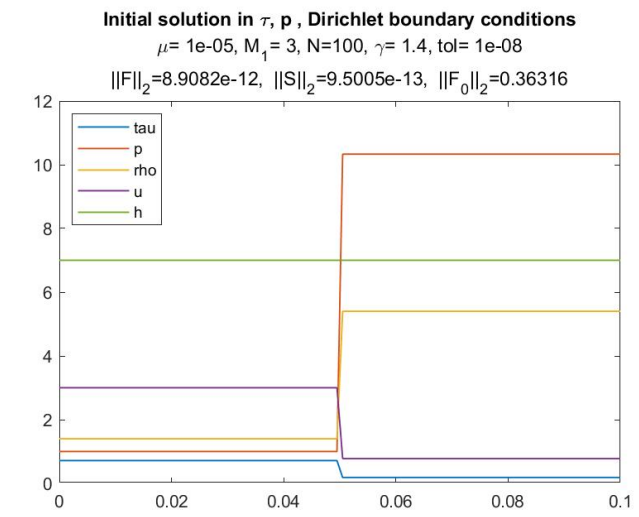

(a) Initial solution

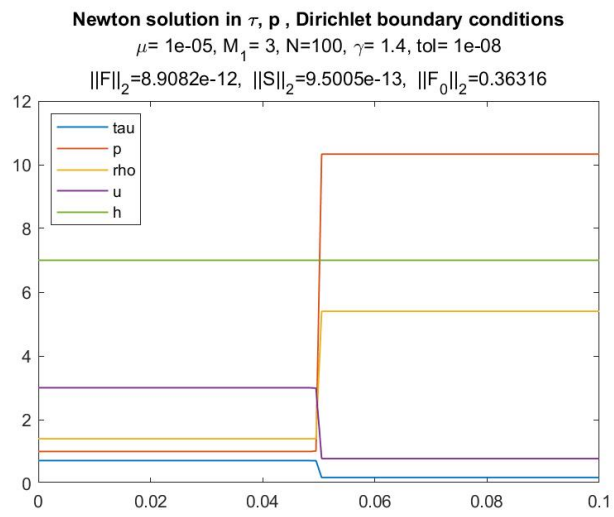

(b) Final solution

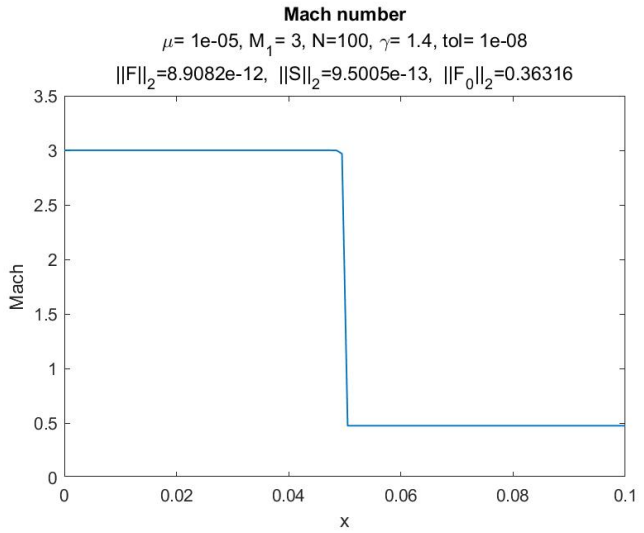

(c) Mach

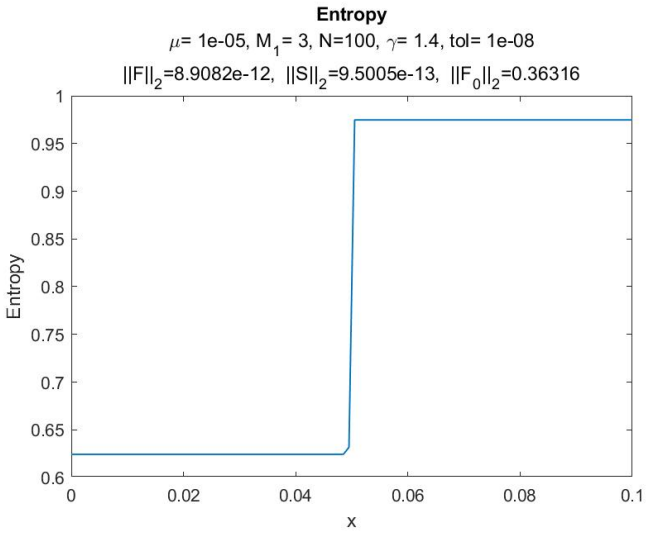

(d) Entropy

Figure 21: Initial solution with shock, system in τ, p

In the final result in Figure 21, we see the highest Mach number and the lowest dynamic viscosity. This results in the sharpest solution yet. Furthermore, the entropy does not decrease for these values.

In all results, we can clearly see the flow moving across a shock wave. The location of the shock waves differs for different combinations of the Mach number and the dynamic viscosity. Along the shock wave, the velocity decreases. As a result of the compressible flow, the density increases. Furthermore, variables which are not shown are the temperature, energy and speed of sound. Across the shock wave, the temperature increases while the energy decreases. Furthermore, the

speed of sound increases. As the speed of sound increases and the velocity decreases, the Mach number decreases. Lastly, the entropy increases across the shock wave. This means that there is less energy available to do work.

Additionally, we compute the Reynolds numbers of the flows. They Reynolds numbers is defined as $\mathrm{Re} = \rho u l/\mu$, where l is a characteristic length. The higher the Reynolds number, the larger the chance for turbulent flow instead of laminar flow. A laminar flow is usually a smooth fluid motion while a turbulent flow is chaotic and shows unstable behaviour. The Reynolds number of these flows will be used later in this report.

Mach \ μ	1e−2	1e−3	1e−5
1.1	15.4	154	1.54e4
2	28	280	2.8e4
3	42	420	4.2e4

Table 1: Reynolds number for varying Mach and dynamic viscosity

Furthermore, we want to note that the location of the shock is difficult to determine. As we have already seen, the shock moves to the right side of the spatial domain when using a higher Mach number. However, the location of the shock is independent of the initial solution. To demonstrate this, we choose two different initial solution shocks and compute the results.

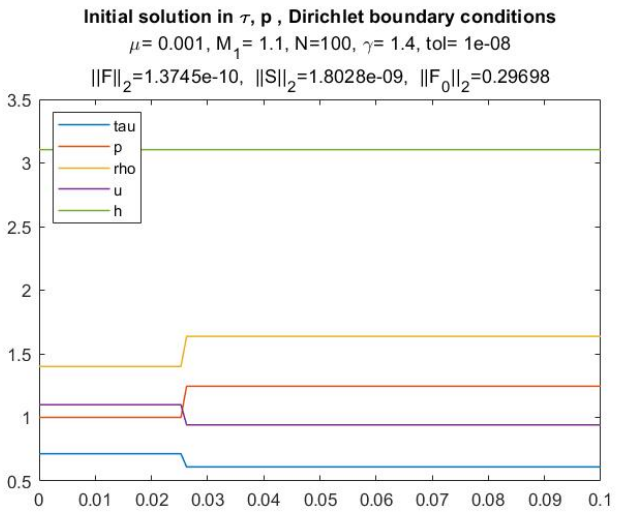

(a) Initial solution

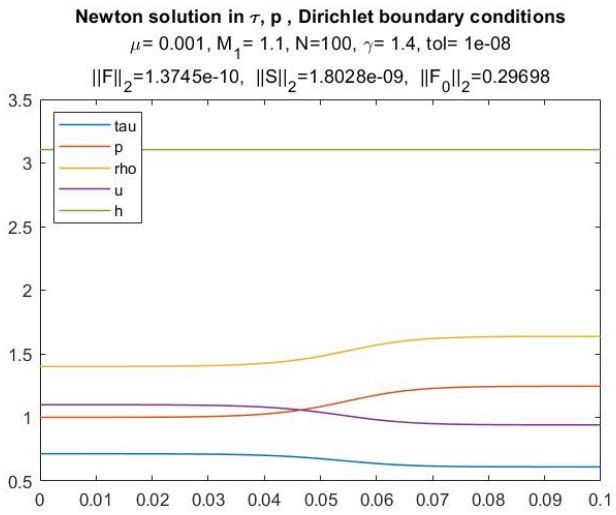

(b) Final solution

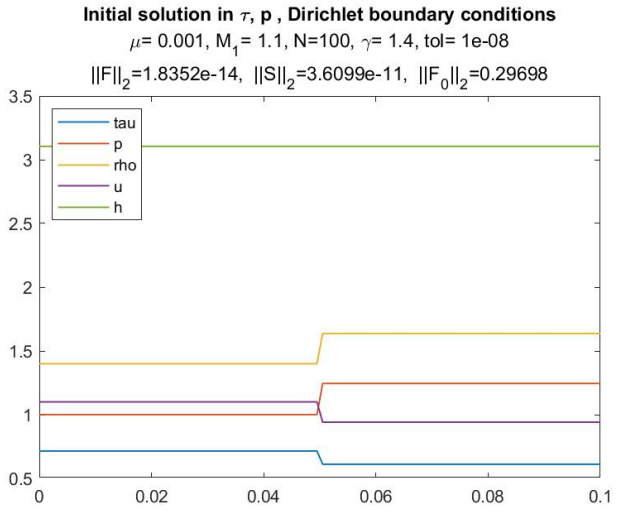

(c) Initial solution

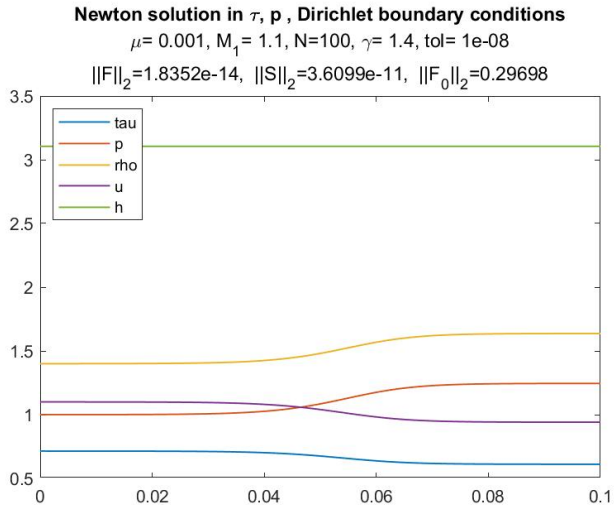

(d) Final solution

Figure 22: Initial solution with shock, system in τ, p

In Figure 22 we can see that the placement of the shock is independent of the placement of the initial shock. Therefore, it is difficult to predict the placement of the final solution shock.

Furthermore, we want to discuss the choice of the solution vector $\underline{y}$. We have chosen to alternate between variables τ, p, i.e., $\underline{y} = (\ldots, \tau_i, p_i, \tau_{i+1}, p_{i+1}, \ldots)$. One could have also chosen a different order, e.g., $\underline{y} = (\ldots, \tau_i, \tau_{i+1}, \ldots, \ldots, p_i, p_{i+1}, \ldots)$. This would influence the Jacobian. However, we have tried this alternative order of y and it gave the same results. The difference in convergence was negligible. This also holds for the system in variables τ, h.

Lastly, we note that all computations were done in less than 10 iterations.

6.3 Convergence analysis

Now that all results are shown, we analyze the convergence of the Newton iteration. This is done using convergence plots in a semilog scale. For each computation, we plot the norm of the residual for each iteration step. This is done for the system in τ, p as well as for the system in τ, h in order to compare the convergence of the two. We note that all methods converge in less than 10 iterations. Furthermore, we note that the stopping criteria that we used for the Newton-Raphson method are $\|\underline{F}\| < \text{tol} \wedge \|\underline{S}\| < \text{tol}$, where S is the update step. As a result, it can be seen that, in some computations, there is an extra iteration although the norm of $\underline{F}$ is already smaller than the tolerance. In these cases, the norm of the update step is not yet small enough and thus extra iterations are needed to satisfy the stopping criteria.

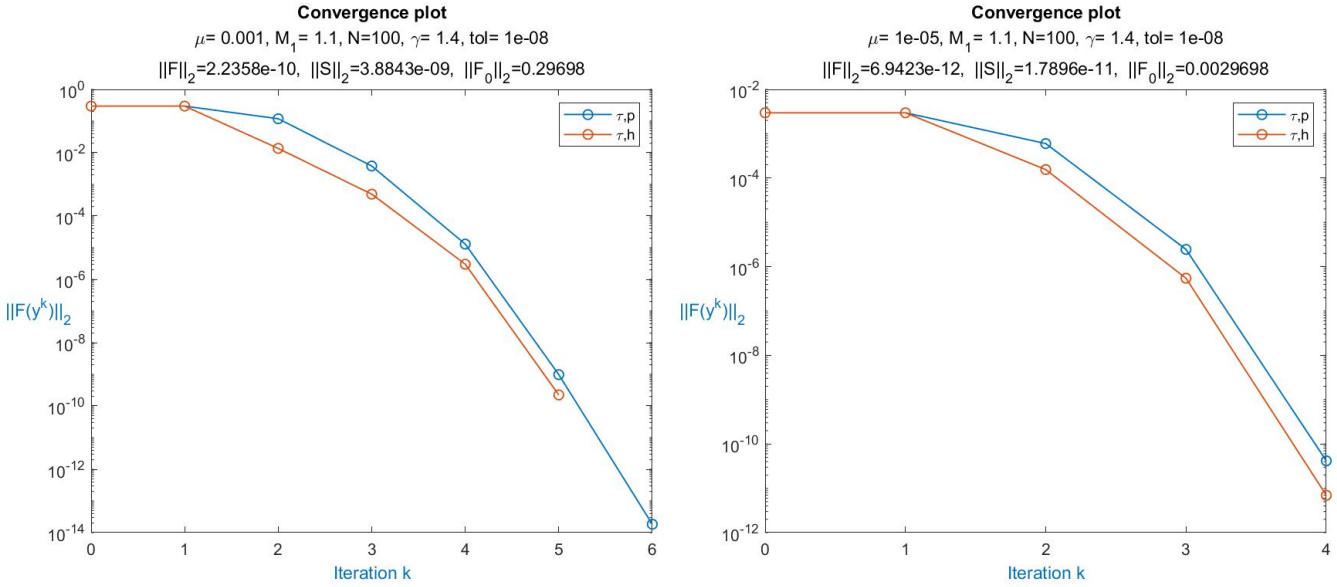

(a) Mach $= 1.1, \mu = 1\text{e}{-3}$

(b) Mach $= 1.1, \mu = 1\text{e}{-5}$

Figure 23: Convergence plots, Mach= 1.1

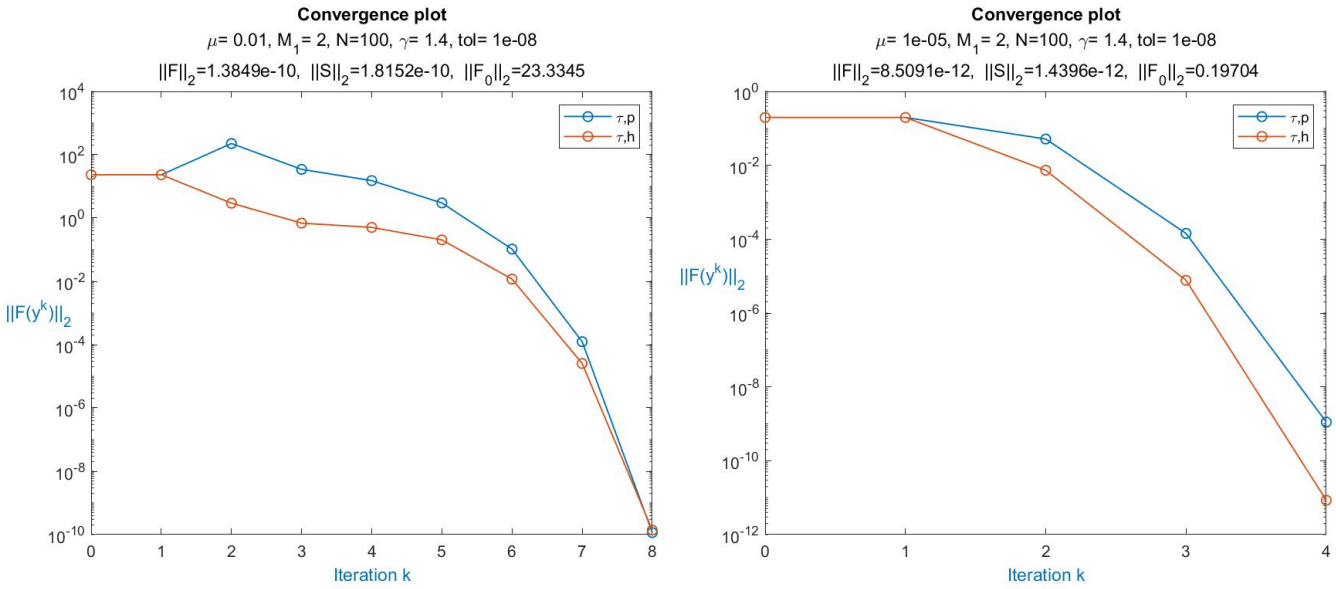

(a) Mach $= 2, \mu =$ 1e$-$2 (b) Mach $= 2, \mu =$ 1e$-$5

Figure 24: Convergence plots, Mach= 2

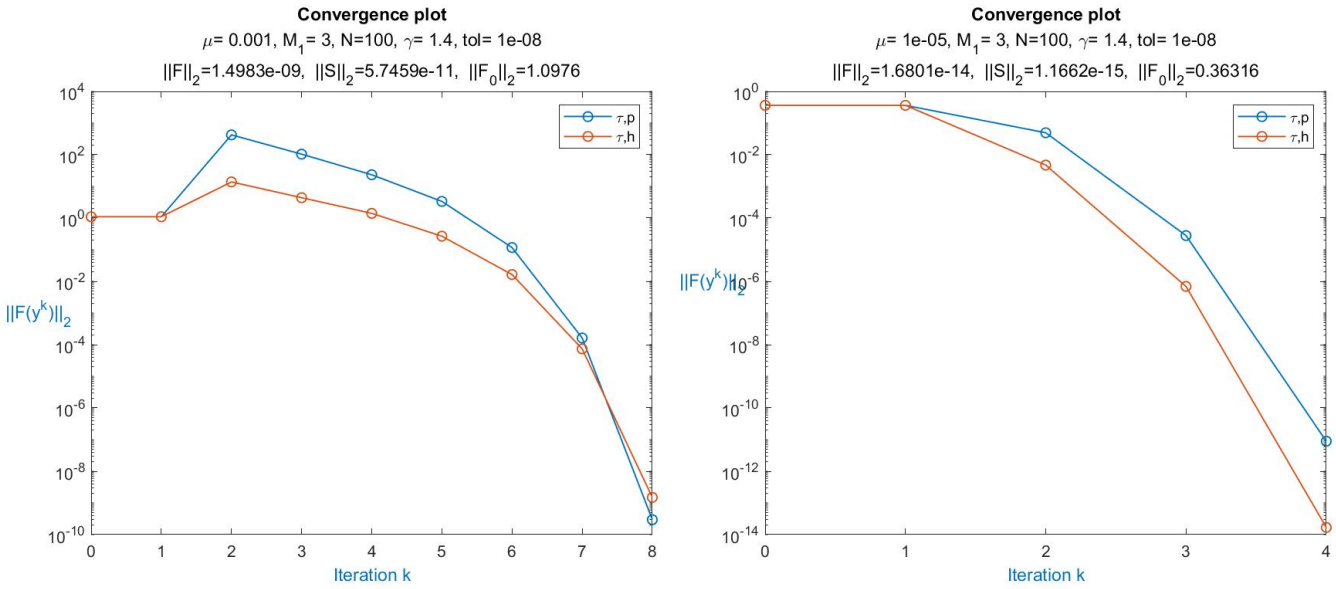

(a) Mach $= 3, \mu =$ 1e$-$3 (b) Mach $= 3, \mu =$ 1e$-$5

Figure 25: Convergence plots, Mach= 3

From Figures 23-25, we see that the rate of converges becomes larger than 2 for the final iterations. Therefore, the method has convergence higher than quadratic convergence while the Newton-

Raphson method has quadratic convergence. Furthermore, the convergence for the system in τ, h is always slightly better than the convergence for τ, p with the exception of the last iteration for Mach $= 3$, $\mu = 1\text{e}{-3}$. This is presumably a result of the equation for F_2. When using variables τ, h, this equation becomes linear and consists of only one matrix product. Furthermore the Jacobian $\mathbf{F_2'}$ is sparser. We do note that for variables τ, p, the equation for $\underline{F}_1$ is also linear but it consists of a sum of two matrix products and its Jacobian is slightly more dense. This can explain the slight difference in convergence. Overall, the convergence is slightly better than expected.

7 Complete flux approach for Prandtl $\neq \frac{3}{4}$

In this extension to the original complete flux approach, we do not limit ourselves to Pr $= \frac{3}{4}$. This choice will result in a different expression for the enthalpy flux. We start with equation (15). If we multiply with the integrating factor and integrate this expression, we obtain

$$\frac{1}{m}(1-e^{-\frac{m}{\varepsilon}})F_{h,j+\frac{1}{2}} = -(e^{-\frac{m}{\varepsilon}}h_R - h_L) - \frac{\alpha}{\varepsilon\Delta x}\int_0^1 e^{-\frac{m\sigma}{\varepsilon}}(p\tau)'\mathrm{d}\sigma.$$

We previously assumed that p is linear, i.e., $p(\sigma) = p_L + (p_R - p_L)\sigma$. Now we also assume that τ is linear: $\tau(\sigma) = \tau_L + (\tau_R - \tau_L)\sigma$. The integral now becomes

$$\frac{1}{m}(1-e^{-\frac{m}{\varepsilon}})F_{h,j+\frac{1}{2}} = -(e^{-\frac{m}{\varepsilon}}h_R - h_L) - \frac{\alpha}{\varepsilon\Delta x}\int_0^1 e^{-\frac{m\sigma}{\varepsilon}}\left[p_L(\tau_R-\tau_L)+\tau_L(p_R-p_L)+2(\tau_R-\tau_L)(p_R-p_L)\sigma\right]\mathrm{d}\sigma.$$

Computing the integral and using the boundary conditions gives

$$F_{h,j+\frac{1}{2}} = \varepsilon\left[B^-h_L - B^+h_R\right] - \frac{\alpha}{\Delta x}\left[p_j(\tau_{j+1}-\tau_j)+\tau_j(p_{j+1}-p_j)+2(\tau_{j+1}-\tau_j)(p_{j+1}-p_j)W^+\right].$$

Equation (18b) now becomes

$$\begin{aligned}\varepsilon\left[-B^-h_{j-1}+(B^-+B^+)h_j - B^+h_{j+1}\right] - \frac{\alpha}{\Delta x}\big[&p_j(\tau_{j+1}-\tau_j)+\tau_j(p_{j+1}-p_j)+2(\tau_{j+1}-\tau_j)(p_{j+1}-p_j)W^+\\ &-p_{j-1}(\tau_j-\tau_{j-1})-\tau_{j-1}(p_j-p_{j-1})-2(\tau_j-\tau_{j-1})(p_j-p_{j-1})W^+\big] = 0.\end{aligned}$$

We now choose Dirichlet boundary conditions and write the system in the variables τ, p, like in Section 5.1.2. The vector $\underline{F_2}$ becomes

$$\underline{F_2} = \varepsilon\mathbf{B}\underline{h} + \underline{f_2} - \frac{\alpha}{\Delta x}\underline{C},$$

where $\underline{C} = (C_2, \dots C_{N-1})^\intercal$,

$$\begin{aligned}C_j =&p_j(\tau_{j+1}-\tau_j)+\tau_j(p_{j+1}-p_j)+2(\tau_{j+1}-\tau_j)(p_{j+1}-p_j)W^+ - p_{j-1}(\tau_j-\tau_{j-1})-\tau_{j-1}(p_j-p_{j-1})\\ &-2(\tau_j-\tau_{j-1})(p_j-p_{j-1})W^+.\end{aligned}$$

In the Jacobian, the matrix $-\frac{\alpha}{\Delta x}C'$ is added to F_2' where

$$\begin{aligned}\frac{\partial C_j}{\partial\tau_{j-1}} &= 2p_{j-1} - p_j + 2(p_j - p_{j-1})W^+,\\ \frac{\partial C_j}{\partial p_{j-1}} &= 2\tau_{j-1} - \tau_j + 2(\tau_j - \tau_{j-1})W^+,\\ \frac{\partial C_j}{\partial\tau_j} &= p_{j+1} - 2p_j - p_{j-1} - 2W^+(p_{j+1}-p_{j-1}),\\ \frac{\partial C_j}{\partial p_j} &= \tau_{j+1} - 2\tau_j - \tau_{j-1} - 2W^+(\tau_{j+1}-\tau_{j-1}),\\ \frac{\partial C_j}{\partial\tau_{j+1}} &= p_j + 2(p_{j+1}-p_j)W^+,\\ \frac{\partial C_j}{\partial p_{j+1}} &= \tau_j + 2(\tau_{j+1}-\tau_j)W^+.\end{aligned}$$

In C as well as C', the Dirichlet boundary conditions need to be substituted for $j = 2, N-1$. For the sake of brevity, we do not show the whole matrix.

7.1 Results

For this section, we use the constants of hydrogen to compute results [12]:

γ	μ	κ	c_p	Re	Pr
1.4005	8.8e-6	0.182	14310	3.1932e4	0.6919

Table 2: Values for hydrogen, measured at 25°C

Note that hydrogen can be considered as an ideal gas. We now compute results for Mach $= [1.1, 1.5, 2, 3]$.

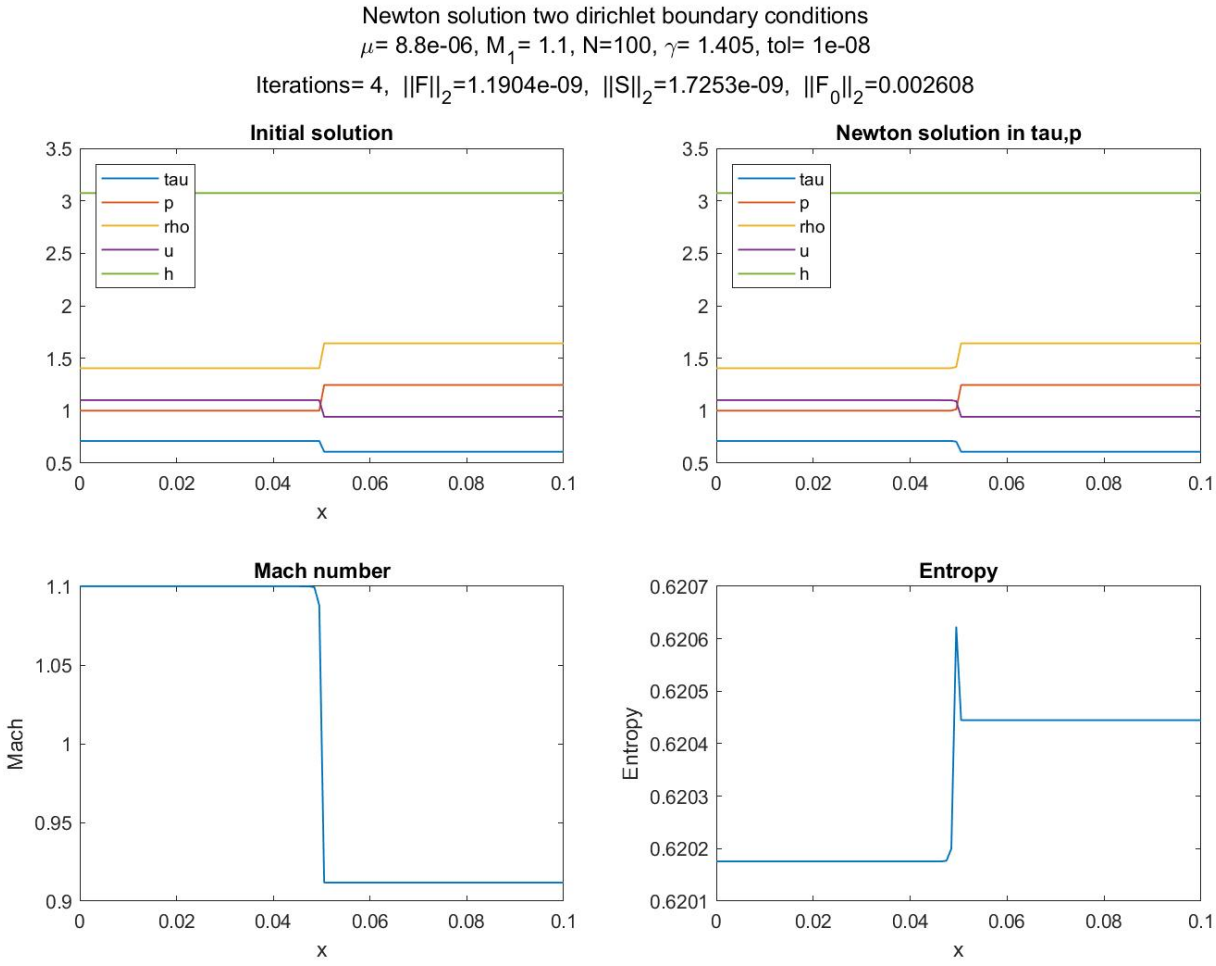

Figure 26: Results for hydrogen, Mach = 1.1

In Figure 26, we see similar behaviour to what we previously saw. A shock wave is again clearly visible. Unfortunately, we do see a slight peak in the entropy around the shock wave.

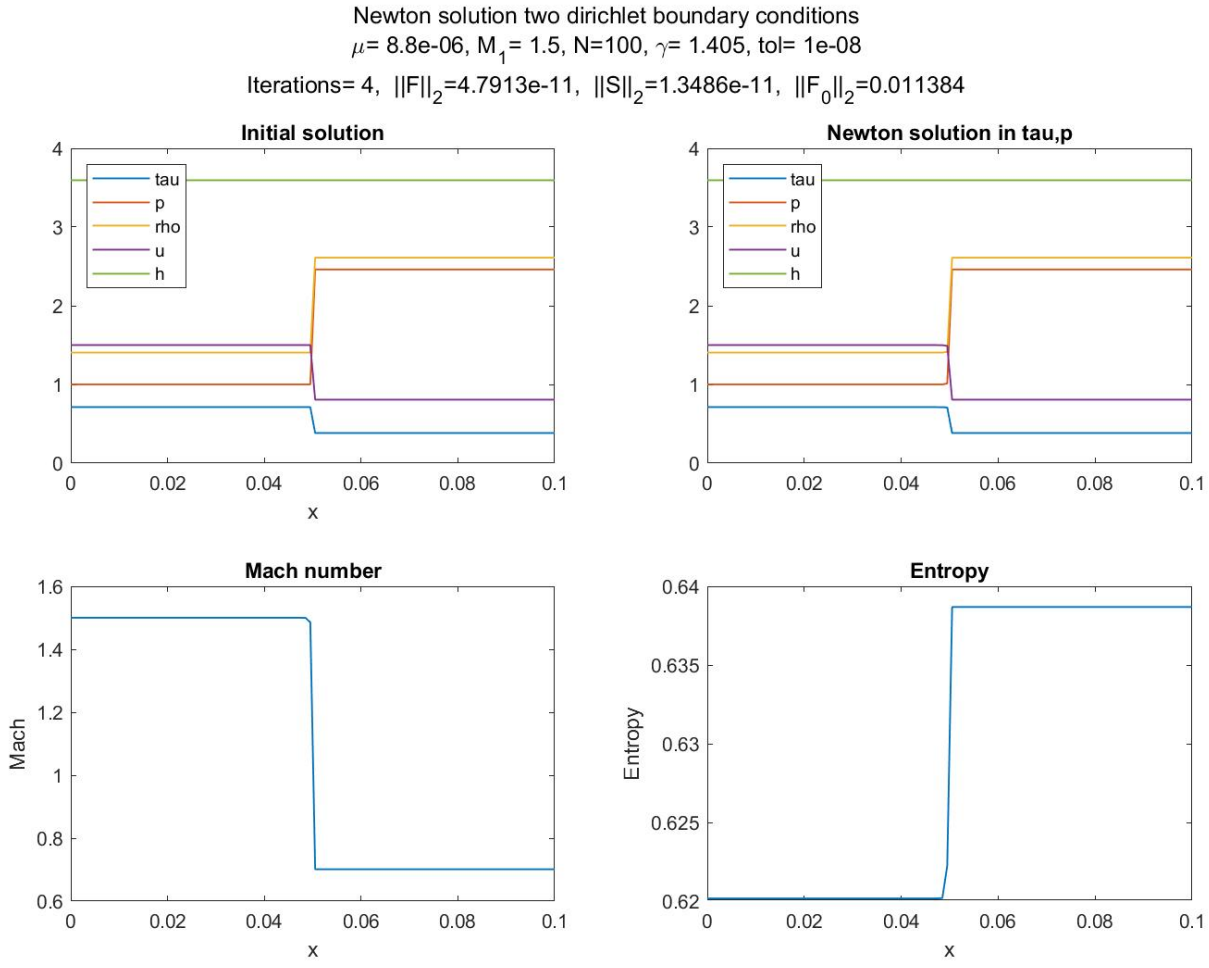

Figure 27: Results for hydrogen, Mach = 1.5

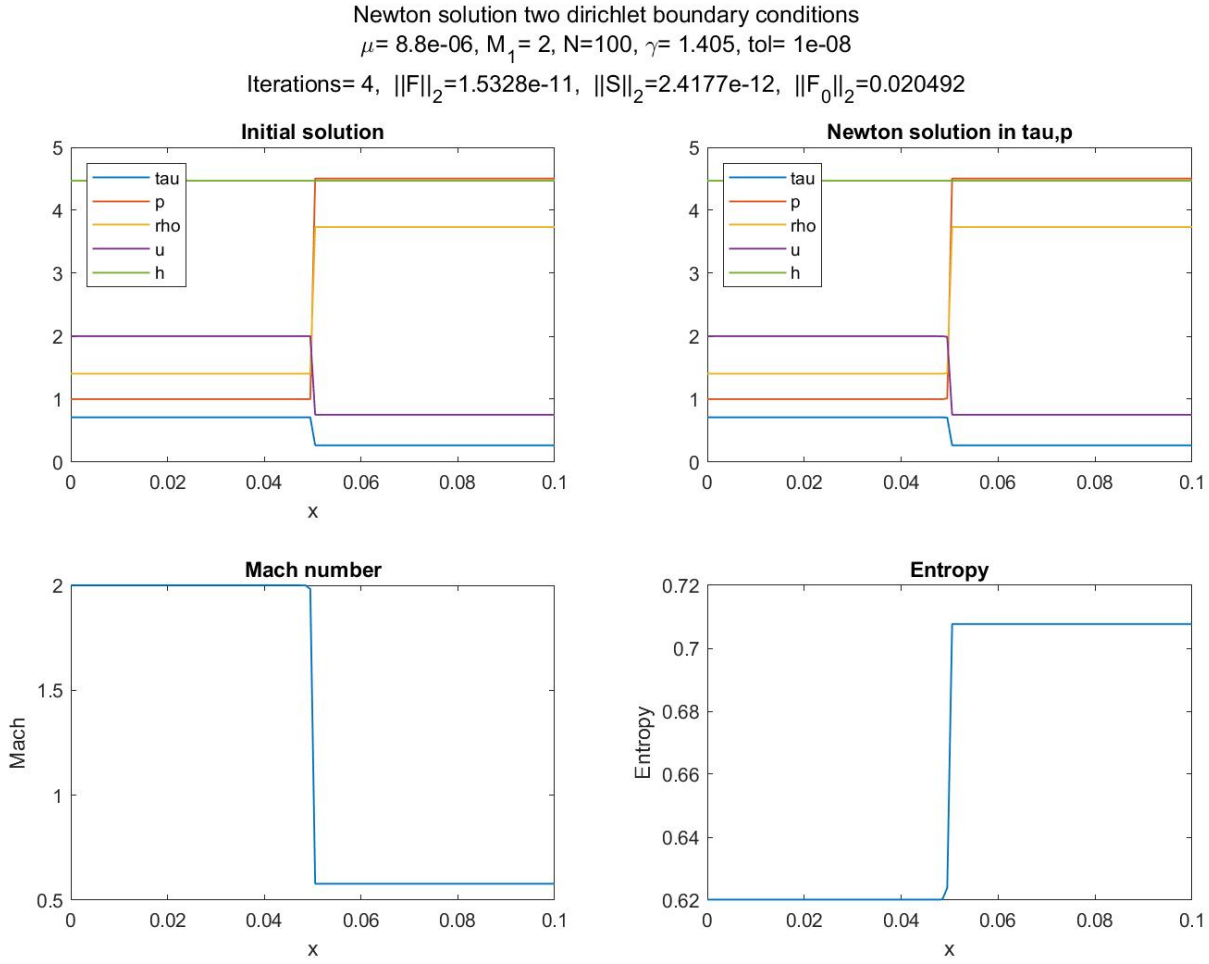

Figure 28: Results for hydrogen, Mach = 2

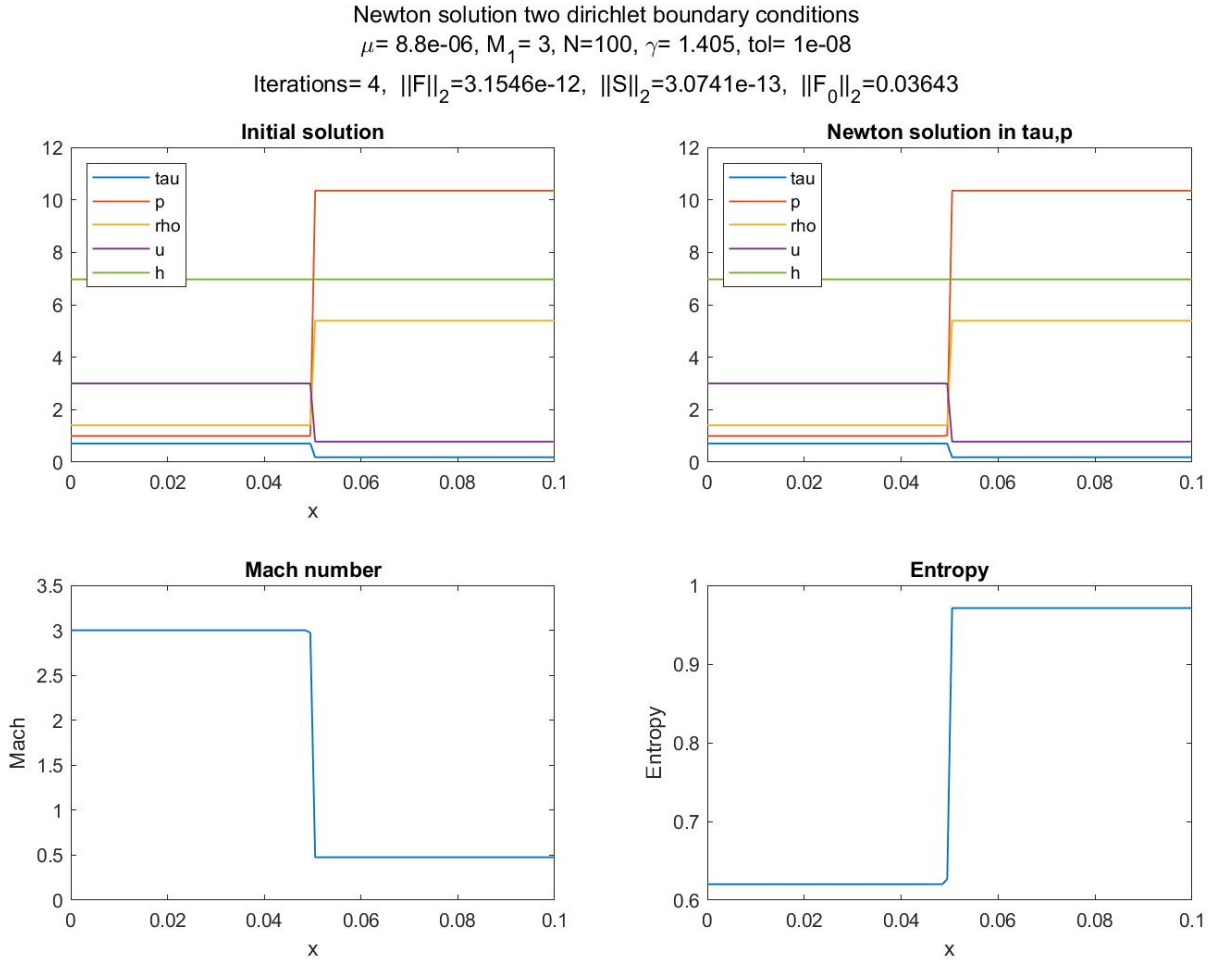

Figure 29: Results for hydrogen, Mach = 3

Figures 27-29 all show similar behaviour. The range of the variables increases for increasing Mach number. Furthermore, the decrease in entropy disappears. Thus, the entropy behaves as expected. As the dynamic viscosity for hydrogen is quite low, all results have quite sharp curves. Furthermore, we note that for $\Pr \neq \frac{3}{4}$, h does not have to be constant. However, h is again constant, with the exception of one finite volume. That is, in the finite volume in which the shock is placed, the value of h differs slightly. Lastly, all physical phenomena across the shock wave, as explained in the previous results, also hold here.

8 Dimensionless system

In this section, we look at the dimensionless system and propose an alternative discretization.

A standard approach to describe and interpret a physical system is through non-dimensional variables. This yields the important non-dimensional variables such as the Prandtl number and the Reynolds number. In this approach, the variables are replaced by dimensionless variables. That is, the whole system is scaled. The new variables that are used are

$$\begin{aligned}
x^* &= x/l, \\
t^* &= t/(l/\bar{u}), \\
\rho^* &= \rho/\bar{\rho}, \\
u^* &= u/\bar{u}, \\
p^* &= p/(\bar{\rho}\bar{u}^2), \\
T^* &= T/(\bar{u}^2/c_v), \\
h^* &= h/\bar{u}^2, \\
e^* &= e/\bar{u}^2,
\end{aligned}$$

where l, $\bar{u}$, $\bar{\rho}$ are the reference length, velocity and density, respectively. These are chosen to be the original length of the spatial domain and the inflow velocity and density that were previously used in Section (5). We note that the dimensionless variables could also be chosen differently, as long as they remain dimensionless. For example, we could have also chosen $T^* = T/(\bar{u}^2/c_p)$. This would result in similar results that are scaled differently.
When substituting these variables into (7a) – (7e), we obtain the following time-dependent equations:

$$\rho_t + (\rho u)_x = 0, \tag{32a}$$
$$(\rho u)_t + (\rho u^2 + p - \tfrac{4}{3}\tfrac{1}{\mathrm{Re}} u_x)_x = 0, \tag{32b}$$
$$(\rho e)_t + (\rho u h - \tfrac{4}{3}\tfrac{1}{\mathrm{Re}} u u_x - \tfrac{\gamma}{\mathrm{RePr}} T_x)_x = 0, \tag{32c}$$
$$p = (\gamma - 1)\rho T, \tag{32d}$$
$$h = \tfrac{1}{2}u^2 + \gamma T, \tag{32e}$$

where $\mathrm{Re} = \rho u l/\mu$ denotes the Reynolds number, Pr denotes the Prandtl number and we have omitted the superscript *. Furthermore, we have that $e = \frac{1}{2}u^2 + T$.

8.1 Dimensionless finite volume discretization

For the dimensionless equations, we can also apply the finite volume discretization and the complete flux approximation as described in Section 3. Here, we will again look at the stationary solution. The specific volume and enthalpy equations (12b) and (12a) become:

$$\begin{aligned}
(m^2\tau + p - \tfrac{4}{3}\tfrac{1}{\mathrm{Re}} m\tau_x)_x &= 0, \\
(mh - \tfrac{4}{3}\tfrac{1}{\mathrm{Re}} h_x - \alpha^*(p\tau)_x)_x &= 0,
\end{aligned}$$

where $\alpha^* = \frac{\gamma}{(\gamma-1)\mathrm{Re}}(\frac{1}{\mathrm{Pr}} - \frac{4}{3})$.
We can see that for the dimensionless approach, only the constants have changed. That is, μ is

replaced by $\frac{1}{\mathrm{Re}}$ and α by α^*. Therefore, the computations also remain the same and the following nonlinear discretized system can be found

$$
\begin{aligned}
&m\varepsilon^* \left[-B^-\tau_{j-1} + (B^- + B^+)\tau_j - B^+\tau_{j+1}\right] - W^-p_{j-1} + (W^- - W^+)p_j + W^+p_{j+1} = 0,\\
&\varepsilon^* \left[-B^-h_{j-1} + (B^- + B^+)h_j - B^+h_{j+1}\right] = 0,\\
&h = \frac{\gamma}{\gamma - 1}p\tau + \tfrac{1}{2}(m\tau)^2,
\end{aligned}
$$

where $\varepsilon^* = \frac{4}{3\Delta x\mathrm{Re}}$ and the Péclet number in B and W becomes $\mathrm{Pe}^* = m/\varepsilon^*$.

8.2 Alternative finite volume discretization

In this alternative approach, we do not omit time integration. Instead we use the method of lines. That is, we first use a spatial discretization based on finite volumes and central differences of the spatial derivatives. Subsequently, we apply a time integration method.
This approach can be seen as an approximation of the previous complete flux approach. Both approaches begin with integration of the conservation laws over a finite volume. Subsequently, a local boundary value problem around $x_{j+\frac{1}{2}}$ is constructed in order to compute the fluxes. In the complete flux scheme, this boundary value problem is solved analytically using the integrating factor. In this alternative approach, we approximate the solution of the boundary value problem using central differences on all spatial derivatives. Additionally, we use the forward Euler method to integrate over time in this alternative approach.

First we use the finite volume method on volume $[x_{j-\frac{1}{2}}, x_{j+\frac{1}{2}}]$ for the spatial derivatives of (32) to obtain:

$$
\begin{pmatrix} \rho u \\ \rho u^2 + p \\ \rho u h \end{pmatrix}_{j+\frac{1}{2}} - \begin{pmatrix} \rho u \\ \rho u^2 + p \\ \rho u h \end{pmatrix}_{j-\frac{1}{2}} - \tfrac{4}{3\mathrm{Re}} \begin{pmatrix} 0 \\ u_x \\ u u_x \end{pmatrix}_{j+\frac{1}{2}} + \tfrac{4}{3\mathrm{Re}} \begin{pmatrix} 0 \\ u_x \\ u u_x \end{pmatrix}_{j-\frac{1}{2}} - \tfrac{\gamma}{\mathrm{RePr}} \begin{pmatrix} 0 \\ 0 \\ T_x \end{pmatrix}_{j+\frac{1}{2}} + \tfrac{\gamma}{\mathrm{RePr}} \begin{pmatrix} 0 \\ 0 \\ T_x \end{pmatrix}_{j-\frac{1}{2}} = \underline{0}. \quad (33)
$$

We now assume that $m_j = \rho_j u_j$ is constant on each volume $[x_j, x_{j+1}]$. As the inflow boundary is located at the left side of the domain, we use m_j when we need to compute the mass flux at an interface $m_{j+\frac{1}{2}}$. Furthermore, there are still two derivatives in (33). For these derivatives, we use central differences to obtain

$$
\begin{aligned}
&\begin{pmatrix} m_j \\ m_j u + p \\ m_j h \end{pmatrix}_{j+\frac{1}{2}} - \begin{pmatrix} m_{j-1} \\ m_{j-1} u + p \\ m_{j-1} h \end{pmatrix}_{j-\frac{1}{2}} - \tfrac{4}{3\mathrm{Re}\Delta x} \begin{pmatrix} 0 \\ u_{j+1} - u_j \\ u_{j+\frac{1}{2}}(u_{j+1} - u_j) \end{pmatrix} + \tfrac{4}{3\mathrm{Re}\Delta x} \begin{pmatrix} 0 \\ u_j - u_{j-1} \\ u_{j-\frac{1}{2}}(u_j - u_{j-1}) \end{pmatrix}\\
&- \tfrac{\gamma}{\mathrm{RePr}\Delta x} \begin{pmatrix} 0 \\ 0 \\ T_{j+1} - T_j \end{pmatrix} + \tfrac{\gamma}{\mathrm{RePr}\Delta x} \begin{pmatrix} 0 \\ 0 \\ T_j - T_{j-1} \end{pmatrix} = \underline{0}. \qquad (34)
\end{aligned}
$$

In order to compute all flux values, we construct a boundary value problem around cell-face $j + \frac{1}{2}$:

$$
\frac{\mathrm{d}}{\mathrm{d}x} \begin{pmatrix} mu + p - \frac{4}{3\mathrm{Re}} u_x \\ mh - \frac{4}{3\mathrm{Re}} u u_x - \frac{\gamma}{\mathrm{RePr}} T_x \end{pmatrix} = \underline{0}, \qquad \begin{aligned} u(x_{j+1}) &= u_{j+1}, \quad & u(x_j) &= u_j \\ p(x_{j+1}) &= p_{j+1}, \quad & p(x_j) &= p_j. \end{aligned}
$$

Instead of applying the integrating factor, as was previously done, we use central differences to compute the solution of the BVP to obtain

$$m_j \frac{u_{j+1}-u_j}{\Delta x} + \frac{p_{j+1}-p_j}{\Delta x} - \tfrac{4}{3\mathrm{Re}} \frac{u_{j+1}-2u_{j+\frac{1}{2}}+u_j}{(\frac{1}{2}\Delta x)^2} = 0, \tag{35a}$$

$$m_j \frac{h_{j+1}-h_j}{\Delta x} - \tfrac{4}{3\mathrm{Re}} \left[\left(\frac{u_{j+1}-u_j}{\Delta x} \right)^2 + u_{j+\frac{1}{2}} \left(\frac{u_{j+1}-2u_{j+\frac{1}{2}}+u_j}{(\frac{1}{2}\Delta x)^2} \right) \right] - \tfrac{\gamma}{\mathrm{RePr}} \frac{T_{j+1}-2T_{j+\frac{1}{2}}+T_j}{(\frac{1}{2}\Delta x)^2} = 0. \tag{35b}$$

From (35a), we can obtain a formula for the velocity flux $u_{j+\frac{1}{2}}$ which reads

$$u_{j+\frac{1}{2}} = \tfrac{1}{2}(u_{j+1}+u_j) - \tfrac{3}{32}\mathrm{Re}\Delta x \left(m_j(u_{j+1}-u_j) + p_{j+1} - p_j \right).$$

In addition, the temperature flux $T_{j+\frac{1}{2}}$ can be computed from (35b) to obtain

$$T_{j+\frac{1}{2}} = \tfrac{1}{2}(T_{j+1}+T_j) - \tfrac{\mathrm{RePr}m_j\Delta x}{8\gamma}(h_{j+1}-h_j) + \tfrac{\mathrm{Pr}}{6\gamma}\left[(u_{j+1}-u_j)^2 + 4u_{j+\frac{1}{2}}(u_{j+1}-2u_{j+\frac{1}{2}}+u_j) \right].$$

Using the equations of state and $m = \rho u$, we can now also compute $\rho_{j+\frac{1}{2}}$ and $h_{j+\frac{1}{2}}$. These interface values can then be substituted into (34) to complete the spatial discretization.

For the time integration, we write the system as

$$\frac{\partial \underline{q}}{\partial t} + \frac{\partial f(\underline{q})}{\partial x} = 0,$$

where

$$\underline{q} = \begin{pmatrix} \rho \\ \rho u \\ \rho e \end{pmatrix}, \qquad f(\underline{q}) = \begin{pmatrix} \rho u \\ \rho u^2 + p - \frac{4}{3}\frac{1}{\mathrm{Re}}u_x \\ \rho u h - \frac{4}{3}\frac{1}{\mathrm{Re}}uu_x - \frac{\gamma}{\mathrm{RePr}}T_x \end{pmatrix}.$$

The spatial discretization of $\partial f(\underline{q})/\partial x$ as shown in (34) will be denoted by $\mathcal{N}(f(\underline{q}))$. If we use forward Euler as the time integration method, we can write the system as

$$\underline{q}_j^{n+1} = \underline{q}_j^n - \Delta t \mathcal{N}(f(\underline{q}_j^n)), \tag{36}$$

where n denotes the time level and j the spatial finite volume. Furthermore, $\underline{q}_j^n \approx q(x_j, t_n)$ and $t_n = n\Delta t$ for $n = 0, 1, 2, \ldots$. Using (36) and a suitable time step, we can compute the stationary solution.

8.3 Dimensionless Dirichlet boundary conditions

Similar as in Section 5.1.2, we can prescribe conditions for the Dirichlet boundary conditions when $m_j = \rho_j u_j$ is constant on each finite volume but not on the whole spatial domain. We use the same approach but now on the following dimensionless equations:

$$\begin{aligned} &m_x = 0, \\ &(m^2\tau + p - \tfrac{4}{3}\tfrac{1}{\mathrm{Re}}u_x)_x = 0, \\ &(mh - \tfrac{4}{3}\tfrac{1}{\mathrm{Re}}uu_x - \tfrac{\gamma}{\mathrm{RePr}}T_x)_x = 0. \end{aligned}$$

Similarly as before, we assume that $u_x = T_x = 0$ at the boundaries and we integrate over $[x_L, x_R]$. We then obtain:

$$m_L = m_R, \tag{37a}$$
$$m_L^2 \tau_L + p_L = m_R^2 \tau_R + p_R, \tag{37b}$$
$$m_L h_L = m_L h_R, \tag{37c}$$

where $h = \frac{1}{2} m^2 \tau^2 + \frac{\gamma}{\gamma - 1} p\tau$.
Substituting (37a) and the expression for h into (37b) and (37c) and eliminating the trivial solutions gives

$$p_R = p_L + m_L^2 (\tau_L - \tau_R),$$
$$\tau_R = \frac{2\gamma p_L}{m_L^2 (\gamma + 1)} + \frac{\gamma - 1}{\gamma + 1} \tau_L.$$

Note that these formulas are similar to those found in Section 5.1.2. The only difference is the replacement of m by m_L. Furthermore, the shock relations found in 5.1.2 remain the same. This means that these boundary conditions again only satisfy the entropy condition for $M_L \geq 1$.

8.4 Results dimensionless systems

We will now compute results for the dimensionless complete flux method as well as for the alternative approach.

8.4.1 Dimensionless complete flux results

For the complete flux approach, the results are computed for Mach $= [1.1, 2, 3]$ and one low and one high Reynolds number for each Mach number. We note that for all results, τ is equal to u and therefore not shown. All results are computed for $\mathrm{Pr} = \frac{3}{4}$. The results will be discussed collectively after all figures.

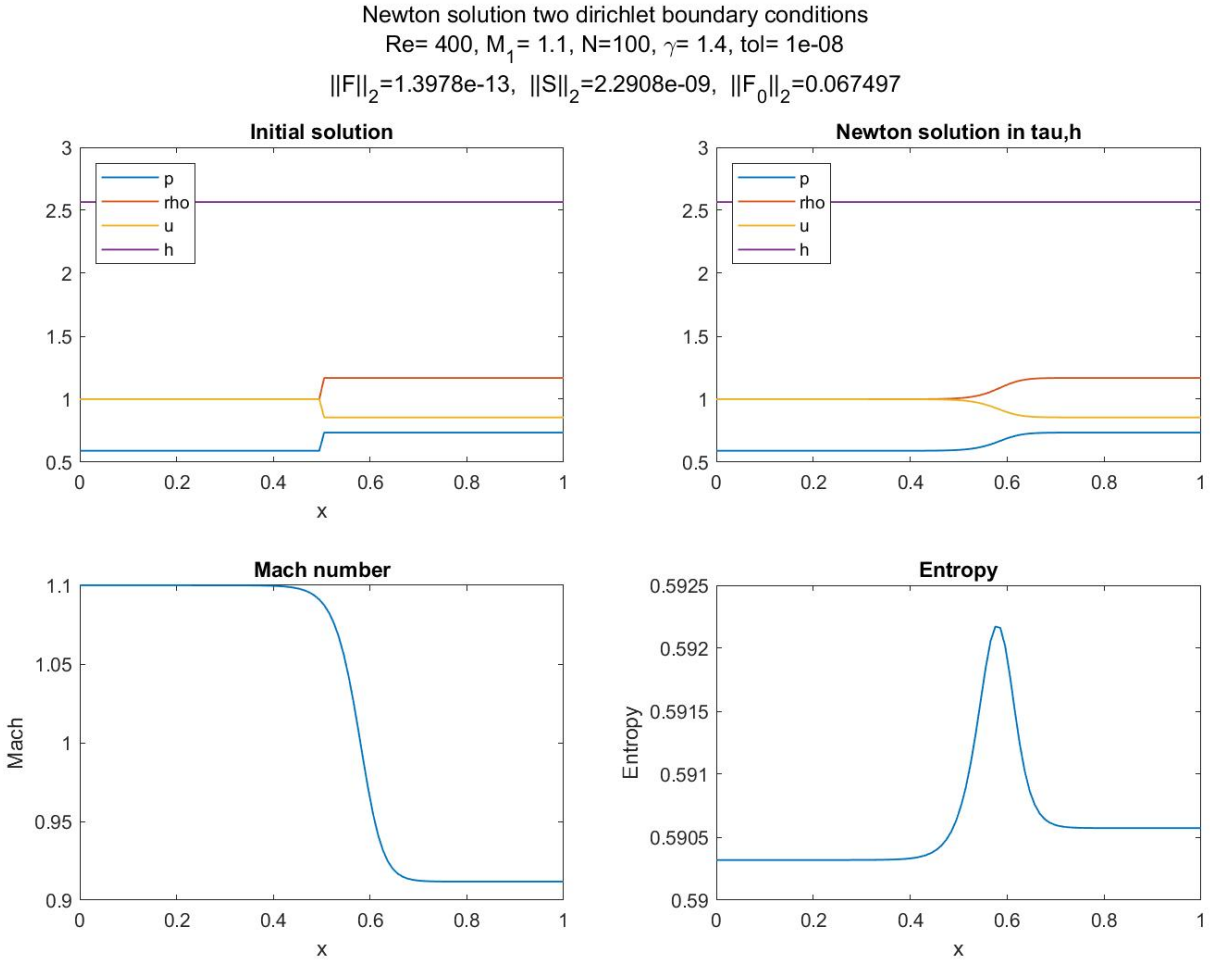

Figure 30: Dimensionless complete flux, Mach= $1.1, \mathrm{Re} = 400$

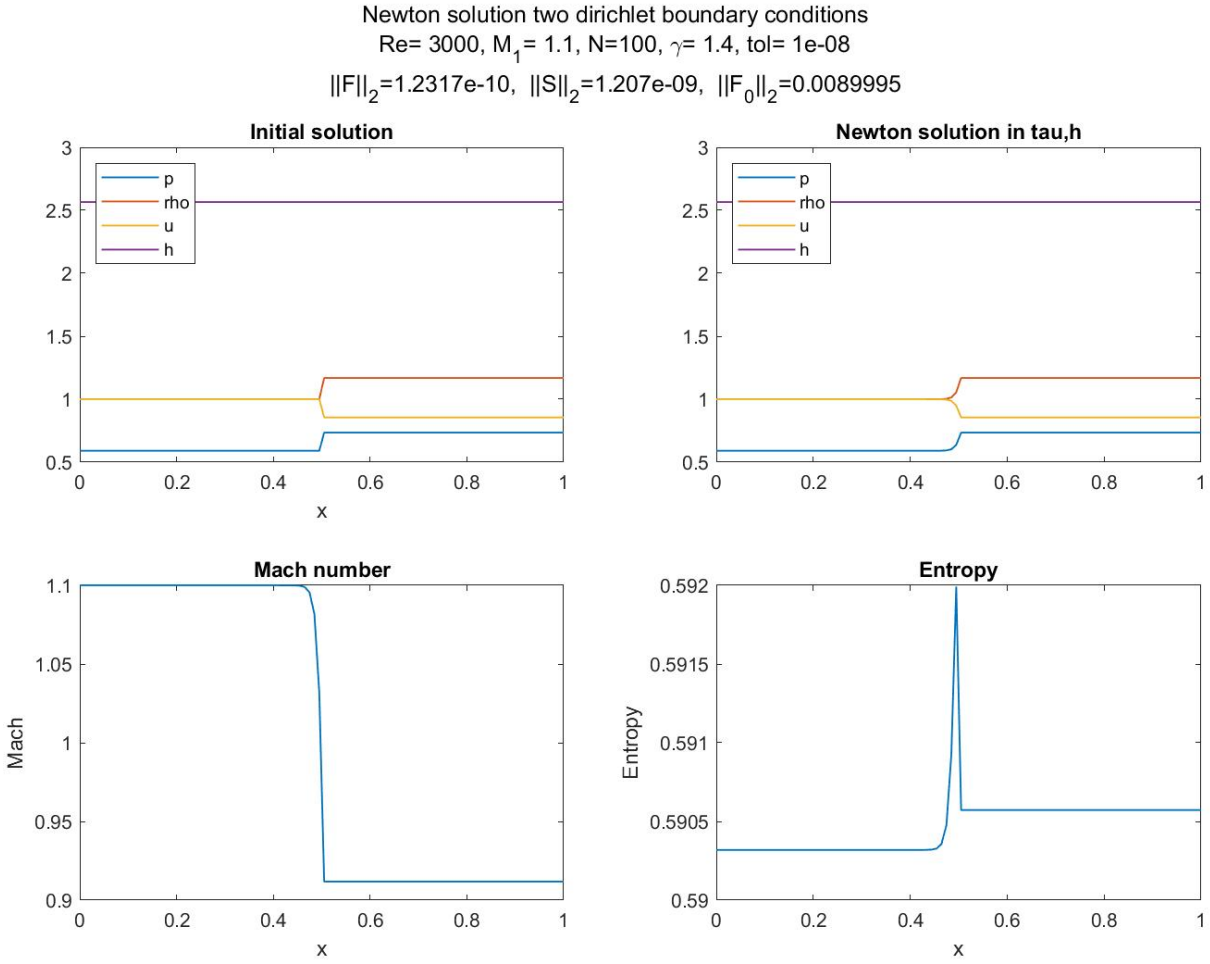

Figure 31: Dimensionless complete flux, Mach= $1.1, \mathrm{Re} = 3000$

In Figures 30 and 31, we see similar results as in the dimensionful results for Mach $= 1.1$. Note that the Reynolds numbers of the dimensionful computations for $\mu = 1e-3, \mu = 1e-5$ were 154 and $1.54e4$, respectively. Thus here we have used a slightly different Reynolds number. Nonetheless, we see similar behaviour. We can still recognize a fluid flow moving across a shock wave. Furthermore, the Mach number also shows similar behaviour. Lastly, there again is a peak in the entropy.

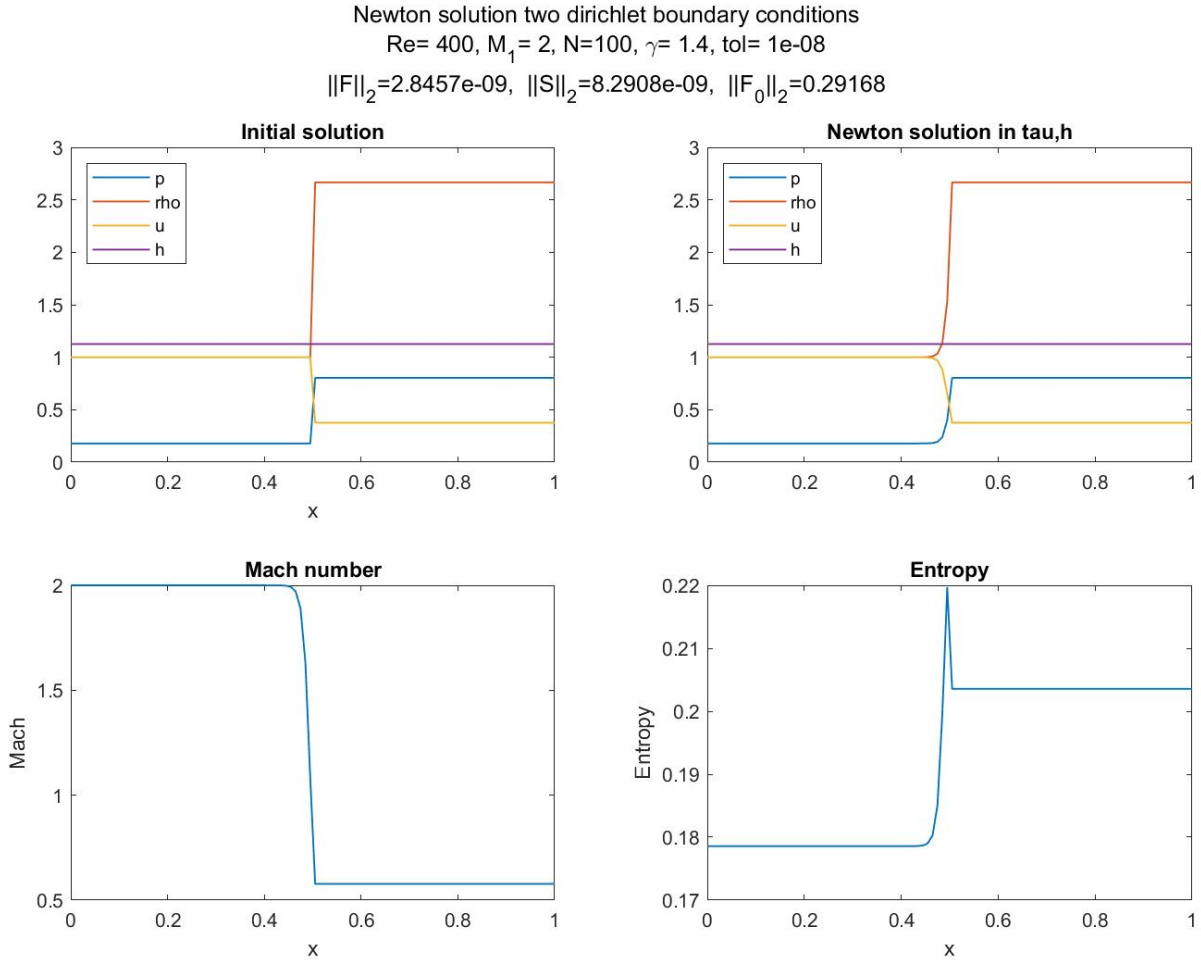

Figure 32: Dimensionless complete flux, Mach$= 2, \mathrm{Re} = 400$

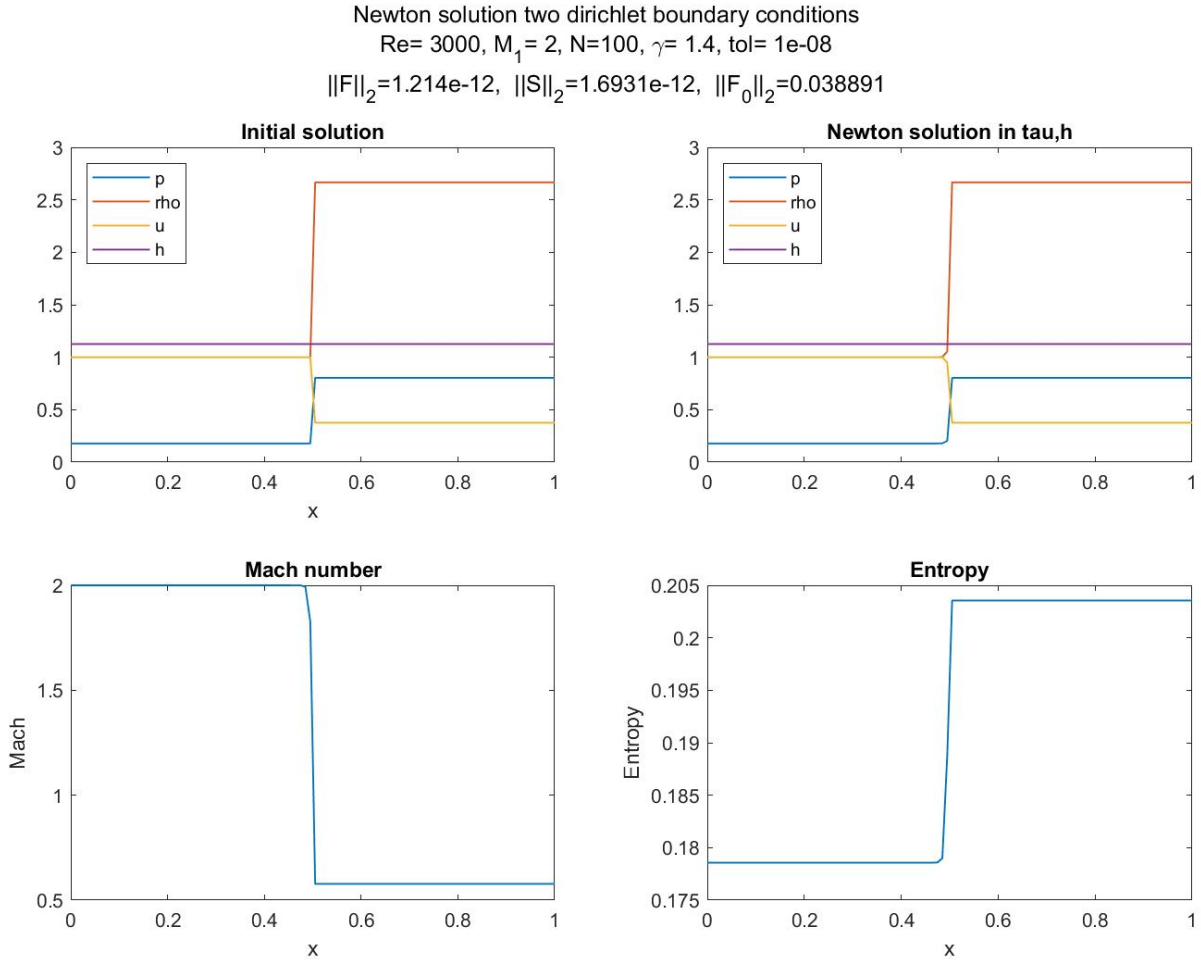

Figure 33: Dimensionless complete flux, Mach= $2, \mathrm{Re} = 3000$

In Figures 32 and 33, we see that for Mach $= 2$, the shock has become sharper. Furthermore, the peak in the entropy has become sharper for $\mathrm{Re} = 400$ and has even disappeared for $\mathrm{Re} = 3000$.

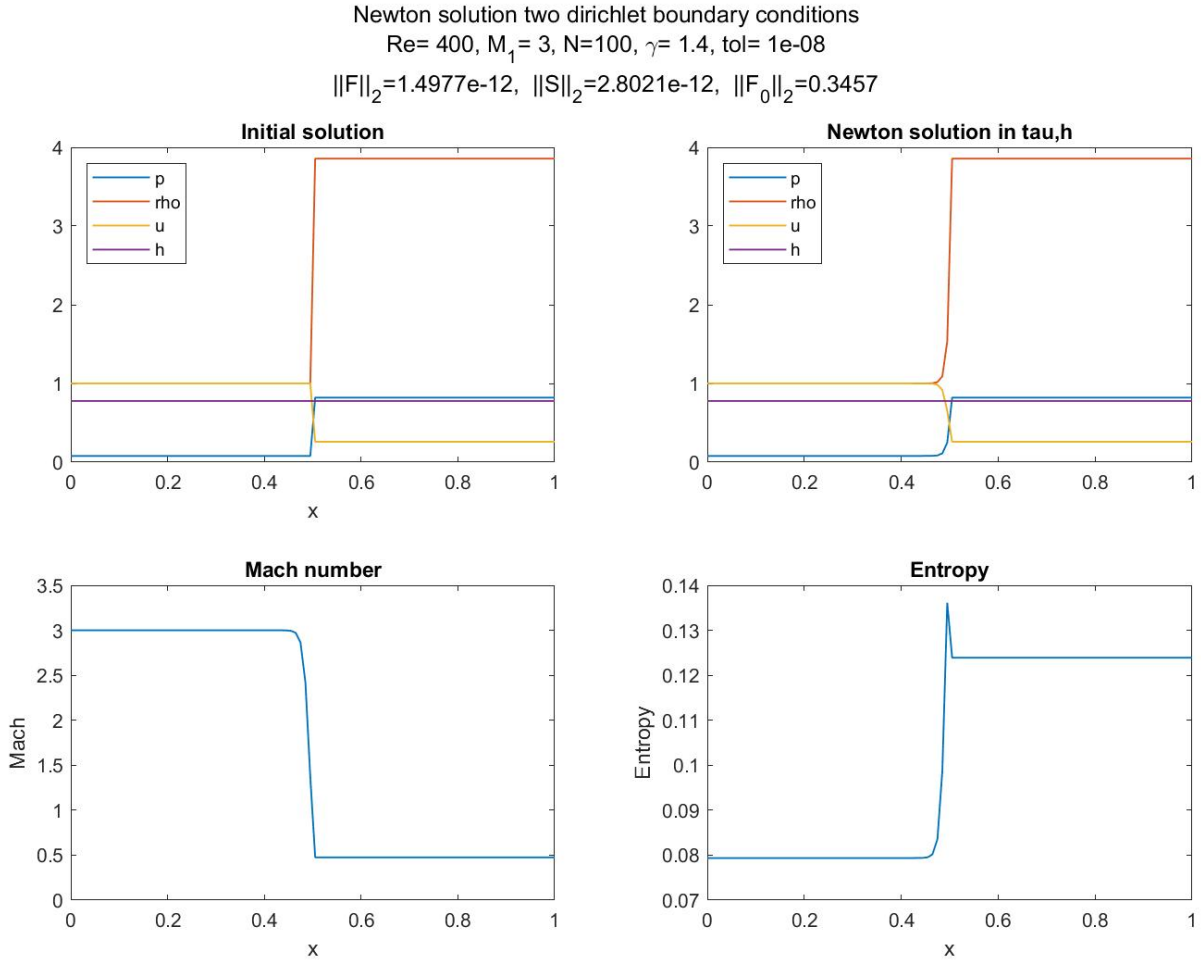

Figure 34: Dimensionless complete flux, Mach= $3, \mathrm{Re} = 400$

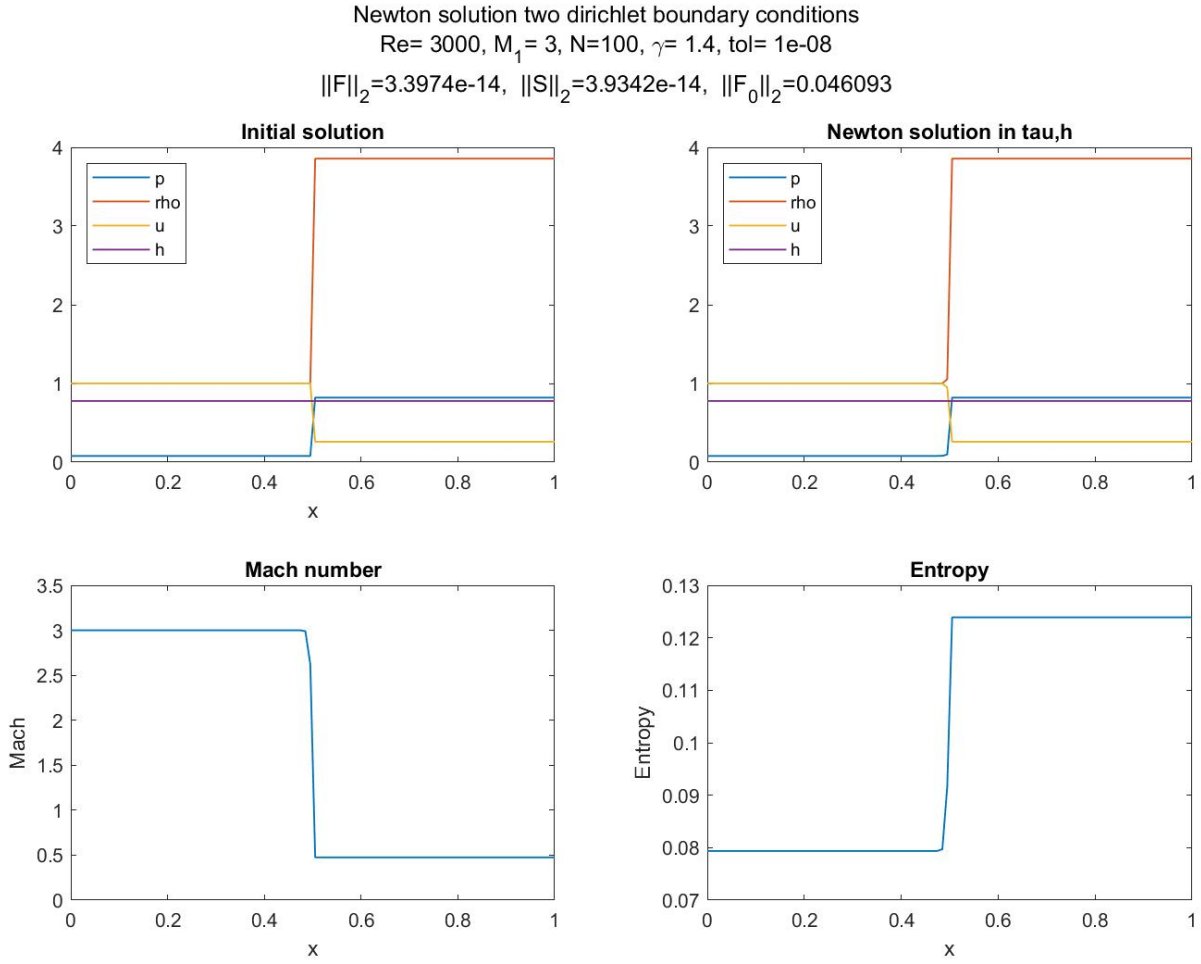

Figure 35: Dimensionless complete flux, Mach= $3, \mathrm{Re} = 3000$

Lastly, Figures 34 and 35 show the results for Mach $= 3$. We again see that for $\mathrm{Re} = 3000$, the peak in the entropy disappears.

In conclusion, all dimensionless results show similar behaviour as the dimensionful previous results. Therefore, we do not get into details here. One important observation is that the entropy behaves better for larger Reynolds number. As the Reynolds number increases, the decrease in the entropy disappears and the entropy forms a smooth graph. Lastly, we note that all results were obtained in less than 10 iterations.

8.4.2 Dimensionless alternative approach results

For the initial solution, we used

1. $\tau_1 = 1$,
2. $p_1 = 1/(\bar{\rho}\bar{u}^2)$,

3. $\mathrm{Pr} = 1$,
4. $\gamma = \frac{7}{5}$,
5. $\mathrm{Re} = 400$,
6. $M_{\text{in}} = 1.1$.

The initial solution is constructed similar as before. Using the Dirichlet boundary conditions, we place a shock in the middle. For the results, we use a time step of $\Delta t = (1/2)\Delta x^2$. It is difficult to derive a stability requirement for this alternative approach using standard approaches based on Fourier theory. Therefore we propose this time step. Presumably, this time step is small enough to guarantee stability. This time step is based on [13].
In the results, we introduce a new variable $\hat{\rho}$. As a consequence of the chosen Dirichlet boundary conditions, $m_j = 1$ in each volume. Therefore, the first row of equation (36) becomes

$$\rho_j^{n+1} = \rho_j^n,$$

for all j. Thus, ρ remains the same as the initial solution. However, u does change in the computation. We use u to compute $\hat{\rho} = m/u$ and see that $\hat{\rho}$ changes over time and shows behaviour which is expected.
The results, starting from $t = 0$, are shown below.

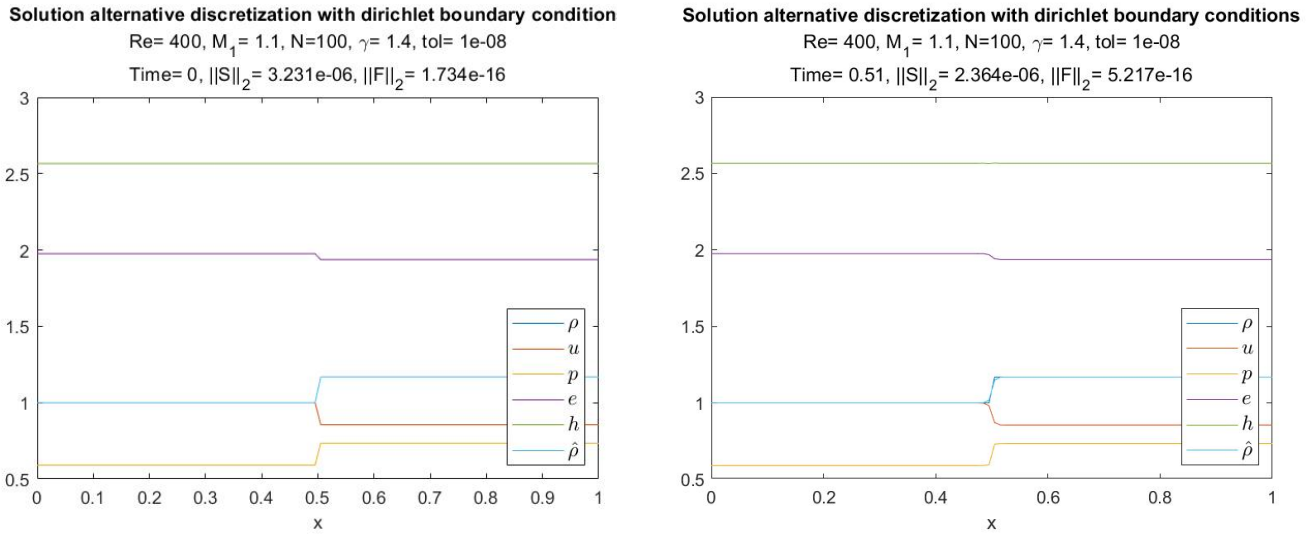

(a) Solution at iteration 0

(b) Solution at iteration 10000

Figure 36: Solution alternative approach, part 1

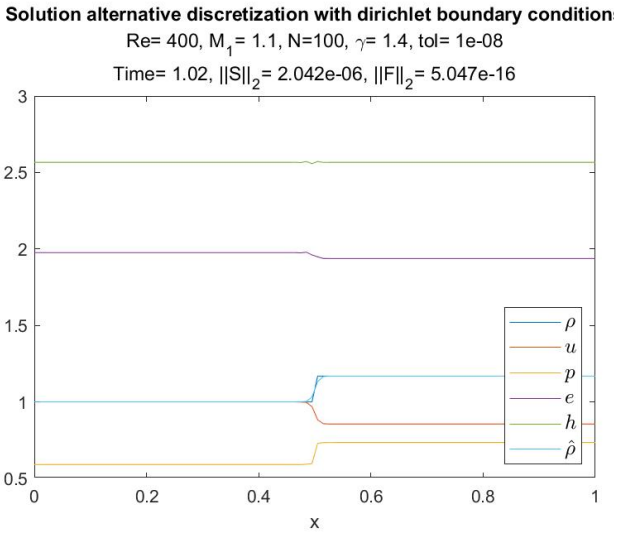

(a) Solution at iteration 20000

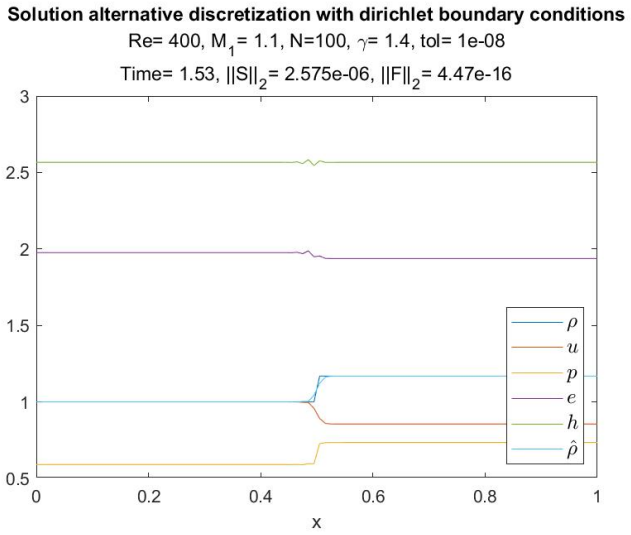

(b) Solution at iteration 30000

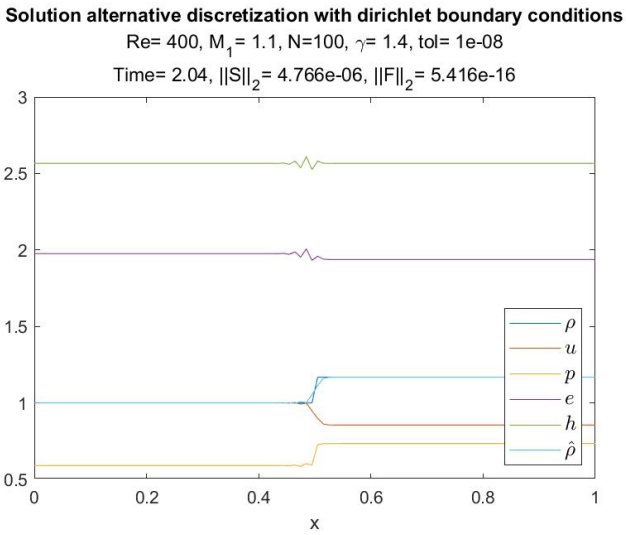

(c) Solution at iteration 40000

Figure 37: Solution alternative approach, part 2

In Figures 36 and 37, we see that oscillations develop over time. This is a indication of instability. However, we already used a restrictive time step. As a result, the run time of the computations has increased significantly. We suspect that the alternative approach is unstable for all time steps when using forward Euler. However, we were unable to prove this.

A possible solution to the stability issue can be to use backward Euler as it is generally unconditionally stable. However, the system would then have to solved using an iterative method such as the Newton-Raphson method. This means that the Jacobian has to be computed which is not

straightforward as the fluxes have quite complex formulas. Therefore, the use of the Newton-Raphson method would not be advised.

Furthermore, we note that the alternative approach could also be implemented as a time-independent approach such as we have also done in the complete flux approach. We have chosen to try the approach on the time-dependent system in order to hopefully also see the progress over time and not only the steady state solution. Furthermore, the time-independent system would again have to solved using the Newton-Raphson method, or a similar method. As previously explained, the Jacobian of the system would be quite complex. Therefore, we did not look at the time-independent system.

Lastly, we remark that there is an issue with the computation of ρ. As a result of the chosen Dirichlet boundary conditions and the initial solution, ρ does not change over time which is not expected. An initial solution in which m_j is not the same in each volume presumably will result in a changing ρ.

9 Conclusion

In this report, we started with the derivation of the Navier-Stokes equations. These equations were derived from the conservation of mass, momentum and energy. Furthermore, the ideal gas law and a caloric equation of state were given. These five equations together form the basis of this report, namely the compressible Navier-Stokes equations.

After the equations were derived, the finite volume discretization was given. For this discretization, the spatial domain was covered with N equidistant grid points and control volumes were given. Subsequently, the momentum flux and enthalpy flux were integrated over each control volume. By defining and solving a local boundary value problem, formulas for the numerical fluxes were derived. These numerical flux formulas were substituted into the discrete conservation laws that were derived. After this, a discrete system was obtained.

Before solving the system, an analytical solution of the momentum equation was found. The starting point of this computation was the integration of the energy equation and imposing inflow boundary conditions. After this, it was found that h was constant when using $\mathrm{Pr} = \frac{3}{4}$. Using this discovery, the momentum equation was integrated and boundary conditions were imposed. This led to an initial value problem for the velocity which could be solved analytically and numerically.

After an impression of the solution was given using the analytical solution of the momentum equation, the discrete system was solved. This was done by imposing several combinations of boundary conditions and solution variables. Subsequently, the results were given. The conclusion of the results was that for the Neumann-Dirichlet boundary conditions, a nontrivial solution is not always guaranteed. However, the Dirichlet boundary conditions always give a nontrivial solution. This is a result of the shock conditions that should hold for the Dirichlet boundary conditions. In these solutions, a shock wave was visible. Along this shock wave, the variables such as velocity and pressure changed. Furthermore, we saw that for the Dirichlet boundary conditions, the rate of convergence was higher than two, indicating convergence better than quadratic convergence.

In the second to last section, an extension to the original finite volume discretization was given. This resulted in an approach which worked for all Prandtl numbers. This approach was applied to the flow of oxygen.

Finally, the dimensionless system was derived. On the dimensionless equations, the original complete flux approach was applied. Furthermore, a new alternative approach that includes time integration was given. This approach integrated the spatial part of the Navier-Stokes equations over a control volume. Subsequently, central differences were used to approximate the spatial derivatives. After this, a boundary value problem similar to that in the original approach was constructed and solved using central differences. Using these equations, formulas for the fluxes could be found. Finally, the time integration was done using the forward Euler method. Using the results on the alternative method, we concluded that the method is unstable when using the forward Euler method.

10 Discussion

In this section, we will discuss the several approaches and give topics for further research.

Firstly, in the complete flux approach, there is one important assumption. Namely, that p (and later also τ) can be approximated by a linear function on each volume. We note that τ could also be computed by solving the momentum equation, assuming that p is linear. However, this would lead to a more complicated expression for τ which subsequently has to be substituted into further computations. Although assuming that p and τ are linear does give good results, it can be argued whether this assumption is justified.

Secondly, the entropy has a small decrease in some of the results. As the entropy is a quantity that can not decrease according to the second law of thermodynamics, this result is undesirable. When using higher Mach numbers and a lower dynamic viscosity (or a higher Reynolds number), this problem disappears. However, it is important to understand what causes the small decrease. A test we performed to remedy this problem was using a smaller grid size Δx. However, the entropy remained unchanged. Unfortunately, we were not able to detect the cause and suggest this topic for further research.

A topic that has not yet been discussed in detail is that for some specific values of the Mach number and the dynamic viscosity (and the Reynolds number), the complete flux approach does not work. For example, when using the dimensionless system, the method does not work for the following values:

- $\text{Mach} = 1.1, \text{Re} \in [400, 1700]$,
- $\text{Mach} = 2, \text{Re} \in [70, 300]$,
- $\text{Mach} = 3, \text{Re} \in [60, 210]$.

We can see that the range of Reynolds numbers for which the method does not work decreases for higher Mach numbers. It is remarkable that the method does work for Reynolds numbers lower as well as higher than this range. For values in these ranges, the method continues to iterate infinitely long or the Jacobian becomes singular. However, we were unable to detect the cause of these problems.

Another possible topic for further research is that of initial solutions for the Neumann-Dirichlet conditions. In Section 6.1 we have shown that for most initial solutions that were tested, the trivial solution was found. However, for some initial solutions, we were able to compute a nontrivial solution. These initial solutions often had a constant value for h. Further research on possible initial solutions with a constant h that result in a nontrivial solution can be done.

Finally, the alternative approach was presumably unstable. Although we had already chosen a very restrictive time step, oscillations occurred. This is a result of the chosen time step method, namely the forward Euler method. A different time integration method could solve the problem of instability, e.g., backward Euler. However, an implicit method does complicate the computations.
Furthermore, the choice of Dirichlet boundary conditions together with the choice of initial solution resulted in ρ not changing over time.
Although the alternative approach seemed a suitable idea, we were unable to compute useful

results using the method. Further research on the stability and boundary conditions can possibly alter this approach into a useful method.

A Results complete flux with Neumann-Dirichlet boundary conditions in τ, h

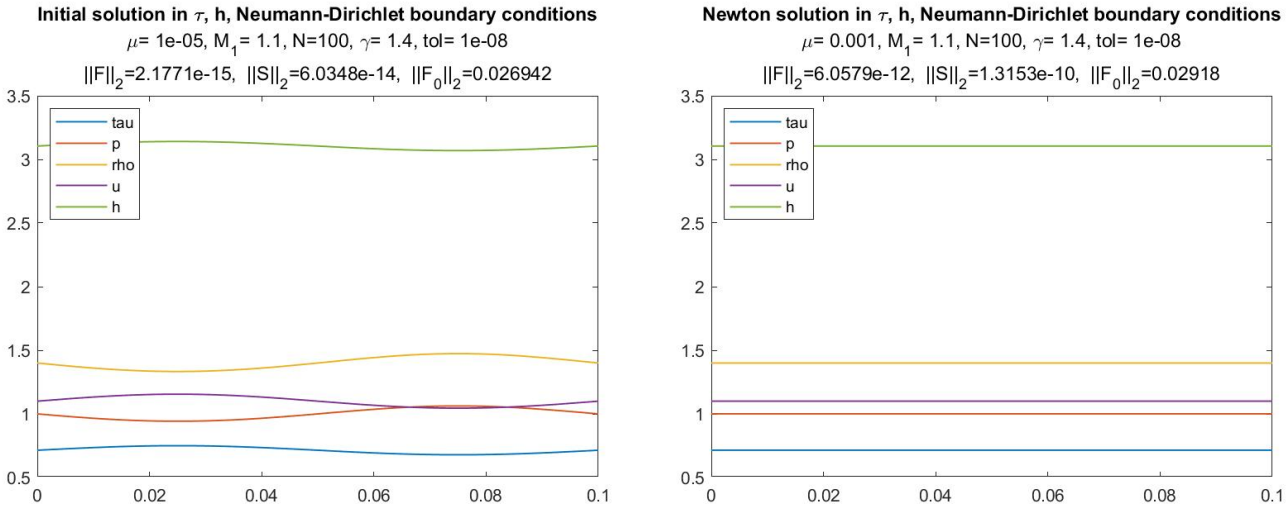

(a) Initial solution

(b) Final solution

Figure 38: Initial solution with distortion, system in τ, h

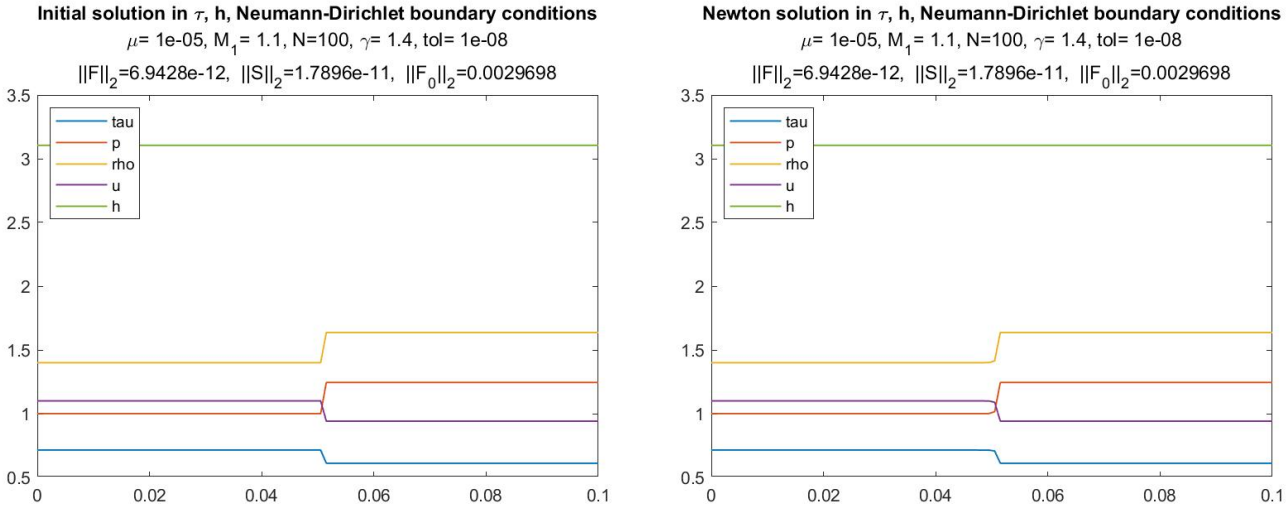

(a) Initial solution

(b) Final solution

Figure 39: Initial solution with Dirichlet shock, system in τ, h

B Results complete flux with Dirichlet boundary conditions in τ, h

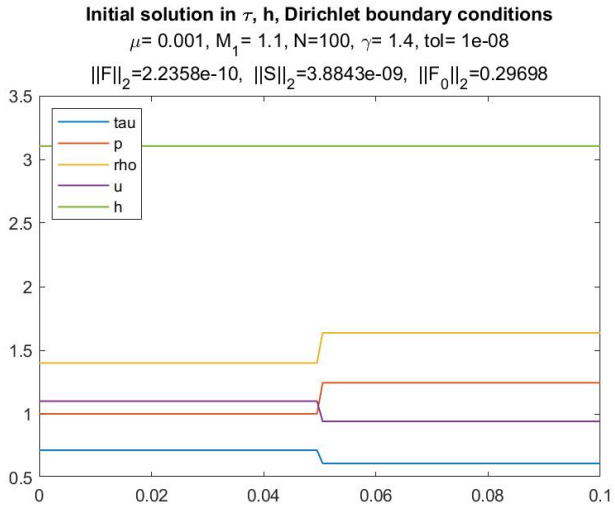

(a) Initial solution

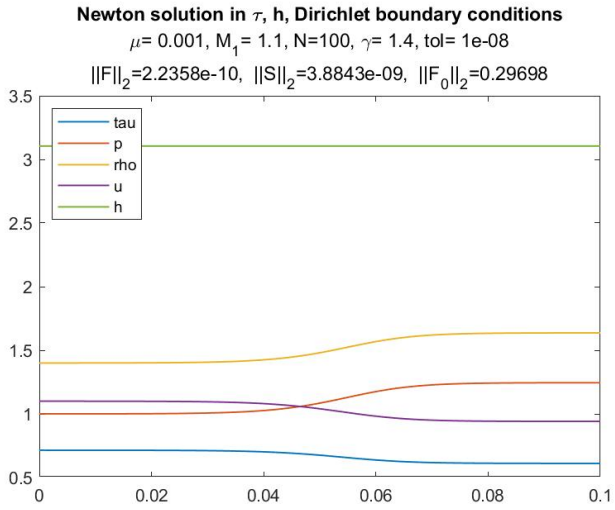

(b) Final solution

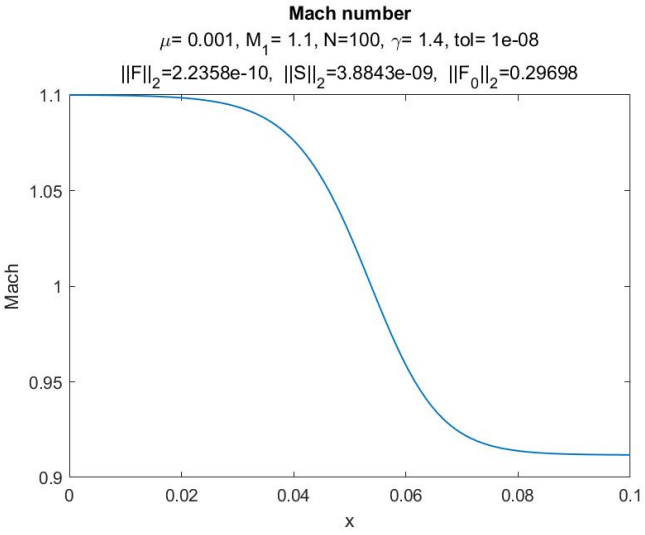

(c) Mach

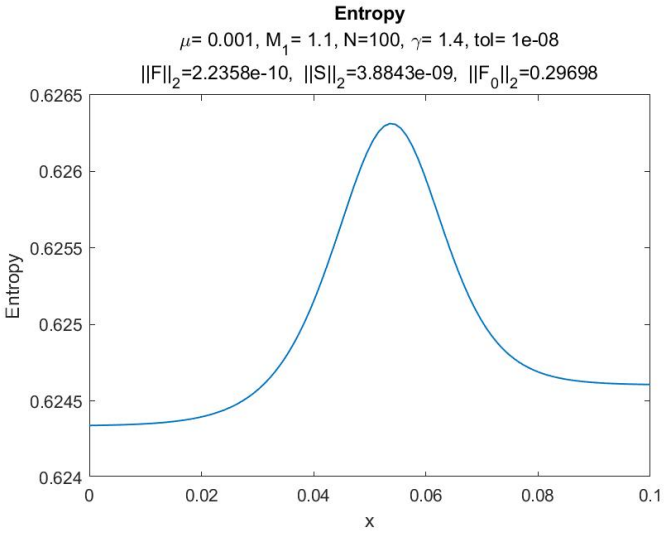

(d) Entropy

Figure 40: Initial solution with shock, system in τ, h

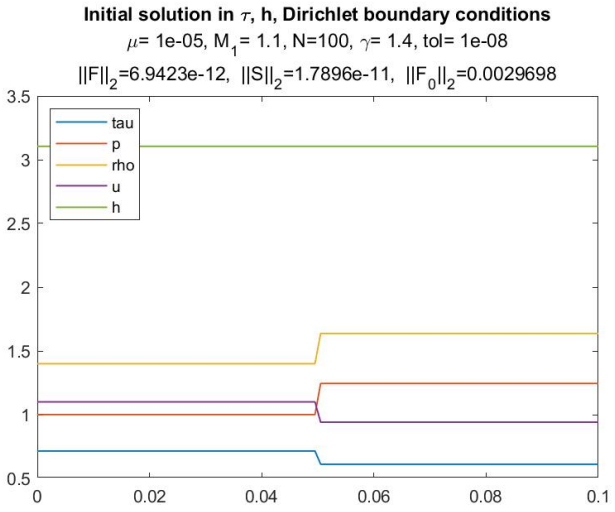

(a) Initial solution

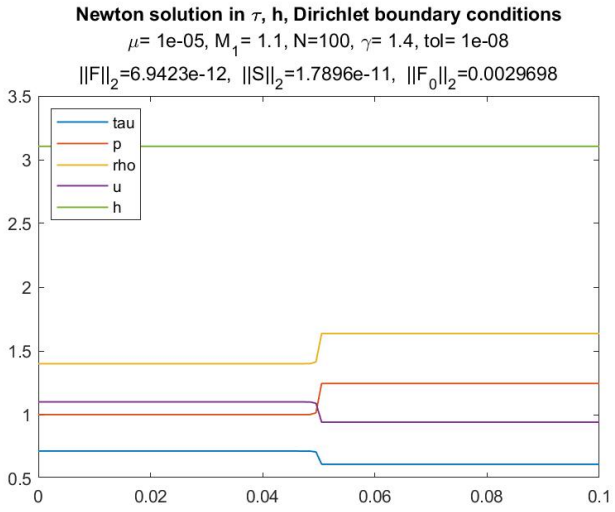

(b) Final solution

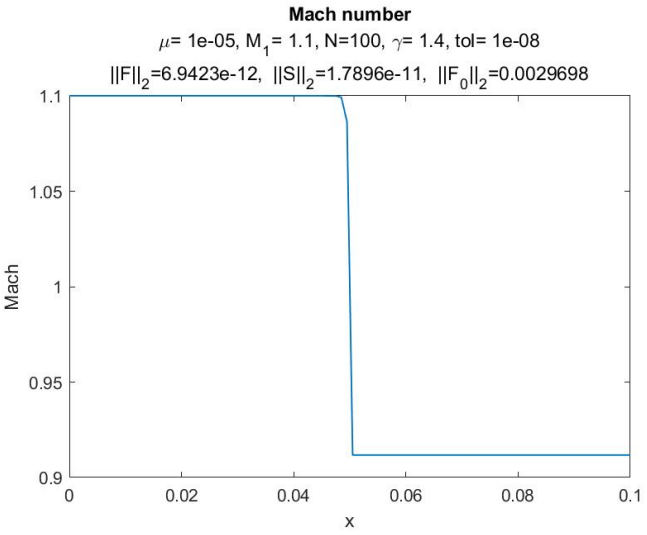

(c) Mach

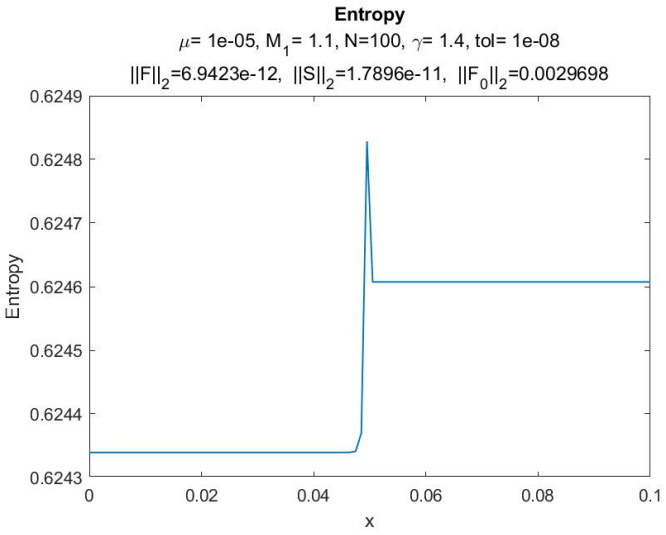

(d) Entropy

Figure 41: Initial solution with shock, system in τ, h

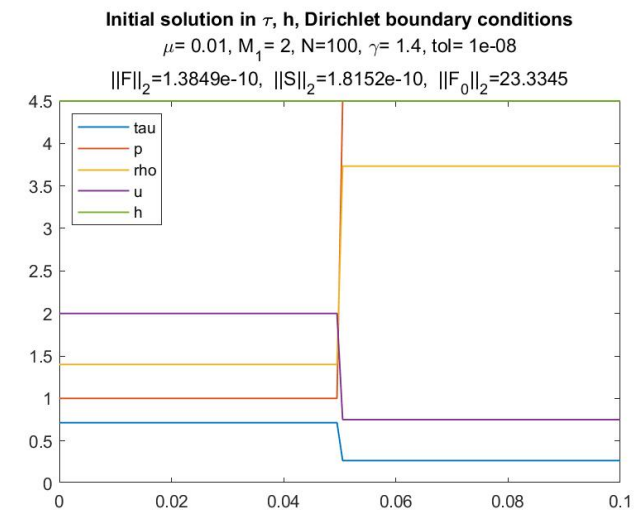

(a) Initial solution

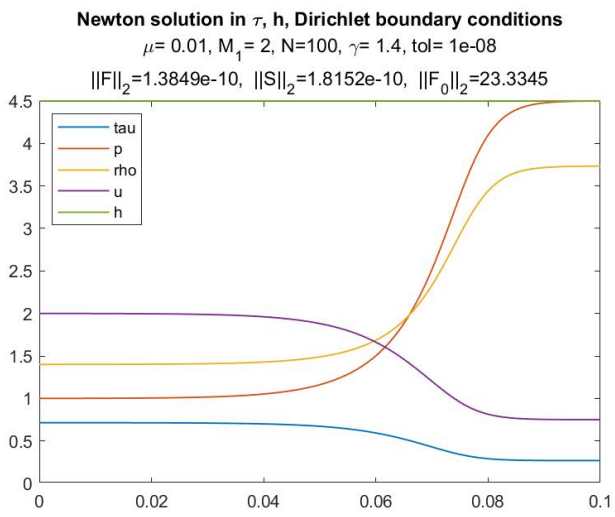

(b) Final solution

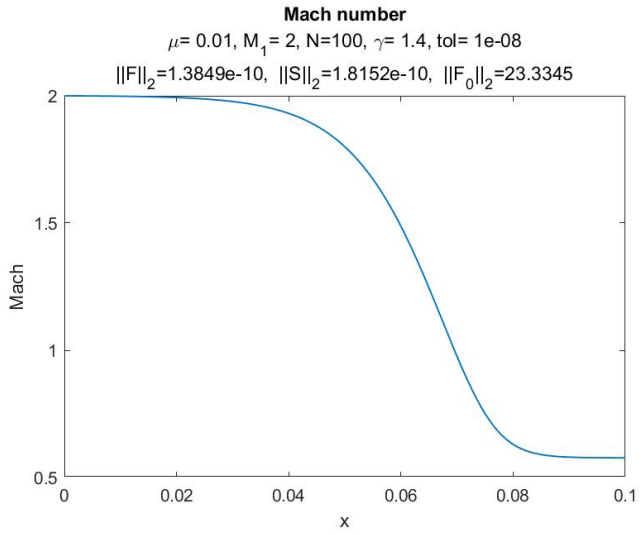

(c) Mach

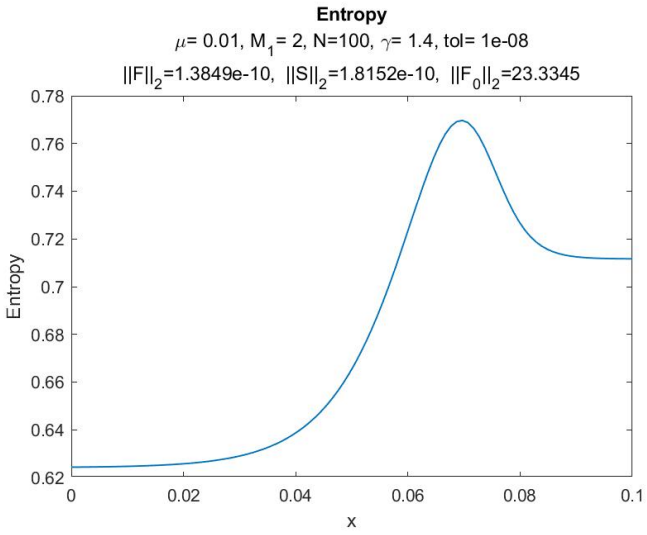

(d) Entropy

Figure 42: Initial solution with shock, system in τ, h

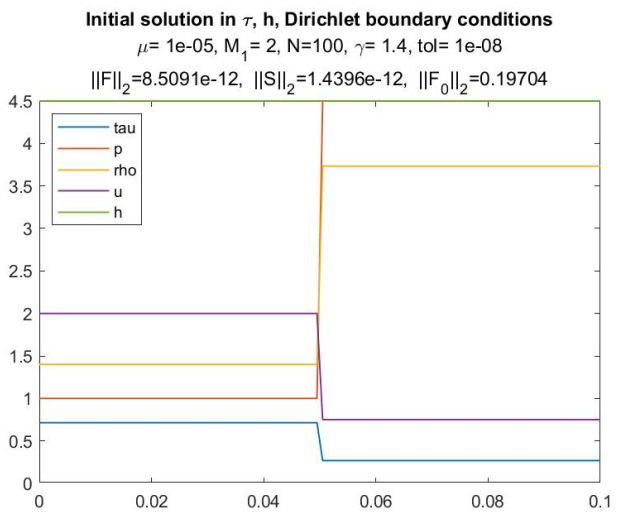

(a) Initial solution

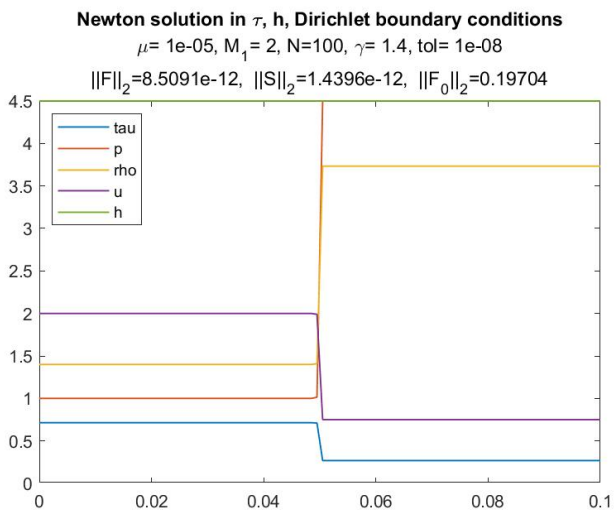

(b) Final solution

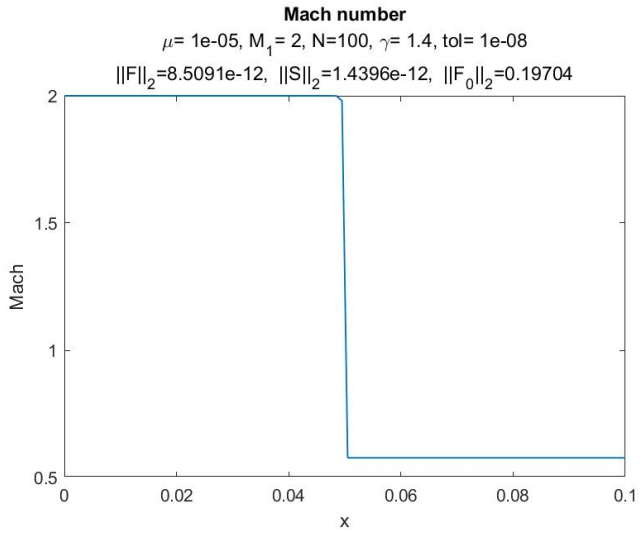

(c) Mach

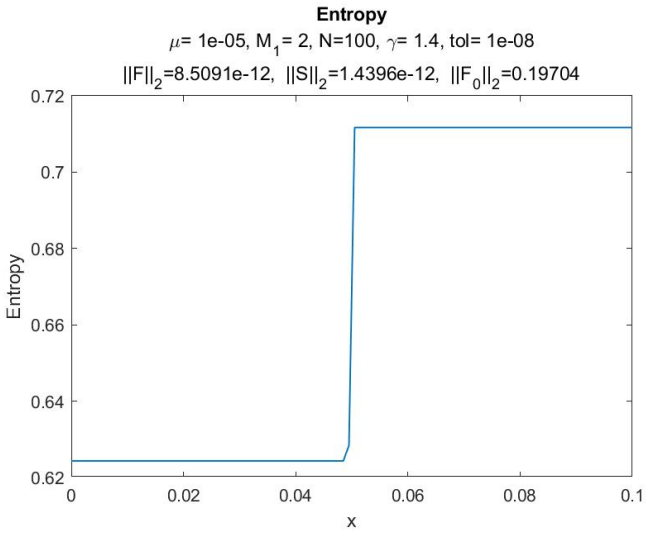

(d) Entropy

Figure 43: Initial solution with shock, system in τ, h

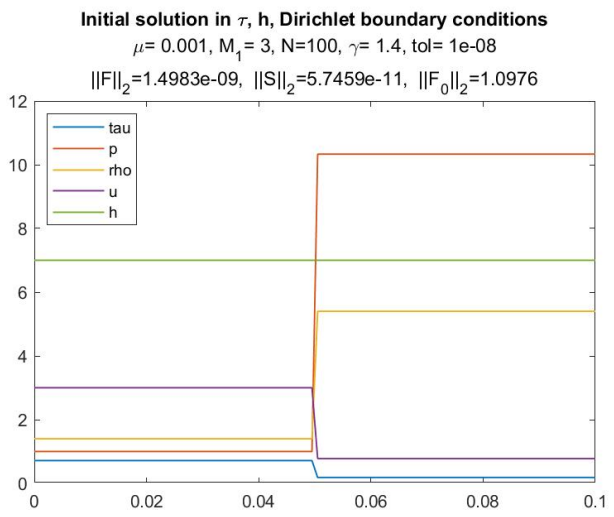

(a) Initial solution

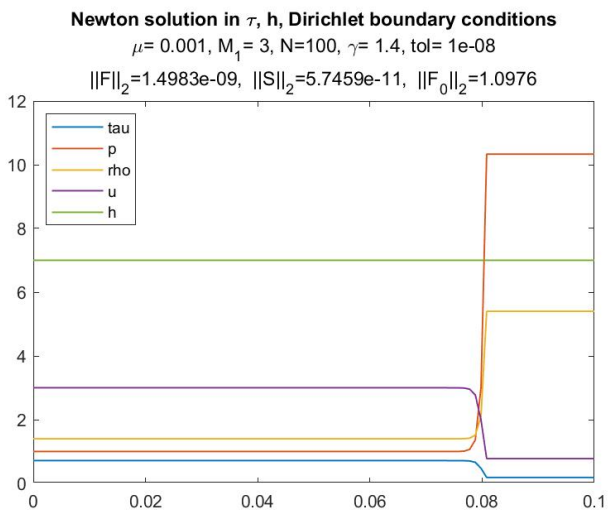

(b) Final solution

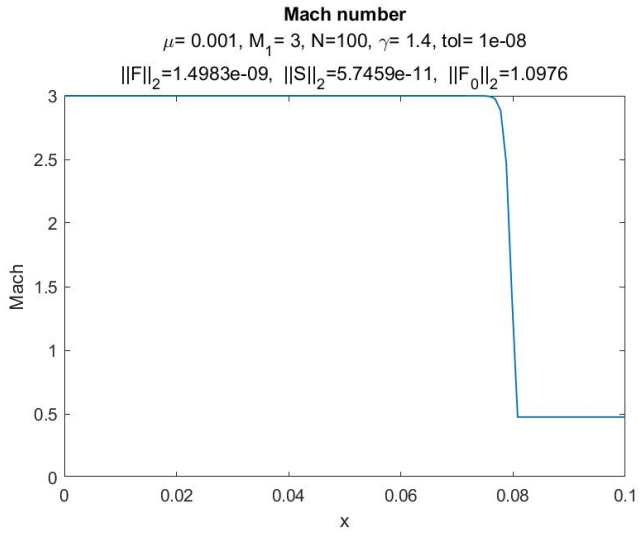

(c) Mach

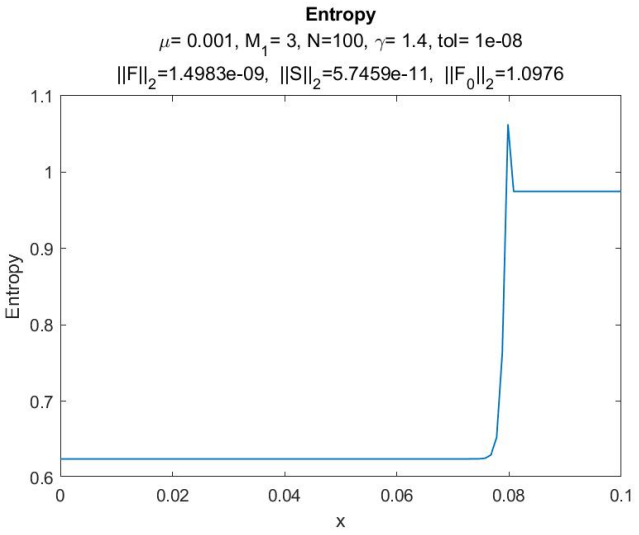

(d) Entropy

Figure 44: Initial solution with shock, system in τ, h

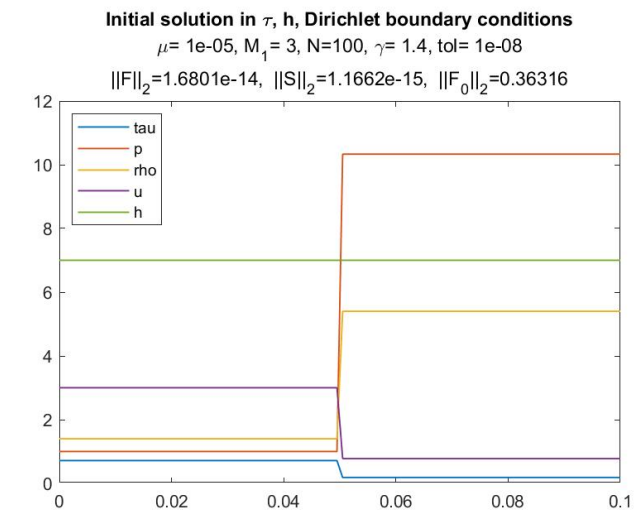

(a) Initial solution

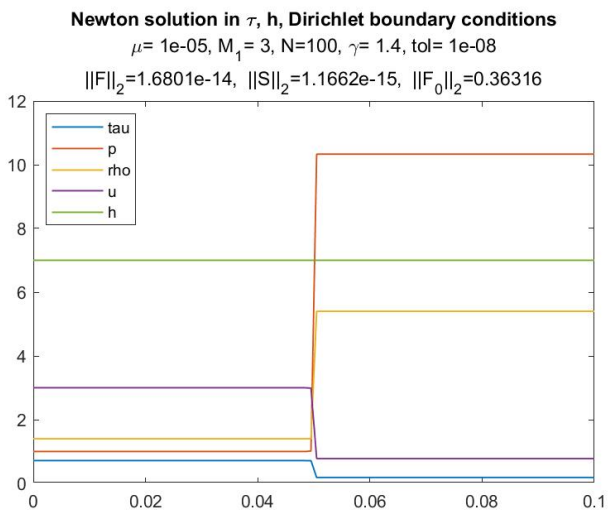

(b) Final solution

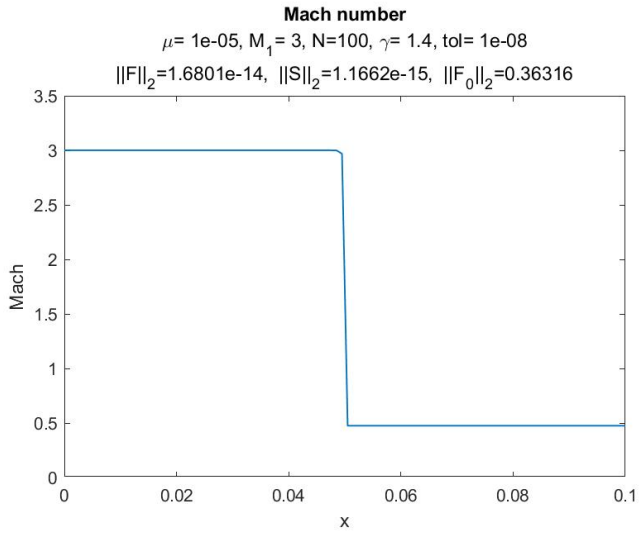

(c) Mach

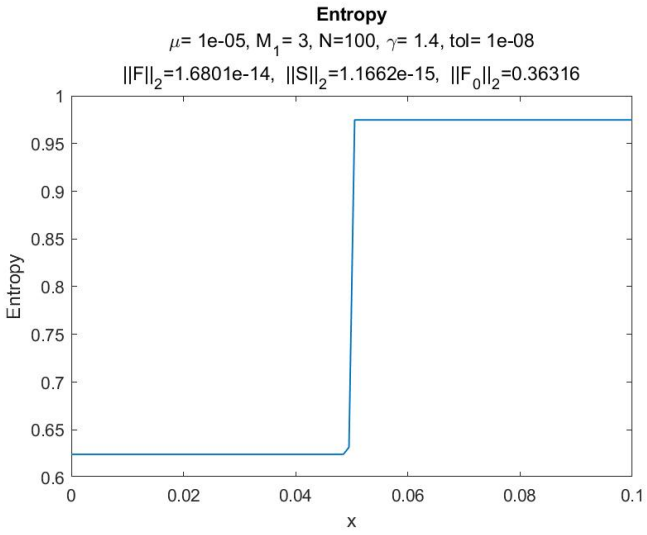

(d) Entropy

Figure 45: Initial solution with shock, system in τ, h

List of Symbols

α	$\alpha = \kappa(1 - \frac{4}{3}Pr)/R$	kg/ms
β	$\beta = \frac{\gamma-1}{\gamma+1} + \frac{2}{(\gamma-1)M_{in}^2}$	
Δx	$\Delta x = x_{j+1} - x_j$	m
$F_{\tau,j+\frac{1}{2}}$	Numerical momentum flux at $x_{j+\frac{1}{2}}$	kg/ms^2
γ	Specific heat ratio, $\gamma = c_p/c_v$	
κ	Thermal conductivity	kgm/s^3K
μ	Dynamic viscosity	kg/ms
Pe	Peclet number, $\mathrm{Pe} = m/\varepsilon$	
Pr	Prandtl number, $\mathrm{Pr} = \mu c_p/\kappa$	
Re	Reynolds number, $\mathrm{Re} = (\bar{\rho}\bar{u}l)/\mu$	
ρ	Density	kg/m^3
$\sigma(x)$	Scaled spatial variable, $\sigma(x) = (x - x_j)/\Delta x$	
τ	Specific volume, $\tau = 1/\rho$	m^3/kg
θ	$\theta = \frac{3m(\gamma+1)}{8\mu\gamma}$	
$\tilde{\gamma}$	$\tilde{\gamma} = \frac{\gamma}{\gamma-1}$	
ε	$\varepsilon = \frac{4}{3}\mu/\Delta x$	kg/m^2s
c_p	Specific heat at constant pressure	m^2/s^2K
c_v	Specific heat at constant volume	m^2/s^2K
f_τ	Momentum flux	kg/ms^2
f_h	Enthalpy flux	J/m^2s
$F_{h,j+\frac{1}{2}}$	Numerical enthalpy flux at $x_{j+\frac{1}{2}}$	J/m^2s
h	Specific enthalpy	m^2/s^2
m	Mass flux	kg/m^2s
p	Pressure	kg/ms^2
R	Specific gas constant, $R = c_p - c_v$	m^2/s^2K
T	Temperature	K
u	Velocity	m/s
V_j	Control volume, $V_j = [x_{j-\frac{1}{2}}, x_{j+\frac{1}{2}}]$	

References

[1] SimScale (2021) *What are the Navier-Stokes Equations?*. Retrievable from https://www.simscale.com/docs/simwiki/numerics-background/what-are-the-navier-stokes-equations/

[2] Clay Mathematics Institute *Millennium problems: Navier-Stokes equation*. Retrievable from https://www.claymath.org/millennium-problems/navier-stokes-equation

[3] R. Panton (2005). *Incompressible flow*. Hoboken, N.J., J. Wiley

[4] Phillip A. Thompson (1972). *Compressible-Fluid Dynamics*. London, McGraw-Hill, Section 1.4

[5] J.H.M. ten Thije Boonkkamp · M.J.H. Anthonissen (2011). *The Finite Volume-Complete Flux Scheme for Advection-Diffusion-Reaction Equations*. Journal of Scientific Computing, v46 n1

[6] C. Hirsch (1988). *Numerical Computation of Internal and External Flows vol. 1*. John Wiley Sons, Section 2.7.1

[7] Phillip A. Thompson (1972). *Compressible-Fluid Dynamics*. London, McGraw-Hill, Section 7.2

[8] Phillip A. Thompson (1972). *Compressible-Fluid Dynamics*. London, McGraw-Hill, Section 2.5

[9] Phillip A. Thompson (1972). *Compressible-Fluid Dynamics*. London, McGraw-Hill, Section 7.4

[10] William C. Davis (1998). *Explosive Effects and Applications*. New York, Springer Science Business Media, Chapter 3: Shock Waves; Rarefaction Waves; Equations of State

[11] Hermann Schlichting and Klaus Gersten (2017). *Boundary-Layer Theory*. Berlin Heidelberg, Springer-Verlag , Sections 3.4 - 3.7

[12] The Engineering Toolbox *Hydrogen - Thermophysical Properties*. Retrievable from https://www.engineeringtoolbox.com/hydrogen-$d_1$419.*html*

[13] J.H.M. ten Thije Boonkkamp, B. Koren (2019). *Lecture Notes Scientific Computing in Partial differential equations 2MMN30*. Eindhoven, 0.1 Time integration methods for parabolic PDE